EFFECTS OF CURVATURE ON THE STRESSES OF A CURVED LAMINATED BEAMS SUBJECTED TO BENDING

by

THIEN NGUYEN

Presented to the Faculty of the Graduate School of
The University of Texas at Arlington in Partial Fulfillment
of the Requirements
for the Degree of

MASTER OF SCIENCE IN MECHANICAL ENGINEERING

THE UNIVERSITY OF TEXAS AT ARLINGTON
MAY 2010

ACKNOWLEDGEMENTS

I would like to sincerely thank and appreciate to my supervising professor, Dr. Wen S. Chan for his guidance, support, and encouragement throughout my research in every aspect. My gratitude goes to the committee members: Dr. Seiichi Nomura and Dr. Haiying Huang, for providing guidance and support.

Most of all, thanks to my up coming son, Dat Nguyen, and my beloved wife, Tram Nguyen, for her love, support, and encouragement. Without her love and support, none of this research work would have proceeded.

Finally, thanks to my parents, my brothers, and my sisters for their love and support.

April 16, 2010

ABSTRACT

EFFECTS OF CURVATURE ON THE STRESSES

OF A CURVED LAMINATED BEAM

SUBJECTED TO BENDING

Thien Nguyen, M.S.

The University of Texas at Arlington, 2010

Supervising Professor: Wen S. Chan

In aircraft structural applications, curved laminated beam structures are often used as part of the internal structure. If the curved composite structure is subjected to bending that tends to flatten or compress the composite structure, interlaminar stresses can be generated in the thickness direction of the composites. These interlaminar stresses are the major factor of delamination failure. Besides these stresses, the in-plane stresses can be also affected by the pre-existence of the beam curvature.

This research has studied the variation of both tangential and radial stresses with respect to the changing in curvature, stacking sequence, and fiber orientation in a curved laminated beam subjected to a bending moment. Three 3-D finite element models of the curved laminated beam have been developed in PATRAN / NASTRAN. These models have been validated for isotropic material, Al-2014-T6, and orthotropic material, T300/977-2

graphite/epoxy, with all 0^0 plies lay-up. The finite element models of the curved laminated beam provide solutions showing an excellent agreement with the exact solutions for both tangential and radial stresses.

An analytical method to calculate the tangential stress was also developed for a curved laminated beam subjected to a bending moment. The tangential stress results from this method were compared well with the results from the finite element method. The analytical closed-form expressions of axial, coupling and bending stiffness, as well as their characteristics were also investigated.

TABLE OF CONTENTS

LIST OF ILLUSTRATIONS

LIST OF TABLES

CHAPTER 1

INTRODUCTION

1.1 Composite Material Overview

1.1.1 History

The composites industry has been in place for over fifty years. It began in earnest in the late 1940s and developed rapidly through the 1950s. Most of the composites processing methods used today were developed by the year 1955. Some aircraft of composite materials began to appear in the late 1930s and 1940s; normally these were plastic-impregnated wood materials. New materials were continually being developed-true carbon fibers in the mid-1960s, aramid fibers in the 1970s, and many advanced resins in subsequent years.

Fiberglass is the most common composite material, and consists of glass fibers embedded in a resin matrix. Fiberglass was first used widely in the 1950s for boats and automobiles, and today most cars have fiber glass bumpers covering a steel frame. Fiberglass was first used in the Boeing 707 passenger jet in the 1950s, where it comprised about two percent of the structure. By the 1960s, other composite materials became available, in particular boron fiber and graphite, embedded in epoxy resins. The first major military production use of boron fiber was for the horizontal stabilizers on the Navy's F-14 Tomcat interceptor. By 1981, the British Aerospace-McDonnell Douglas AV-8B Harrier flew with over 25 percent of its structure made of composite materials. Recently, in December 2009, the Boeing 787-8 Dreamliner flew with 50 percent of the primary structure-including the fuselage and wing- made of composite materials.

1.1.2 Definition and Applications

What are composite materials? And why have composite materials been using widely? Composite material consists of two or more materials macroscopically mixed together to form a

useful new material. This new material contains on constituent to reinforce the other constituent. The composite reinforcement is often in the form of continuous fibers which are high specific stiffness and strength. To take advantages of these unique properties of the fiber reinforced composites, a structure often contains multiple layers laminated together with each layer oriented in the direction of the pre-determined structural function. Due to lack of the thickness reinforcement, laminate is prone to delamination resulting in loss of stiffness, strength and fatigue life.

Composite materials are now the most preferred materials in aircraft structures. Many aircraft are currently undergoing the design that takes advantage of composite materials for primary structure applications. Composites are different from metals in several ways. These include their largely elastic response, their ability for tailoring of strength and stiffness, their damage tolerance characteristics, and their sensitivity to environmental factors. However, unlike metals, composite materials often give little or no warning before weakening the structural members in aircraft.

1.1.3 Curved Laminated Beam

Most of structural components in aircraft structures in general and in composite structures in particular could contain curved beam regions or could be in the form of curved panels. In structural applications, beam is one of the primary structures that used to support the bending and transverse loads. Beams can be straight or curved. Examples include Z-stiffener, angle clip, angle bracket and panel with supporting stringers in aircraft system, as shown in Figure 1.1. Improper design of these curved beam/panel structures may lead to structural failures.

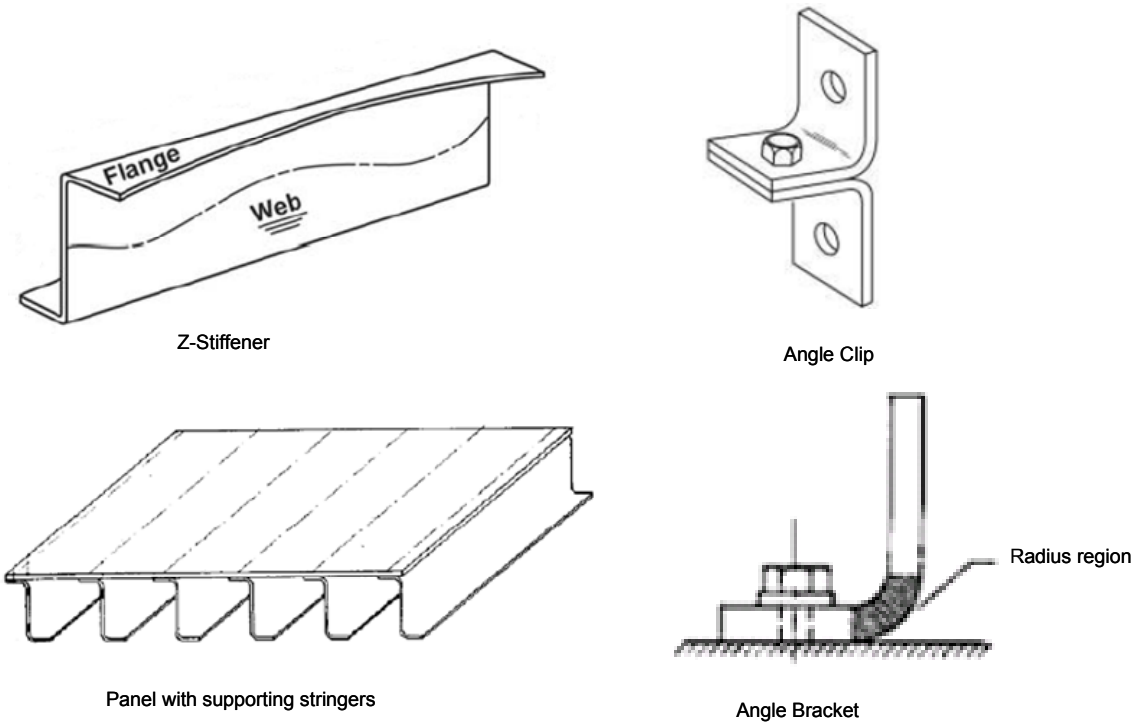

Figure 1.1. Examples of aircraft structural components.

1.1.4 Past works in Composite Curved Beam

Numerous of studies, researches had been done in the linear/or nonlinear for straight beams. However, much less works have been done for the laminated beams, particularly the curved beams.

Sayegh and Dong [1] in 1970 investigated the stresses and displacements of a three-layer curved beam subjected to loading conditions of pure flexure and applied axial force using both technical theory and orthotropic elasticity. It was shown that for a beam, whose radius of curvature is large compared to the total thickness, technical theory gives adequate results provided the properties of the layer are approximately the same. For large differences, the prediction by the technical theory may be in considerable error.

Cheung and Sorensen [2] provided additional insight into the effect on the radial stresses due to the axial loads that are present in the curved beams. Equations of tangential,

radial, and shear stress were developed for curved beams under an axial load. The theory of elasticity with polar coordinates for plane stress applied to an orthotropic material was used. The theoretical radial stresses predicted by Wilson's equation were verified by a rigorous theory of elasticity solution as both solutions gave almost identical results. They concluded that the effect of axial load on the radial stress in curved beams is small.

Graff and Springer [3] developed a finite element code to calculate the stresses and strains in thick, curved composite laminates subjected to an arbitrary, but consistent, combination of forces and displacements. The analysis was formulated using anisotropic, bilinear quadrilateral and tri-linear hexahedral continuum elements. A computer code was then written for either three-dimensional or two-dimensional (plane stress or plane strain) analysis of curved laminates. The accuracy of the computer code was evaluated by generating numerical results for three problems for which analytical solutions exist, and by comparing the numerical and analytical results. In every case the agreement between the numerical and analytical results was excellent.

Barbero et al. [4] investigated the bending behavior of glass fiber reinforced composite beam. They showed that the bending stiffness is low compared to that of steel sections of the same shape. They concluded that shear deformation effects are important for composite beams. This is due to relatively low elastic modulus of glass fibers when compared to steel and the low shear modulus of matrix resin.

Madabhusi-Raman and Davalos [5] later derived a form for the shear correction factor for laminated rectangular beams with symmetric or asymmetric cross-ply or angle-ply lay-ups. In this work, the shear correction factor was computed by equating the shear strain energy obtained from the constitutive relations of first order shear deformable laminated plate theory to that obtained using the “actual” shear stress distribution calculated *a posteriori*, i.e. computed using the equilibrium equations of elasticity.

Kasal and Heiduschle [6] studied the application of fiber composite materials in reinforcement of laminated wood arches subjected to radial tension. An experimental program was designed that included testing of mechanical properties of composite tubes, studying properties of the wood-composite tube interface, testing of the wood-steel rod interface, and testing of models of laminated wood arches. The application of composite materials in radial reinforcement of arches is feasible and possibly has advantages over the glued-in steel rods because of greater flexibility of sizes and properties of reinforcing elements, low mass, and potential ease of installation.

Wang and Shenoi [7] studied the through-thickness tension in curved sandwich beam using an elasticity-theory-based approach. This approach ensures an accurate description of the through-thickness stresses in curved sandwich beam. The critical load for instability of a curved beam on an elastic foundation which is correspondent to the skin of sandwich beam, is considered and compared with the result for a flat beam on an elastic foundation. Wang and Shenoi also studied the flexural strength of sandwich beam to identify debonding and local instability characteristics. The effects of various parameters, such as geometrical configuration, stiffness of the skin and core, on through-thickness tension stress and local instability respectively are included in this study.

Qatu [8] in 2004 addressed the vibration of laminated curved beams and rings subjected to combined loading, bending and shear loads. The fundamental equations and energy functional for laminated curved beams and closed rings were developed and presented in both exact and approximate solutions. These equations are very useful for design engineers.

1.2 Objectives and Approach to the Thesis

The composite curved beam regions are vulnerable to out-of-plane failures. Loads which tend to open or close the curved beam regions result in tensile or compressive radial stress, respectively, as shown in Figure 1.2.

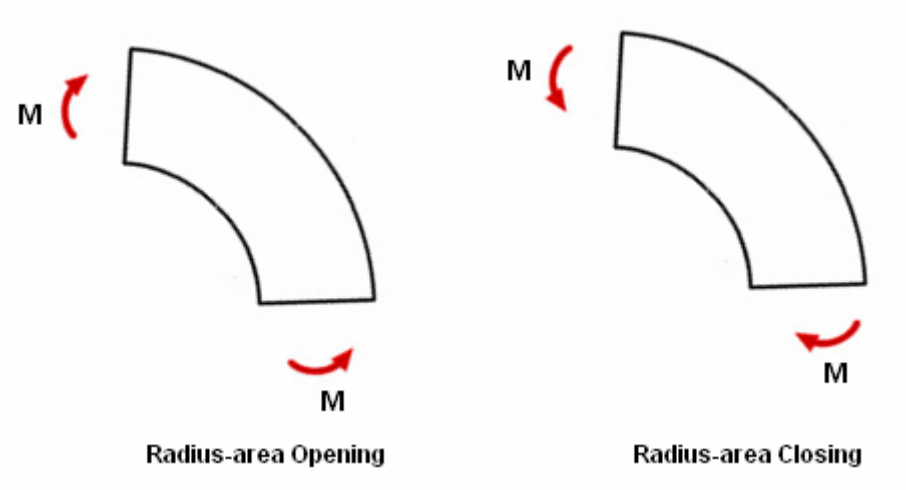

Figure 1.2. Opening and Closing modes of composite curved beam.

The typical failure mode for this region is delamination in the radius area. Delamination is one of the major causes of failure in laminated composite structures, in which the layers of the material separate from each other. Delamination can be caused by interlaminar shear stresses ($\tau_{r\theta}$) between the layers, or tensile radial stresses (σ_r) across the layers. Tensile radial stress (out-of-plane stress) is the principal cause of delamination in the composite curved beam structures (see Figure 1.3). Once the delamination takes place, the composite structure could lose their strength and stiffness significantly, and may lead to a catastrophic structural collapse.

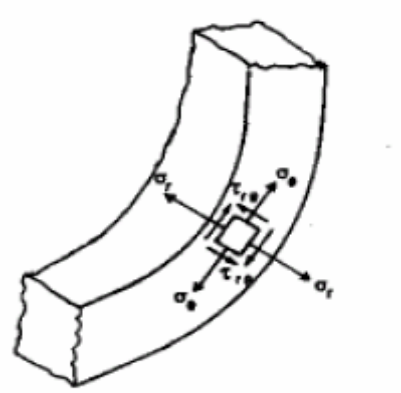

Figure 1.3. Interlaminar stresses in radius region.

Interlaminar stress is a key parameter to be taken into consideration for any composite structural design, especially for structures that contain radius areas. Composite structures are often optimized for minimum weight and maximum strength. Thus, design of composite structures to meet the structural specifications is a challenge problem. Understanding the behavior of the interlaminar stresses in the composite curved beam structures is significant to structural design in many fields. The variation of interlaminar stresses can lead to the changing in geometry design of structural components. Thus, interlaminar stresses must be considered in the design, validation, and certification phases of airframe development.

The primary objective of this study is to investigate the laminate stresses in a curved laminated beam subjected to a pure bending moment. The study was focused on both radial stress (out-of-plane stress) and tangential stress (in-plane stress) effects due to the curvatures, stacking sequences and fiber orientations. An approximated closed-form relationship of laminate constitutive equation is developed to understanding the characteristics of a curved laminate. A 3-D finite element model of PATRAN / NASTRAN was developed to investigate both radial and tangential stress distribution.

This study intended to provide the better understanding about the variation of radial and tangential stresses due to laminate curvature, stacking sequence, and fiber orientation in the curved beam.

1.3 Outline of the Thesis

Chapter 2 presents procedure to develop the geometry, the 3-D finite element model, the material used and its boundary conditions. The validation of analyzed model and the convergence for stresses are also included.

Chapter 3 presents a brief review of lamination theory. An analytical method to calculate the tangential ply stress in a curved laminated beam is presented.

Effects of the tangential and radial ply stresses with the variation of curvature are included in Chapter 4. Effects of the ply stresses due to stacking sequence such as symmetrical versus unsymmetrical and balanced versus unbalanced are also investigated in this Chapter. A comparison of the results between the analytical method and FEM method is included in this Chapter as well.

Chapter 5 concludes the work and provides a future work.

CHAPTER 2

FINITE ELEMENT MODEL

This Chapter describes in detail the geometry, material used in the model, how the model constructed, and the boundary conditions used. PATRAN / NASTRAN was used to develop the required 3-D finite element model.

2.1 Geometry and Material Used

2.1.1. Geometry of Curved Laminated Beam

Three semicircular curved beam models with different curvatures were constructed. The dimensions of these three models are listed in Table 2.1. Figure 2.1 shows the geometry of a typical curved beam 3-D model.

Figure 2.1. Iso view of 3-D curved beam.

Table 2.1. Geometric parameters for three different curved beam models.

Configuration	Inner Radius, Ri (inches)	Outer Radius, Ro (inches)	Mid-Plane Curvature, R (inches)	Width w (inches)
Model I	0.2	0.2888	0.2444	1
Model II	0.6	0.6888	0.6444	1
Model III	1.8	1.8888	1.8444	1

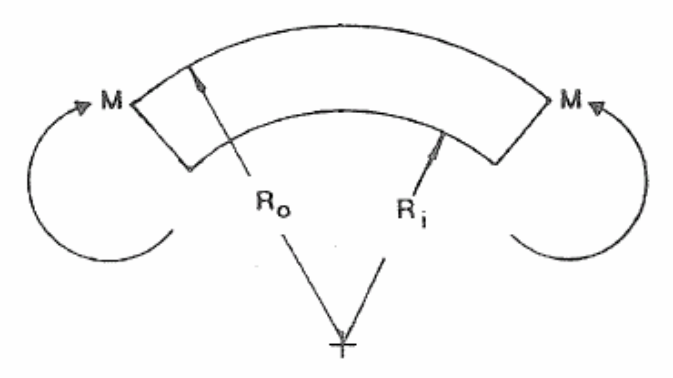

Figure 2.2. Pure bending loading.

2.1.2 Material of Composite Laminate

The material properties required to define the NASTRAN MAT9 card are shown in Table 2.2 below. Four MAT9 cards are used for the curved beam, one for 0^0-ply elements, one for 90^0-ply elements, one for the -45^0-ply elements, and one for the $+45^0$-ply elements.

Table 2.2. Required material properties for NASTRAN MAT 9 Card

Required Material Properties	
E_1	Material 1, Material 2, and Material 3 Directions Correspond to the Element Material Directions Defined in Figure 2.1 & 2.7.
E_2	
E_3	
v_{12}	
v_{23}	
v_{31}	
G_{12}	
G_{23}	
G_{31}	

The material used for a laminate composite is T300/977-2 graphite/epoxy. The lay-up of the laminate is chosen as symmetric and balanced laminate to eliminate the coupling effects of bending and shear in the flat laminate. The stacking sequence is $[-45/+45/90_2/0_2]_S$. The unidirectional orthotropic material properties for graphite/epoxy at 70^0F/ambient temperature are tabulated in Table 2.3.

Table 2.3. Material properties for Graphite/Epoxy at 70^0 F Ambient

Lamina Properties for Graphite/Epoxy at 70^0F/Ambient	
E_1 = 21.75 Msi	Material 1, Material 2, and Material 3 Directions Correspond to the Element Material Directions Defined in Figure 2.1 & 2.7.
E_2 = 1.595 Msi	
E_3 = 1.595 Msi	
ν_{12} = 0.25	
ν_{13} = 0.25	
ν_{23} = 0.45	
G_{12} = 0.8702 Msi	
G_{23} = 0.5366 Msi	
G_{13} = 0.8702 Msi	
t_{ply} = 0.0074 in	

The constants E_1, E_2 and E_3 are the nominal Young moduli of composite ply. The subscripts 1, 2, and 3 are fiber direction, transverse to the fiber direction, and out-of-plane direction, respectively. The constants G_{12}, G_{23} and G_{13} are the shear moduli with respect to 1-2, 2-3, and 1-3 planes, respectively. The constants ν_{12}, ν_{13} and ν_{23} are Poisson's ratios. Material property values for the NASTRAN MAT9 card per Table 2.2 requirement are derived from the graphite/epoxy lamina property values tabulated in Table 2.4.

Table 2.4. Material properties for Graphite/Epoxy at 70^0 F Ambient in NASTRAN MAT 9

Material Properties for NASTRAN MAT9 for Graphite/Epoxy at 70^0F/Ambient	
E_1 = 21.75 Msi	Material 1, Material 2, and Material 3 Directions Correspond to the Element Material Directions Defined in Figure 2.1 & 2.7.
E_2 = 1.595 Msi	
E_3 = 1.595 Msi	
ν_{12} = 0.25	
ν_{31} = 0.0183	
ν_{23} = 0.45	
G_{12} = 0.8702 Msi	
G_{23} = 0.5366 Msi	
G_{31} = 0.8702 Msi	
t_{ply} = 0.0074 in	

Where, $\upsilon_{31} = \upsilon_{13} \times \frac{E_3}{E_1} = 0.25 \times \frac{1.595}{21.75} = 0.0183$

2.2 Development of Finite Element Model

2.2.1 Modeling Creation

PATRAN has been used to develop the 3-D solid finite element model. PATRAN uses the Global Model Tolerance when it creates geometry. The default value is 0.005. When creating geometry, if two points are within a distance of the Global Model Tolerance, then PATRAN will only create the first point and not the second. This rule also applies to curves, surfaces, and solids. Due to the thickness of each ply in the curved beam model is 0.0074 inch (greater than the default value 0.005), the Global Model Tolerance is set at 0.0005 to improve the model usability. The procedure for generating 3-D Solid FEM for this study is shown below.

1. The 1^{ST} curved surface with inner radius Ri was created.
2. Then 11 more curved surfaces were created by using the “Normal to Surface” method. The distance between each surface is 0.0074 inches.
3. 12 solids were created from these 12 surfaces with the thickness of 0.0074 for each solid.

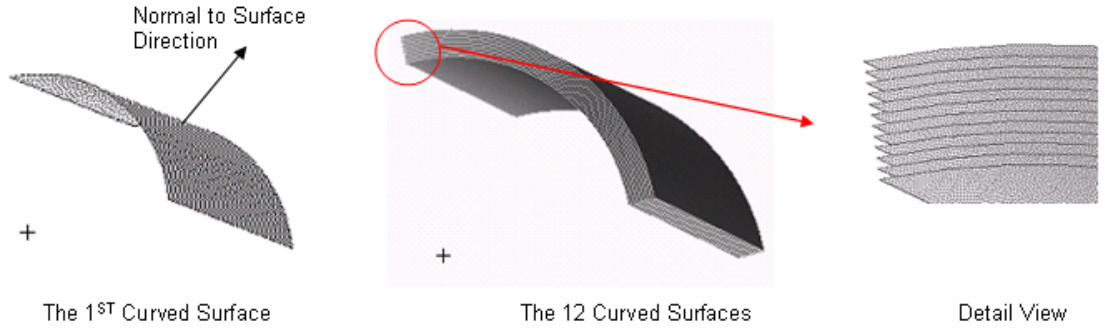

Figure 2.3. The creation of 12 surfaces.

2.2.2 Meshing Generation

At first, the mesh seeds are defined for each edge differently. By doing this, the edges of solid model will have a uniform element edge length specified by a total number of elements. The mesh seed will be represented by small circles in Figure 2.4 below.

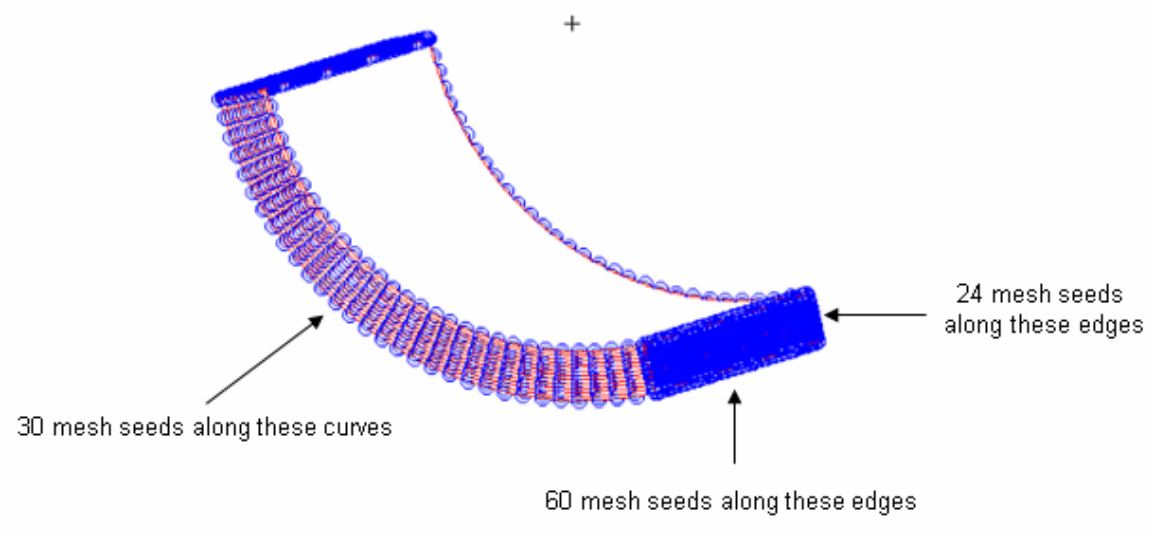

Figure 2.4. The defined mesh seeds of 3-D solid model.

The finite elements for this 3-D Solid Model were then created by using Isomesh method with Hex 8 topology (Hex element shape with 8 corner nodes).

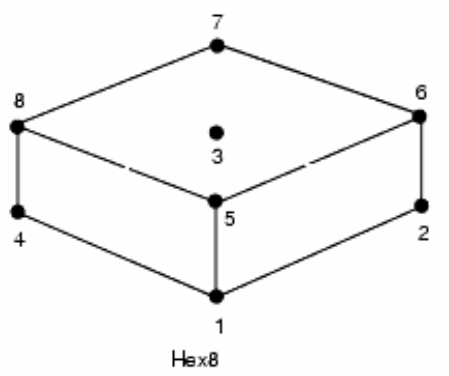

Figure 2.5. Hex 8 element.

This Isomesh created equally-spaced nodes along each edge in the model. A real value will be assigned to the element edge length for a given mesh. This value is known as *global element edge length*. This global element edge length was calculated automatically as 0.0264. This value can be adjusted in case of encounter difficulties.

The action of equivalence was applied for the entire model with equivalencing tolerance of 0.0005 to delete any duplicated nodes or extra nodes in the model. This 3-D Solid Model contains 43200 Hex 8 elements with the aspect ratio of 9.7 for all elements generated. The meshing is shown in Figure 2.6 below.

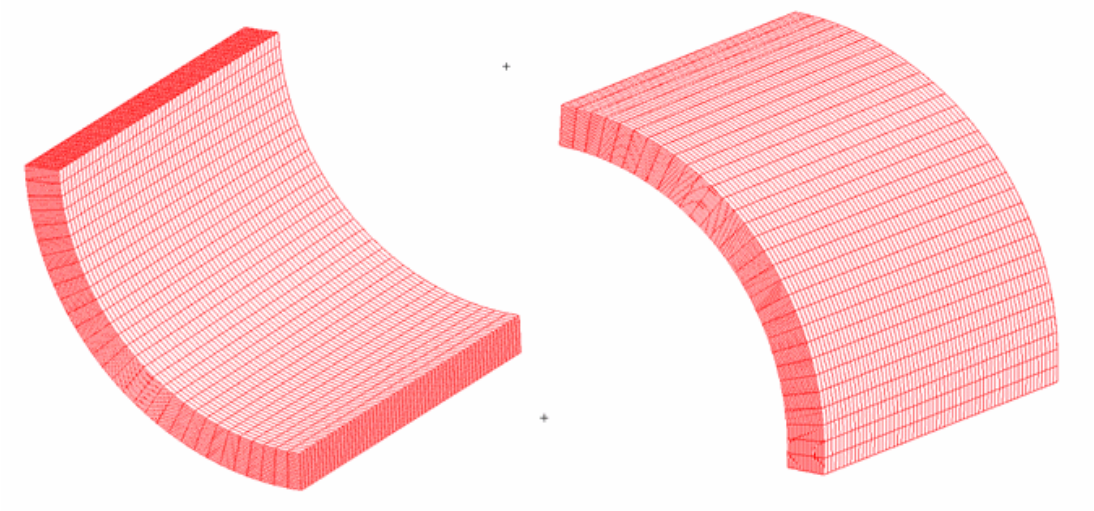

Figure 2.6. Isomesh of 3-D solid model.

2.2.3 Creation of Local Coordinate Systems

The composite curve beam is modeled by NASTRAN 3-D CHEXA Solid elements. The curved beam model contains 12 plies lay-up. Each ply is explicitly modeled by two rows of elements. The model was divided into 30 groups, as shown in Figure 2.7. By doing this, the curved beam is represented by several straight beam elements. Each group was assigned to different local coordinate systems, corresponding to the angle of fiber orientation of each layer of laminated composite. The material X-direction, Y-direction and Z-direction for the elements in the curved beam model were established to be the fiber direction (material direction 1), the transverse to the fiber direction (material direction 2) and the out-of plane direction (material direction 3), respectively. Four local coordinate systems were assigned to each element group. At first, a local coordinate was created for 0^0 ply. Then, this local coordinate was rotated at $-45^{0,}$ $+45^0$ and $90^{0.}$ This procedure created four different local coordinates which associate to four different angle of fiber orientation: 0^0, -45^0, $+45^0$ and 90^0. The creation of local coordinates for each element group is shown in Figure 2.8.

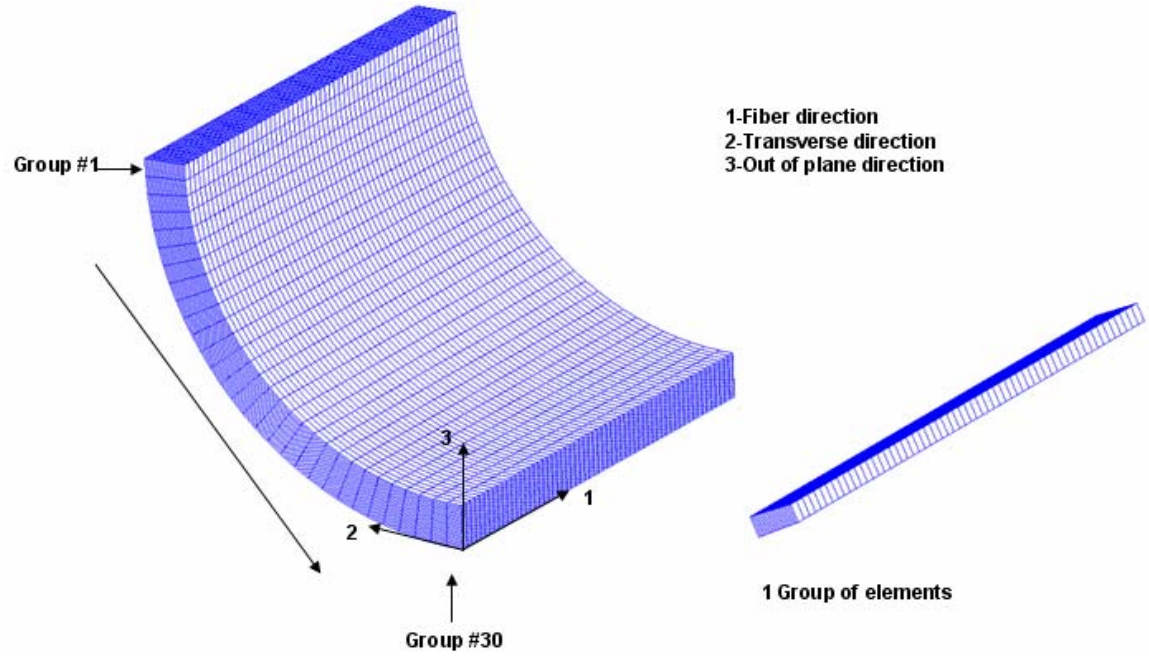

Figure 2.7. 30 Groups of elements along the transverse direction.

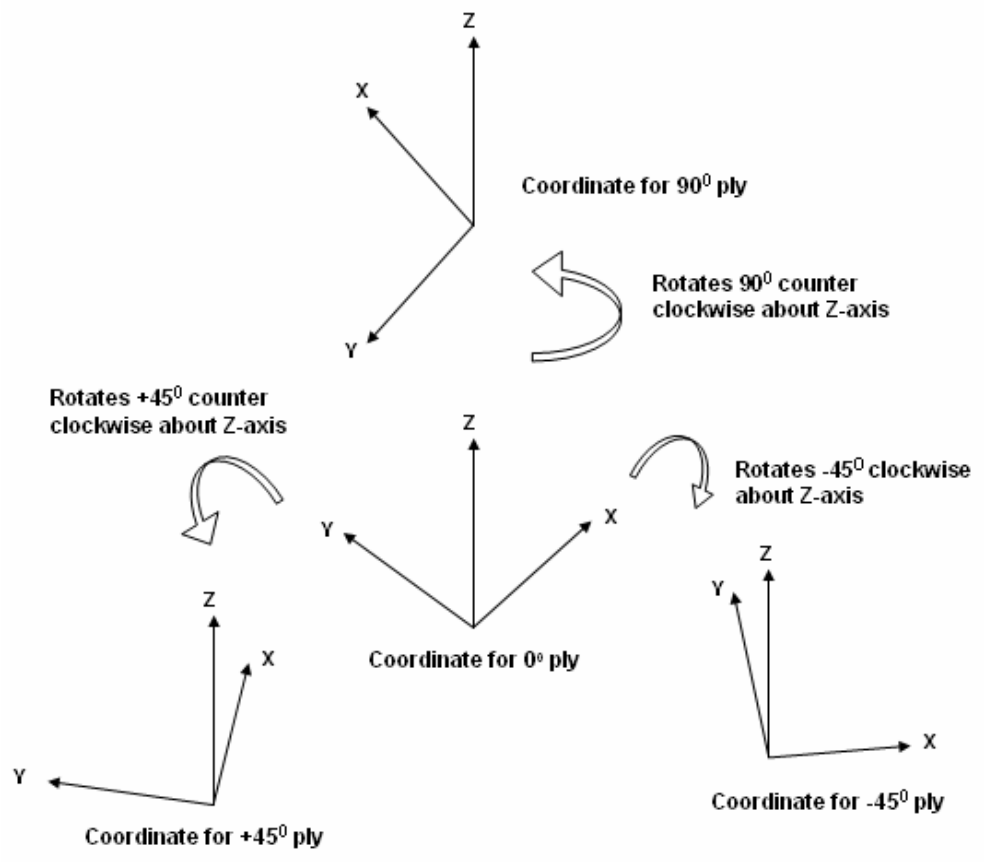

Figure 2.8. The creation of local coordinate for each ply.

2.2.4 Boundary and Loading Conditions

Two boundary conditions were enforced with respect to the global coordinate system

1. Because of the symmetry in geometry of the curved beam model, all nodes at one end were constrained. There were no translation and rotation for these nodes on x, y, and z-direction (Ux = Uy = Uz =0; Rx = Ry = Rz =0).
2. All nodes at another free end (dependent nodes) were constrained to a dummy node (independent node) on the same surface by using the Multi-Point Constraint method (MPC). The pure bending moment of Mz = -100 lbs-in (respect to global coordinate in Figure 2.9) was applied at the independent node. This moment tends to open the curved beam regions resulting in tensile radial stress (out-of –plane stress).

The boundary conditions are shown in Figure 2.9 below.

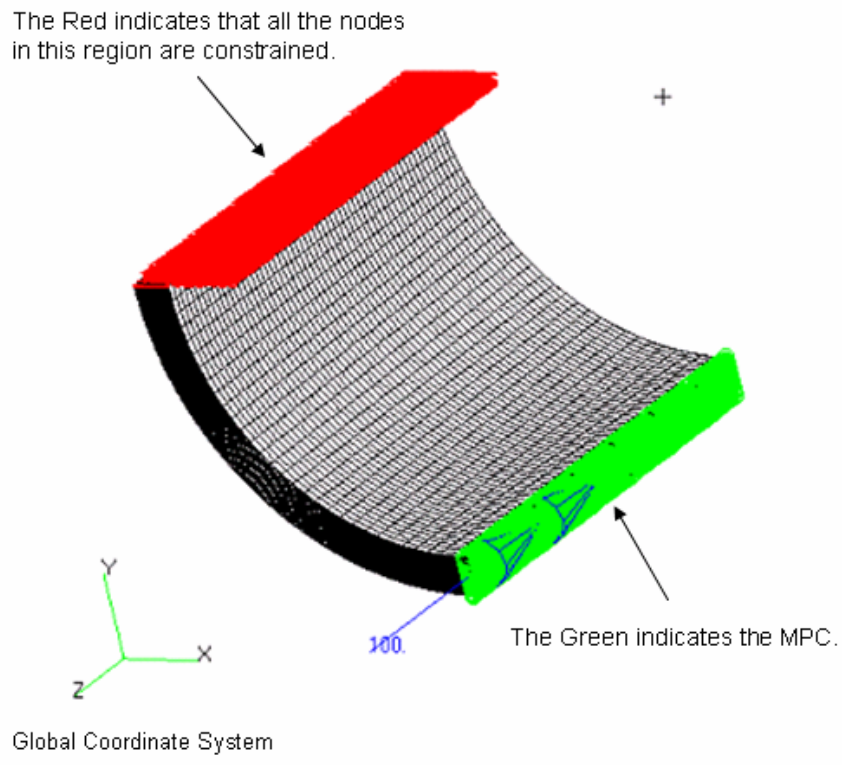

Figure 2.9. Two boundary conditions respect to global coordinate system.

2.3 Model Validation

The purpose of this section is to validate the curve beam FEM using the closed-form solution. The geometry, meshing, elements, boundary conditions, and loading conditions for this curve beam remained the same as defined in the sections above.

2.3.1 Isotropic Material

2.3.1.1 FEM Result

An isotropic material, Al-2014-T6, was used instead of T300/977-2 graphite/epoxy. Because of the uniformity in all directions, one cylindrical coordinate system was used for the entire model. The material properties for Al-2014-T6 are shown in Table 2.5.

Table 2.5. Material properties for Al-2014-T6 in NASTRAN MAT 1

Material Properties for NASTRAN MAT1 for Al-2014-T6	
E	10.6 Msi
ν	0.35
G	3.9 Msi

For the most accuracy in the results from FEM, a group of through thickness elements in the middle of the model was selected to eliminate the “edge effective”.

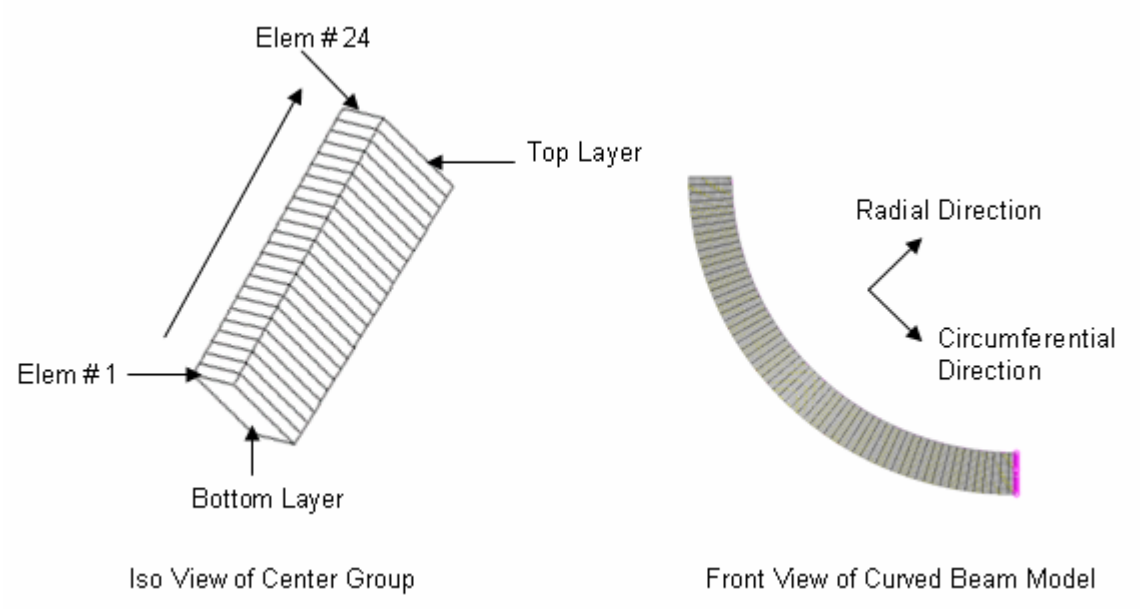

Figure 2.10. Center group and its radial and circumferential directions.

The radial stress and tangential (along circumferential direction) stress at the Centroid of each element in center group, as shown in Figure 2.10, were recorded from the output results in PATRAN. Table 2.6 summarizes these stresses respect to radial position (the distance from the center of curved beam, as shown in Figure 2.14, to the centroid of each element).

Table 2.6. The recorded stress values from FEM for isotropic material.

Layer #	Elem #	Radial Position r (inch)	Radial Stress σ_r (psi)	Tangential Stress σ_θ (psi)
1	1	0.60185	3.12E+02	8.08E+04
	2	0.60555	7.68E+02	7.33E+04
2	3	0.60925	1.18E+03	6.59E+04
	4	0.61295	1.53E+03	5.86E+04
3	5	0.61665	1.84E+03	5.14E+04
	6	0.62035	2.10E+03	4.43E+04
4	7	0.62405	2.31E+03	3.73E+04
	8	0.62775	2.48E+03	3.04E+04
5	9	0.63145	2.60E+03	2.35E+04
	10	0.63515	2.69E+03	1.67E+04
6	11	0.63885	2.73E+03	1.00E+04
	12	0.64255	2.73E+03	3.39E+03
7	13	0.64625	2.69E+03	-3.15E+03
	14	0.64995	2.62E+03	-9.63E+03
8	15	0.65365	2.51E+03	-1.60E+04
	16	0.65735	2.37E+03	-2.24E+04
9	17	0.66105	2.20E+03	-2.86E+04
	18	0.66475	1.99E+03	-3.48E+04
10	19	0.66845	1.75E+03	-4.09E+04
	20	0.67215	1.48E+03	-4.70E+04
11	21	0.67585	1.19E+03	-5.30E+04
	22	0.67955	8.64E+02	-5.89E+04
12	23	0.68325	5.21E+02	-6.48E+04
	24	0.68695	1.44E+02	-7.06E+04

2.3.1.2 Exact Solution

Consider a curved beam subjected to equal end couples moment M such that bending takes place in the plane of curvature, as shown in Figure 2.11. This beam is characterized by a constant rectangular cross section and a circular axis. The axis of symmetry of the cross section lies in a single plane throughout the length of the member [9]. The dimensions of this curved beam are shown in Table 2.7 below.

Table 2.7. Dimensions of curved beam model

Dimensions of Curved Beam Model	
Inner radius, a = Ri	0.6 in
Outer radius, b = Ro	0.6888 in
Width, w	1 in
Height, h	0.0888 in

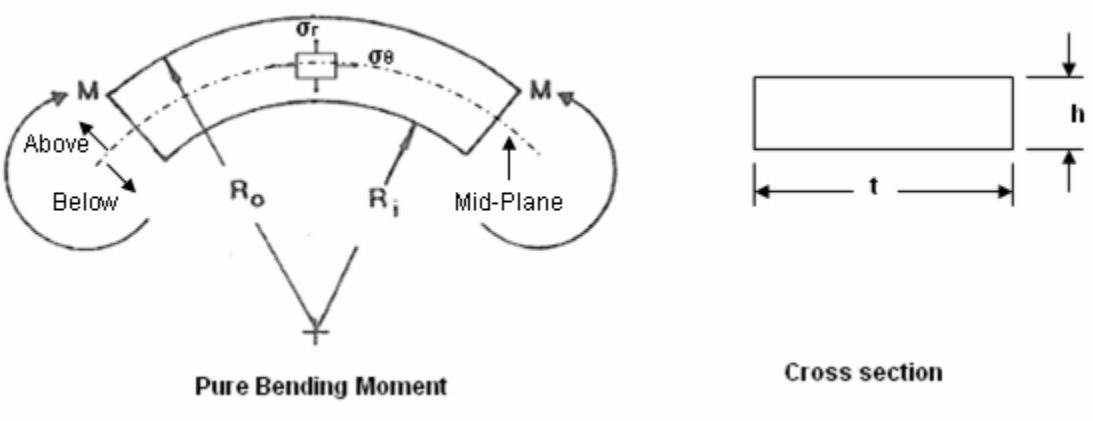

Figure 2.11. Curved beam subjected to bending moment and its cross section.

The radial and tangential stresses were calculated by following equations:

$$\sigma_r = \frac{4M}{tb^2N}\cdot\left[\left(1-\frac{a^2}{b^2}\right)\cdot\left(\ln\frac{r}{a}\right)-\left(1-\frac{a^2}{r^2}\right)\cdot\left(\ln\frac{b}{a}\right)\right]$$

$$\sigma_\theta = \frac{4M}{tb^2N}\cdot\left[\left(1-\frac{a^2}{b^2}\right)\cdot\left(1+\ln\frac{r}{a}\right)-\left(1+\frac{a^2}{r^2}\right)\cdot\left(\ln\frac{b}{a}\right)\right] \qquad \text{(Section 5.13, [9])}$$

Where, $N = \left(1-\frac{a^2}{b^2}\right)^2 - 4\frac{a^2}{b^2}\ln^2\left(\frac{b}{a}\right)$,

$M = 100\ lbs-in$, and $R_i < r < R_o$; ($a = R_i$; $b = R_o$)

These equations are applicable throughout the curved beam. The radial stresses σ_r as determined from the equation above are found positive (tensile). The tangential stresses σ_θ are found positive (tensile) for the elements below the mid-plane, and negative (compressive) for the elements above the mid-plane, as shown in Figure 2.11. Table 2.8 summarizes the calculated radial stresses σ_r and tangential stresses σ_θ with respect to 24 different radial positions.

Table 2.8. The calculated stress values from exact solution.

Layer #	Elem #	Radial Position r (inch)	Radial Stress σ_r (psi)	Tangential Stress σ_θ (psi)
1	1	0.60185	2.40E+02	7.61E+04
	2	0.60555	6.81E+02	6.89E+04
2	3	0.60925	1.07E+03	6.18E+04
	4	0.61295	1.42E+03	5.47E+04
3	5	0.61665	1.72E+03	4.78E+04
	6	0.62035	1.97E+03	4.09E+04
4	7	0.62405	2.18E+03	3.42E+04
	8	0.62775	2.35E+03	2.74E+04
5	9	0.63145	2.48E+03	2.08E+04
	10	0.63515	2.57E+03	1.43E+04
6	11	0.63885	2.62E+03	7.82E+03
	12	0.64255	2.63E+03	1.42E+03
7	13	0.64625	2.60E+03	-4.90E+03
	14	0.64995	2.54E+03	-1.11E+04
8	15	0.65365	2.45E+03	-1.73E+04
	16	0.65735	2.32E+03	-2.34E+04
9	17	0.66105	2.16E+03	-2.95E+04
	18	0.66475	1.97E+03	-3.54E+04
10	19	0.66845	1.74E+03	-4.14E+04
	20	0.67215	1.49E+03	-4.72E+04
11	21	0.67585	1.21E+03	-5.30E+04
	22	0.67955	8.95E+02	-5.87E+04
12	23	0.68325	5.57E+02	-6.44E+04
	24	0.68695	1.92E+02	-7.00E+04

The radial stresses and tangential stresses in Table 2.6 and Table 2.8 were plotted in two different graphs with respect to the variation of radial positions for comparison purposes. The graphs in Figure 2.12, and Figure 2.13, as shown on the next page, show a good agreement between FEM results for isotropic material and Exact solutions. Since these results compared well, the isotropic curved beam model is validated.

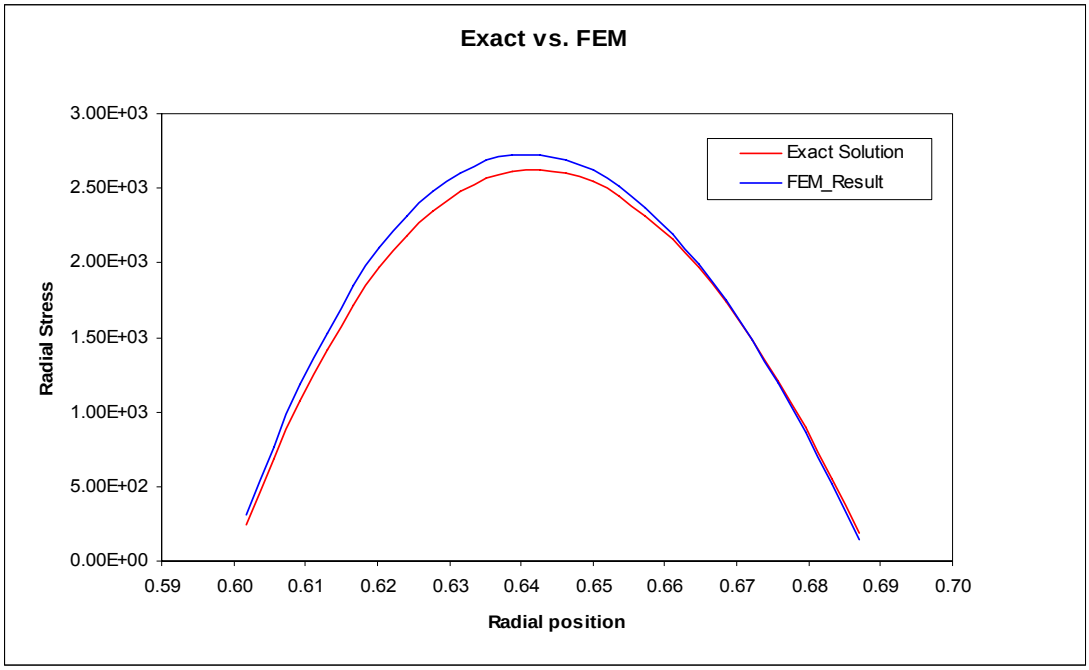

Figure 2.12. Radial stress comparison between isotropic FEM and exact solution.

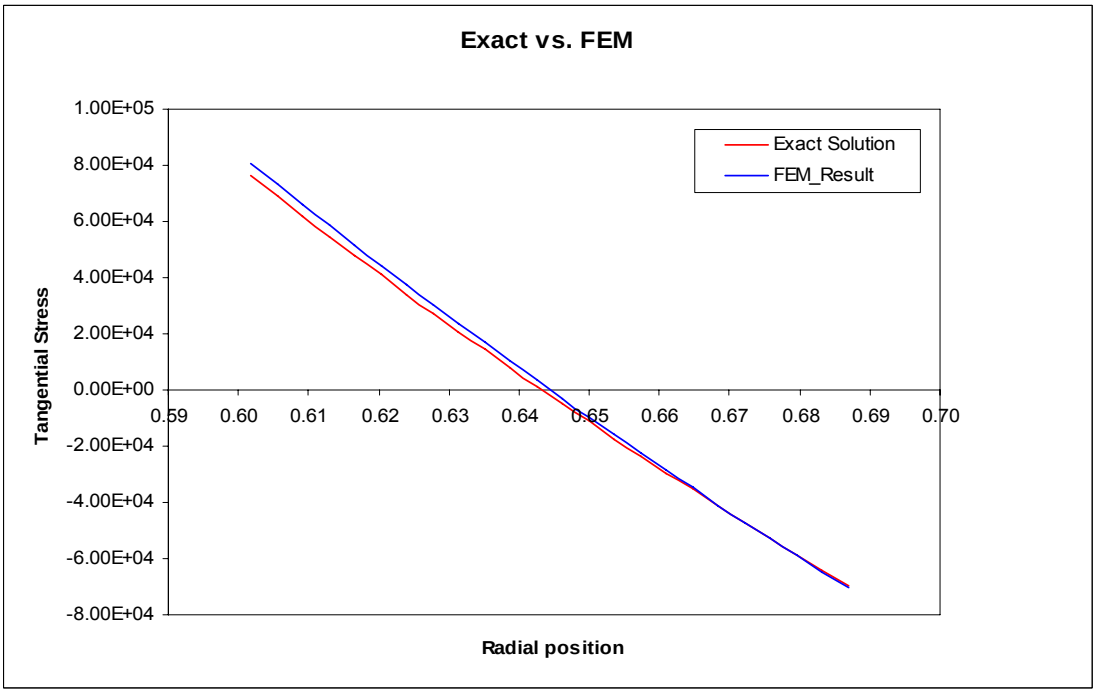

Figure 2.13. Tangential stress comparison between isotropic FEM and exact solution.

2.3.2 Orthotropic Material

An orthotropic material, T300/977-2 graphite/epoxy, was used. The required material properties for NASTRAN MAT9 Card are shown in Table 2.4. All 0^0 plies lay-up was applied for this curved beam model. The material properties of T300/977-2 graphite/epoxy for 0^0-ply elements were assigned to a different element group associated with a different local coordinate system. There were thirty element groups associated with thirty local coordinate systems.

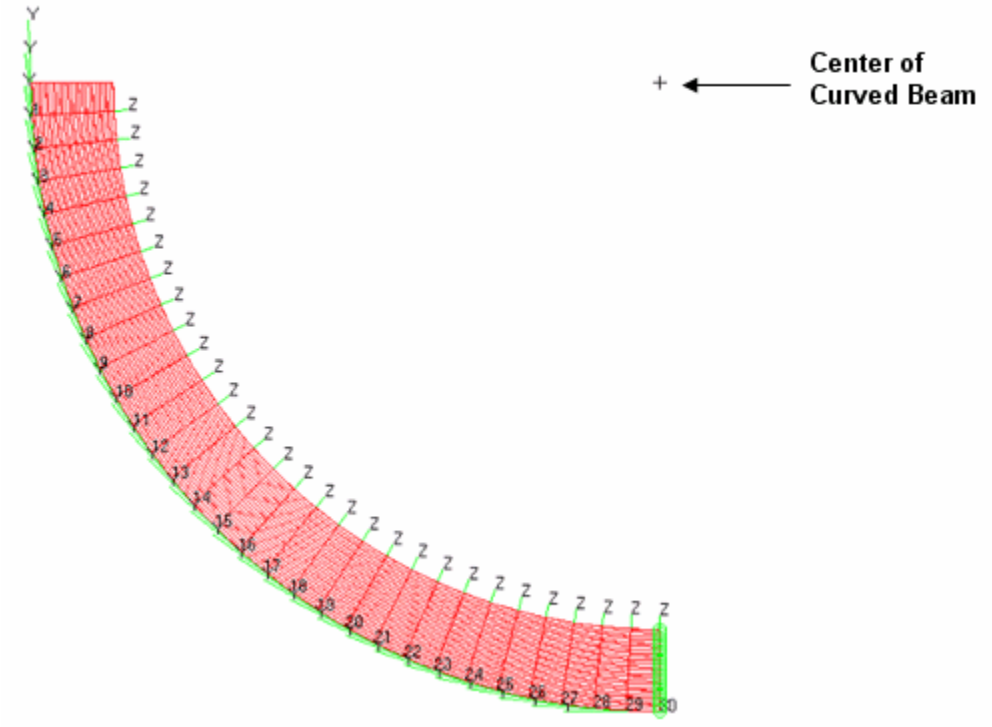

Figure 2.14. Local coordinate system for each element group.

The material X-direction (perpendicular to the Y-Z plane), Y-direction, and Z-direction were established to be the fiber direction, the transverse to fiber direction and the out-of plane direction, respectively. The behavior of the curved beam with the orthotropic material contains all 0^0 plies lay-up similar to the curved beam with the isotropic material. The recorded radial and tangential stress values, as shown in Table 2.9, were compared to the results from the isotropic material and exact solution in Section 2.3.1.

Table 2.9. The recorded stress values from FEM for orthotropic material

Layer #	Elem #	Radial Position r (inch)	Radial Stress σ_r (psi)	Tangential Stress σ_θ (psi)
1	1	0.60185	2.97E+02	7.70E+04
	2	0.60555	7.31E+02	6.98E+04
2	3	0.60925	1.13E+03	6.27E+04
	4	0.61295	1.47E+03	5.57E+04
3	5	0.61665	1.76E+03	4.87E+04
	6	0.62035	2.01E+03	4.19E+04
4	7	0.62405	2.22E+03	3.51E+04
	8	0.62775	2.38E+03	2.84E+04
5	9	0.63145	2.50E+03	2.18E+04
	10	0.63515	2.58E+03	1.52E+04
6	11	0.63885	2.62E+03	8.77E+03
	12	0.64255	2.63E+03	2.38E+03
7	13	0.64625	2.59E+03	-3.93E+03
	14	0.64995	2.53E+03	-1.02E+04
8	15	0.65365	2.43E+03	-1.63E+04
	16	0.65735	2.29E+03	-2.24E+04
9	17	0.66105	2.13E+03	-2.85E+04
	18	0.66475	1.93E+03	-3.44E+04
10	19	0.66845	1.70E+03	-4.04E+04
	20	0.67215	1.44E+03	-4.62E+04
11	21	0.67585	1.16E+03	-5.20E+04
	22	0.67955	8.42E+02	-5.77E+04
12	23	0.68325	5.07E+02	-6.33E+04
	24	0.68695	1.43E+02	-6.89E+04

The stress data from Table 2.6, Table 2.8, and Table 2.9 are combined together to generate two separate plots for comparison: one for the radial stress, and one for the tangential stress, as shown in the Figure 2.15 and Figure 2.16 on the next page. The values of radial and tangential stresses for orthotropic material with all 0^0 lay-up are comparable to the isotropic material solution and exact solution. This is the good evidence to confirm about the validation of the composite curved beam model.

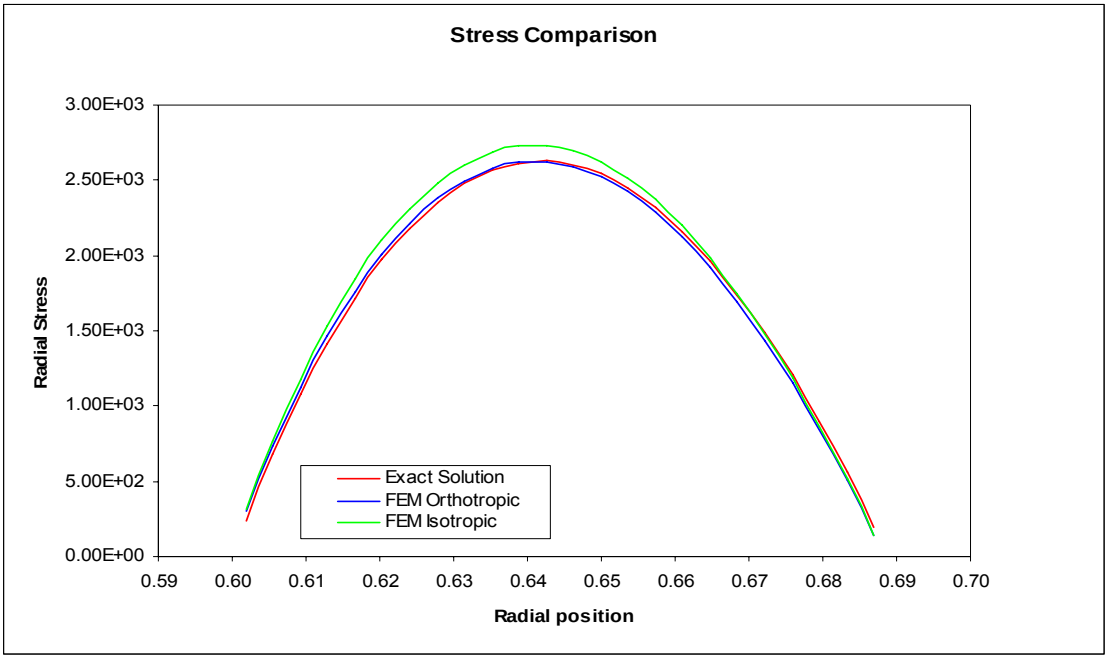

Figure 2.15. Radial stress comparison for isotropic, orthotropic and exact solution.

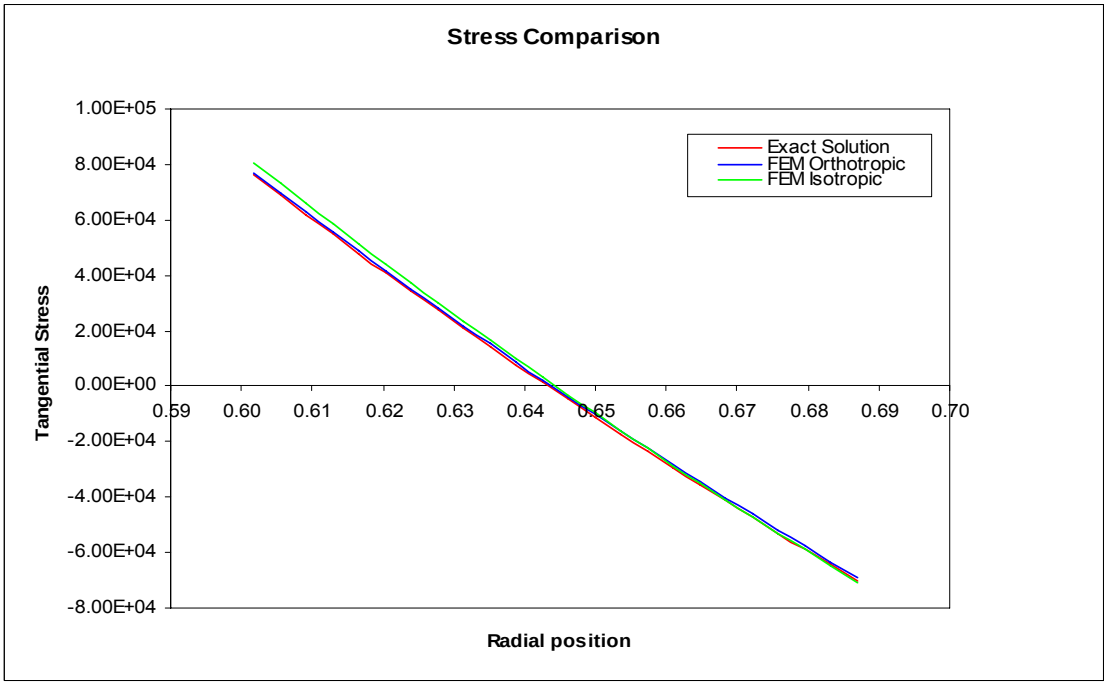

Figure 2.16. Tangential stress comparison for isotropic, orthotropic and exact solution.

2.4 Convergence

The convergence study was conducted for an isotropic semicircular curved beam, Model I (mid-plane curvature R_1 = 0.2444 inches). The geometry dimensions of this Model I are shown in Table 2.1. The isotropic material, Al-2014-T6, was used. Due to the uniformity in all direction of isotropic material, one cylindrical coordinate system was used for the entire model. The meshing, boundary conditions, and loading conditions remained the same as defined in Section 2.2. This curved beam model contains 12 plies. Each ply is explicitly modeled by one row of element. The mesh of this analyzed curved beam model was refined six times. The number of elements was recorded as: 5400, 7200, 9000, 10800, 12600, and 14400 elements. The tangential (in-plane) stress and radial (out-of-plane) stress of twelve different elements from selected center group (through thickness) in this curved beam model were examined. The values of these stresses were recorded and plotted for convergence examination.

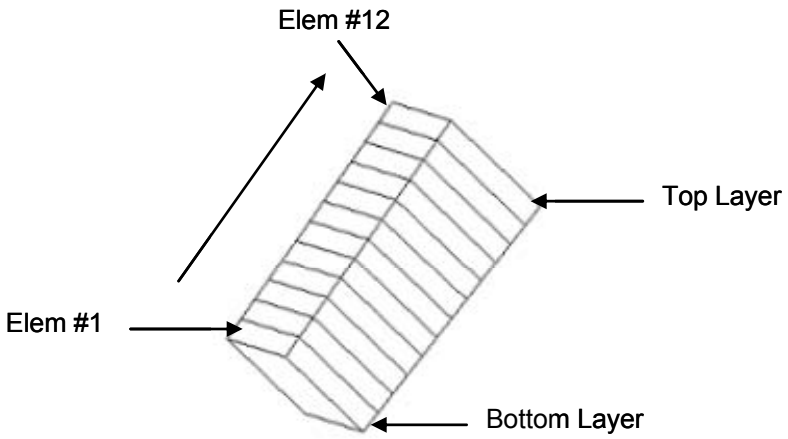

Figure 2.17. Selected center group.

Figure 2.18 and Figure 2.19 on the next page show that stresses approach to a constant with the increasing number of elements in the model. These figures highlight that the tangential and radial stresses for isotropic curved beam converged.

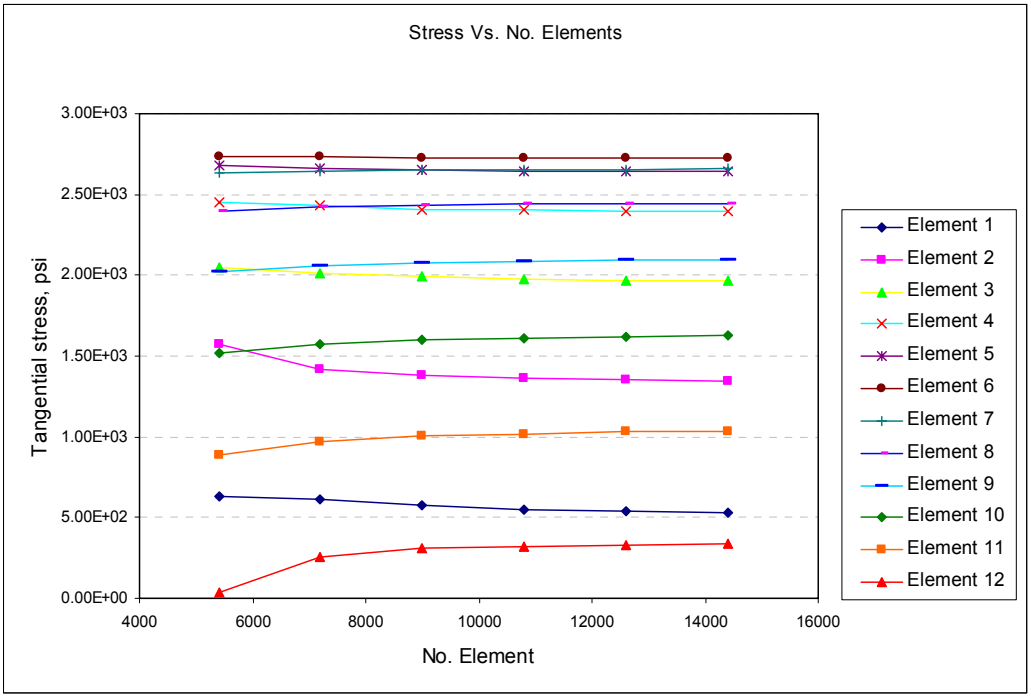

Figure 2.18. The convergence of tangential stress.

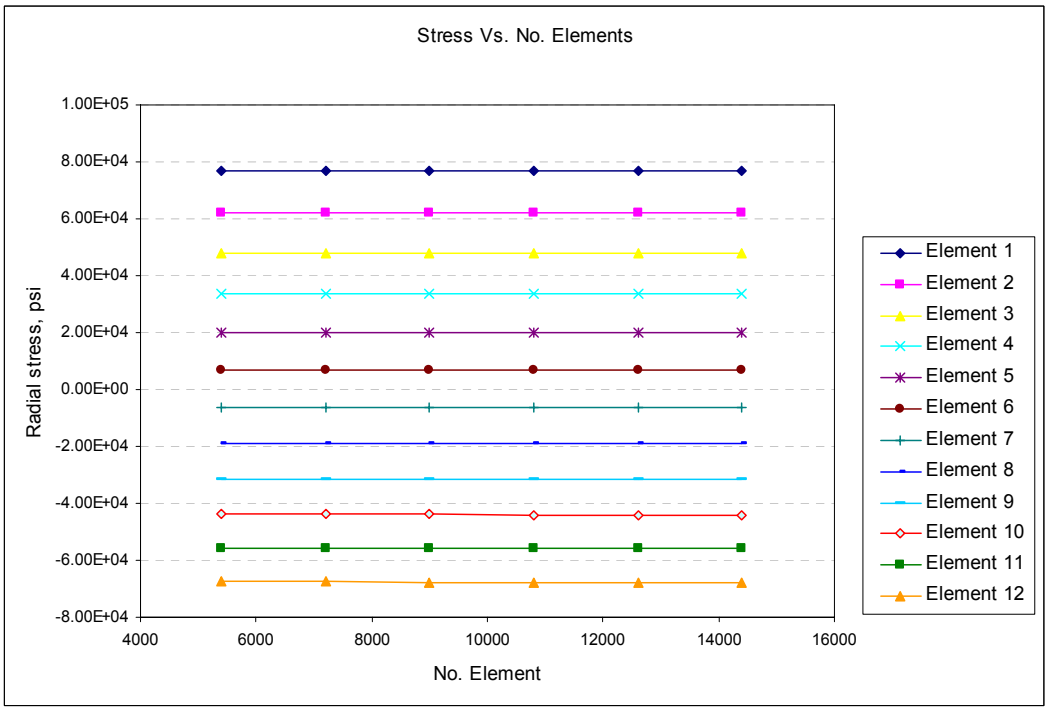

Figure 2.19. The convergence of radial stress.

CHAPTER 3

ANALYTICAL METHOD FOR CURVED LAMINATED BEAM

This Chapter will cover the development of equations used to calculate the tangential ply stress σ_θ in the curved laminated beam under bending based upon the Classical Lamination Theory (CLT). A brief description of the Lamination Theory is depicted below. The detail of derivation can be found in Ref. [10]. The constitutive equation for a narrow laminated beam is also included.

3.1 Review of Lamination Theory

The overall behavior of a multidirectional laminate is a function of the properties and stacking sequence of the individual layers. Classical Lamination Theory (CLT) is the most commonly used to analyze the behavior of laminated plate. It is also used to evaluate strains and stresses of plies in the laminate. CLT is based on the following assumption to analyze the behavior of laminate:

1. Each layer (lamina) of the laminate is quasi-homogeneous and orthotropic.
2. The laminate is thin with its lateral dimensions much larger than its thickness. Hence, the laminate and its layers are in a state of plane stress.
3. All displacements are small compared with the thickness of the laminate.

A laminate contains multiple layers. Each layer has its preferred fiber orientation. Hence, it is convenient to use one coordinate system to represent the fiber direction of a layer and another coordinate system common to all the layers for the laminates. These coordinate systems are described in Figure 3.1.

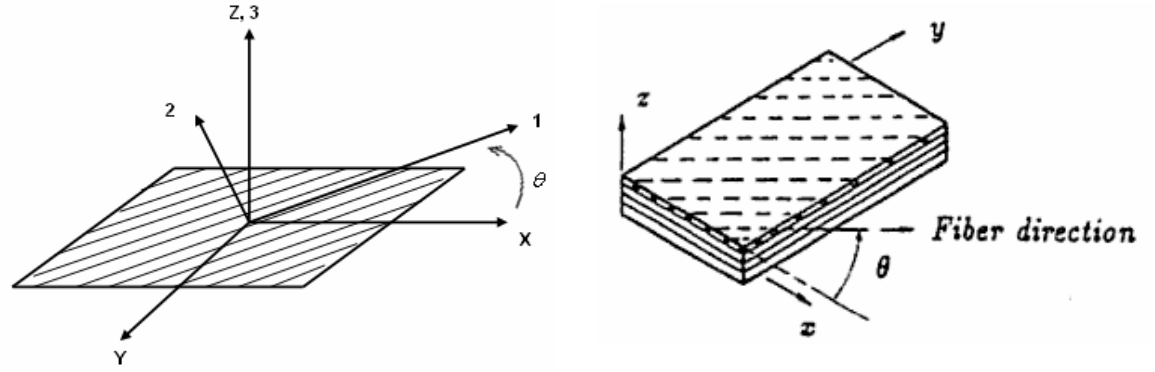

Figure 3.1. Coordinate systems of lamina and laminate.

3.1.1. Elastic Stress-Strain Relationship of Lamina

A 0^0 lamina is treated as an orthotropic thin layer material which requires four independent material constants sufficiently to specify their elastic structural response. These constants refer to E_1 and E_2 being the Young's moduli of lamina along and transverse to the fiber direction, respectively, v_{12}, the Poisson's ratio and G_{12}, the shear modulus of lamina under a loading along the fiber direction. Since the composite layer is very thin, the plane stress condition is considered. The generalized Hook's law gives the stress-strain relationship of 0^0 lamina and the matrix [Q] in terms of engineering constants is given as:

$$Q_{11} = \frac{E_1}{1-\nu_{12}\nu_{21}} \quad Q_{22} = \frac{E_2}{1-\nu_{12}\nu_{21}} \quad Q_{12} = \frac{\nu_{12}E_2}{1-\nu_{12}\nu_{21}} = \frac{\nu_{21}E_1}{1-\nu_{12}\nu_{21}}$$
$$Q_{66} = G_{12} \qquad Q_{16} = Q_{26} = 0 \tag{3-1}$$

For a lamina at angle θ with respect to the reference axes x and y, the stress/strain relation in the x-and y-coordinates is given as:

$$\begin{bmatrix} \sigma_x \\ \sigma_y \\ \tau_{xy} \end{bmatrix} = \begin{bmatrix} \overline{Q}_{11} & \overline{Q}_{12} & \overline{Q}_{16} \\ \overline{Q}_{12} & \overline{Q}_{22} & \overline{Q}_{26} \\ \overline{Q}_{16} & \overline{Q}_{26} & \overline{Q}_{66} \end{bmatrix} \cdot \begin{bmatrix} \varepsilon_x \\ \varepsilon_y \\ \gamma_{xy} \end{bmatrix} \tag{3-2}$$

where $\left[\overline{Q}_{x-y}\right]$ matrix (Q-bar matrix) is obtained by transforming $[Q_{1\text{-}2}]$ matrix of lamina from 1-2 material coordinates to the laminate x-y coordinates. Mathematically, it can be expressed as:

$$\left[\overline{Q}_{x-y}\right]=\left[T_{\sigma}(-\theta)\right]\cdot\left[Q_{1-2}\right]\cdot\left[T_{\varepsilon}(\theta)\right] \quad (3\text{-}3)$$

$[T_{\sigma}(+\theta)]$ and $[T_{\varepsilon}(+\theta)]$ are the transformation matrices that relate the stress and strain components in x-y coordinates to the 1-2 coordinates, respectively. They are defined as where m=cosθ, n= sinθ and θ is the fiber orientation of the lamina [11].

$$\left[T_{\sigma}(\theta)\right]=\begin{bmatrix} m^2 & n^2 & 2mn \\ n^2 & m^2 & -2mn \\ -mn & mn & \left(m^2-n^2\right) \end{bmatrix} \text{ and } \left[T_{\varepsilon}(\theta)\right]=\begin{bmatrix} m^2 & n^2 & mn \\ n^2 & m^2 & -mn \\ 2mn & -2mn & \left(m^2-n^2\right) \end{bmatrix} \quad (3\text{-}4)$$

Substituting equations 3.4 and 3.1 into 3.3, the components of the Q-bar matrix can be explicitly expressed as:

$$\begin{aligned}
\overline{Q}_{11} &= m^4Q_{11}+n^4Q_{22}+2m^2n^2\left(Q_{12}+2Q_{66}\right)\\
\overline{Q}_{12} &= m^2n^2\left(Q_{11}+Q_{22}-4Q_{66}\right)+\left(m^4+n^4\right)Q_{12}\\
\overline{Q}_{22} &= n^4Q_{11}+m^4Q_{22}+2m^2n^2\left(Q_{12}+2Q_{66}\right)\\
\overline{Q}_{16} &= m^3n(Q_{11}-Q_{12}-2Q_{66})-mn^3(Q_{22}-Q_{12}-2Q_{66})\\
\overline{Q}_{26} &= mn^3(Q_{11}-Q_{12}-2Q_{66})-m^3n(Q_{22}-Q_{12}-2Q_{66})\\
\overline{Q}_{66} &= m^2n^2(Q_{11}+Q_{22}-2Q_{12}-2Q_{66})+(m^4+n^4)\ Q_{66}
\end{aligned} \quad (3\text{-}5)$$

Strains at any point in the k^{th} ply of a laminate can be calculated using the following relationship:

$$\begin{bmatrix} \varepsilon_x \\ \varepsilon_y \\ \gamma_{xy} \end{bmatrix}_k = \begin{bmatrix} \varepsilon_x^0 \\ \varepsilon_y^0 \\ \gamma_{xy}^0 \end{bmatrix} + z_k \cdot \begin{bmatrix} k_x \\ k_y \\ k_{xy} \end{bmatrix} \quad (3\text{-}6)$$

where ε_x^0, ε_y^0 and γ_{xy}^0 are the mid-plane strains, and κ_x, κ_y and κ_{xy} are the mid-plane curvatures. z_k is the z- coordinate of the interested point within the k^{th} layer measured from the mid-plane to the lamina and ε_x, ε_y and γ_{xy} are the strains in the k^{th} ply.

3.1.2. Constitutive Equation of Laminate (Lamination Theory)

The structural response of a laminate is represented by the strains and curvatures about its mid-plane. The total in-plane forces $[N]$ and moments $[M]$ per unit width of the laminated plate are obtained by integrating forces of each ply through the laminate thickness as shown in Figure 3.2. Mathematically, they are expressed as:

$$\begin{bmatrix} N_x \\ N_y \\ N_{xy} \end{bmatrix} = \sum_{k=1}^{n} \int_{z_{k-1}}^{z_k} \begin{bmatrix} \sigma_x \\ \sigma_y \\ \tau_{xy} \end{bmatrix}_k dz \quad \text{and} \quad \begin{bmatrix} M_x \\ M_y \\ M_{xy} \end{bmatrix} = \sum_{k=1}^{n} \int_{z_{k-1}}^{z_k} \begin{bmatrix} \sigma_x \\ \sigma_y \\ \tau_{xy} \end{bmatrix}_k \cdot z dz \qquad (3\text{-}7)$$

where $z_{k-1}$and z_k are the distances from the reference plane (often chosen at the mid-plane of the laminate, as shown in Figure 3.3) to the k^{th}-layer's lower and upper surfaces, respectively.

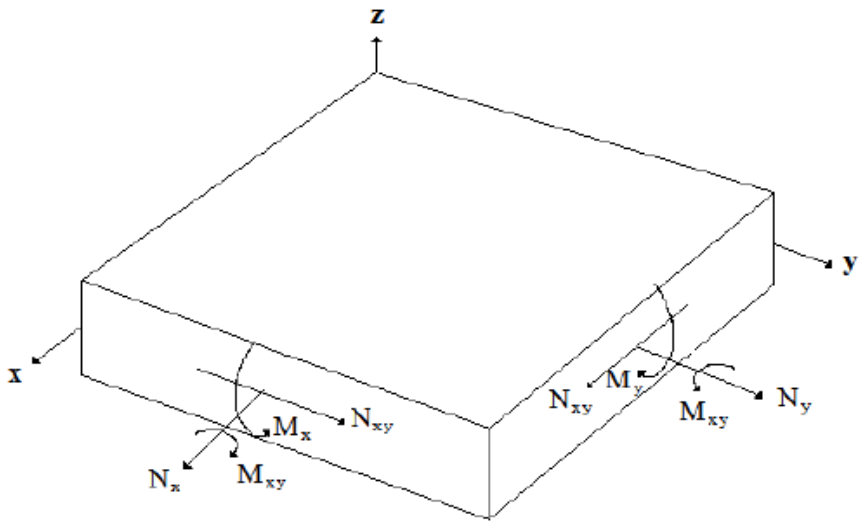

Figure 3.2. Element of single layer with force and moment resultants.

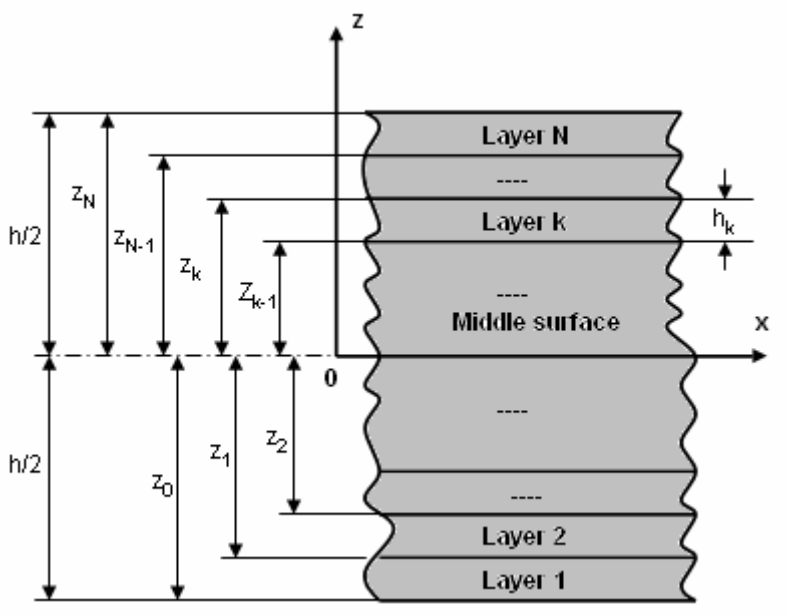

Figure 3.3. Laminate plate geometry and layer numbering system.

Substituting Equations 3.2, 3.6 into 3.7, the general load-deformation relation of laminate can be written in terms of the mid-plane strain and curvature as shown below:

$$\begin{bmatrix} N \\ M \end{bmatrix} = \begin{bmatrix} A & B \\ B & D \end{bmatrix} \cdot \begin{bmatrix} \varepsilon^0 \\ \kappa \end{bmatrix} \tag{3-8}$$

The [A], [B] and [D] matrices are given as

$$\begin{aligned} [A] &= \sum_{k=1}^{n} [\overline{Q}_{x-y}]_k (z_k - z_{k-1}) \\ [B] &= \frac{1}{2} \sum_{k=1}^{n} [\overline{Q}_{x-y}]_k (z_k^2 - z_{k-1}^2) \\ [D] &= \frac{1}{3} \sum_{k=1}^{n} [\overline{Q}_{x-y}]_k (z_k^3 - z_{k-1}^3) \end{aligned} \tag{3-9}$$

where z_{k-1} and z_k are the z-coordinates of the bottom and upper surfaces of the k^{th} layer, respectively. The matrix $\left[\overline{Q}_{x-y}\right]_k$ is the stiffness matrix of k^{th} layer.

The [A] matrix is called in-plane extensional stiffness matrix because it directly relates the in-plane strains ($\varepsilon_x^0, \varepsilon_y^0, \gamma_{xy}^0$) to the in-plane forces per unit width (N_x, N_y, N_{xy}). The [B] matrix is called extensional-bending coupling stiffness matrix. This matrix relates the in-plane strains to the bending moments and curvatures to in-plane forces. The [D] matrix is the bending stiffness matrix because it relates the curvatures (K_x, K_y, K_{xy}) to the bending moments per unit width (M_x, M_y, M_{xy}).

3.2 Curved Laminated Beam

Beams are the primary structural members that carry bending loads. Beams are slender and are considered as one-dimensional members. Consider a curved beam as shown.

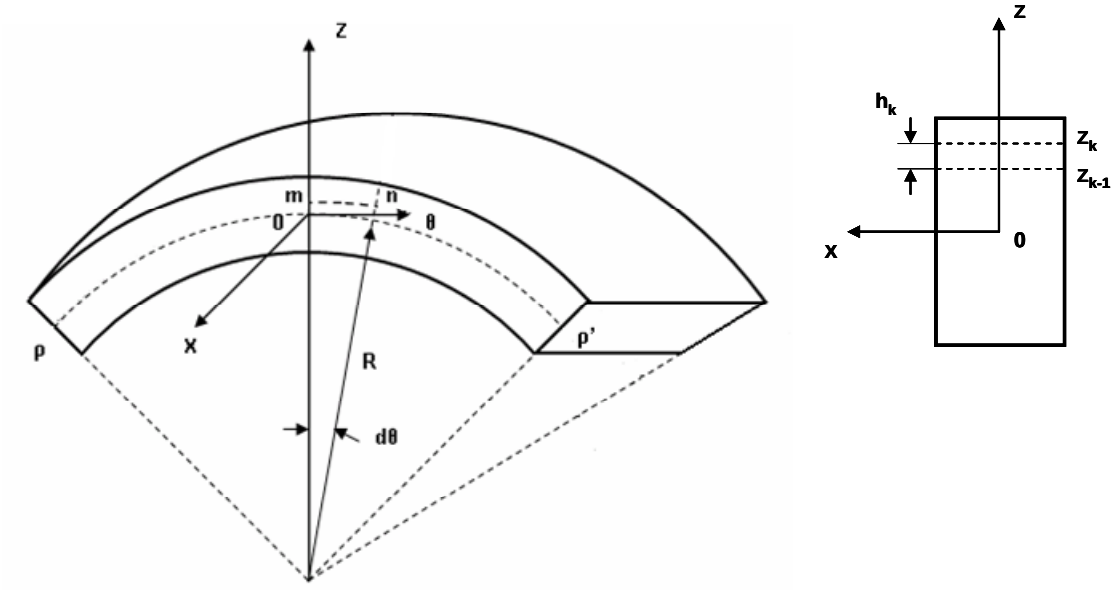

Figure 3.4. The configurations of curved beam and its cross section.

Let $\rho\rho'$ be the mid-axis of the beam. The differential element at the k[th] layer from the mid-axis is $\overline{mn}$. Then, the elongation after deformation can be written as:

$$(R+z)d\theta \cdot \varepsilon_\theta \tag{3-10}$$

This elongation can be also described in terms of the mid-plane strain ε_0 and their curvature κ.

$$R \cdot d\theta(\varepsilon_0 + z \cdot \kappa) \tag{3-11}$$

Combining 3-10 and 3-11, we have:

$$\varepsilon_\theta = \frac{R}{R+z}(\varepsilon_0 + z \cdot \kappa) \tag{3-12}$$

For simplicity, the stress σ_θ at the k[th] layer can be approximated by:

$$\sigma_{\theta,k} = \overline{Q}_{\theta\theta,k}\, \varepsilon_{\theta,k} \tag{3-13}$$

The resultant force and moment per unit width, N_θ and M_θ are obtained as:

$$N_\theta = \sum_{k=1}^{n} \int_{h_{k-1}}^{h_k} \sigma_{\theta,k} dz = \sum_{k=1}^{n} \int_{h_{k-1}}^{h_k} \overline{Q}_{\theta\theta,k} \frac{R}{R+z}(\varepsilon_0 + z \cdot k) dz$$

$$= A_{\theta\theta}\varepsilon_0 + B_{\theta\theta}k_\theta \tag{3-14}$$

$$M_\theta = \sum_{k=1}^{n} \int_{h_{k-1}}^{h_k} \sigma_{\theta,k} z \cdot dz = B_{\theta\theta}\varepsilon_0 + D_{\theta\theta}k_\theta \tag{3-15}$$

where,

$$A_{\theta\theta} = \sum_{k=1}^{n} \overline{Q}_{\theta\theta,k} \int_{z_{k-1}}^{z_k} \frac{R \cdot dz}{R+z}$$

$$B_{\theta\theta} = \sum_{k=1}^{n} \overline{Q}_{\theta\theta,k} \int_{z_{k-1}}^{z_k} \frac{R \cdot z dz}{R+z}$$

$$D_{\theta\theta} = \sum_{k=1}^{n} \overline{Q}_{\theta\theta,k} \int_{z_{k-1}}^{z_k} \frac{R \cdot z^2 dz}{R+z}$$

Explicitly,

$$A_{\theta\theta} = R\sum_{k=1}^{n} \overline{Q}_{\theta\theta,k} \ln \frac{R+z_k}{R+z_{k-1}} \tag{3-16}$$

$$B_{\theta\theta} = R\sum_{k=1}^{n} \overline{Q}_{\theta\theta,k}\left[\left(z_k - z_{k-1}\right) - R\cdot\ln\frac{R+z_k}{R+z_{k-1}}\right] \tag{3-17}$$

$$D_{\theta\theta} = R\sum_{k=1}^{n} \overline{Q}_{\theta\theta,k}\left[\frac{1}{2}\left(z_k^2 - z_{k-1}^2\right) - R\left(z_k - z_{k-1}\right) + R^2\ln\left(\frac{R+z_k}{R+z_{k-1}}\right)\right] \tag{3-18}$$

Combining Equations 3-14 and 3-15, we have:

$$\begin{bmatrix} N_{\theta\theta} \\ M_{\theta\theta} \end{bmatrix} = \begin{bmatrix} A_{\theta\theta} & B_{\theta\theta} \\ B_{\theta\theta} & D_{\theta\theta} \end{bmatrix}\begin{bmatrix} \varepsilon_0 \\ \kappa_\theta \end{bmatrix} \quad \text{or} \quad \begin{bmatrix} \varepsilon_0 \\ \kappa_\theta \end{bmatrix} = \begin{bmatrix} A_{\theta\theta} & B_{\theta\theta} \\ B_{\theta\theta} & D_{\theta\theta} \end{bmatrix}^{-1}\cdot\begin{bmatrix} N_{\theta\theta} \\ M_{\theta\theta} \end{bmatrix} \tag{3-19}$$

Since $M_{\theta\theta}$ is the only load applied to the laminated curved beam, Equation 3-19 can be re-written as:

$$\varepsilon_{\theta\theta} = -\frac{B_{\theta\theta}}{\Delta}; \quad \text{and} \qquad M_{\theta\theta} = \frac{A_{\theta\theta}}{\Delta}$$

where $\Delta = A_{\theta\theta}D_{\theta\theta} - B_{\theta\theta}^2$

$A_{\theta\theta}$, $B_{\theta\theta}$ and $D_{\theta\theta}$ are referring to the extensional, coupling and bending stiffness along the θ direction, respectively. They are equivalent to A_{22}, B_{22} and D_{22} for the plate laminate as the mid-plane curvature R approaches to ∞. This is proved and shown in Appendix B. It is also noted that $B_{\theta\theta}$ is not equal zero even if the laminate is symmetric with respect to its mid-plane.

With the values of ε_0 and κ_θ, the in-plane stress σ_θ at any given position can be obtained from Equations 3-12 and 3-13.

CHAPTER 4

STRESS EFFECT OF CURVATURE AND STACKING SEQUENCE

This Chapter discusses the tangential and radial stresses due to the variation of the laminate curvature. The characteristics of the axial, bending and their coupling stiffness of the curved beam are also investigated.

4.1 The Curvature Effect on Laminate Stresses

Three curved beam models with the difference in geometry dimensions were examined. The meshing, number of elements, boundary conditions, and loading conditions remained the same as defined in Chapter 2. Four local coordinate systems were assigned to each element group. Each of these four local coordinate systems was associated to a different angle of fiber orientation: 0^0, -45^0, $+45^0$, and 90^0, as shown in Figure 2.4. The T300/977-2 graphite/epoxy laminate with stacking sequence of $[+45/-45/90_2/0_2]_S$, quasi-orthotropic material, was used for these three models. The required material properties for NASTRAN MAT9 Card are shown in Table 2.4.

4.1.1 Stress Distribution

Model I with the mid-plane curvature of $R_1 = 0.2444$ inches was examined and analyzed in PATRAN/NASTRAN. The geometrical dimensions of this Model I are shown in Table 2.1. Four plies (0^0 ply#6, -45^0 ply#2, $+45^0$ ply#1 & and 90^0 ply#4) from the lower half and four plies from the upper half (0^0 ply#7, -45^0 ply#11, $+45^0$ ply#12, and 90^0 ply#9) of analyzed model were selected to show different stresses distributions. The ply in the model and its sequence are shown below.

Table 4.1. Ply sequence for 12-ply composite curved beam.

Ply #	Orientation
1	$+45^0$
2	-45^0
3	90^0
4	90^0
5	0^0
6	0^0
Mid-Plane	
7	0^0
8	0^0
9	90^0
10	90^0
11	-45^0
12	$+45^0$

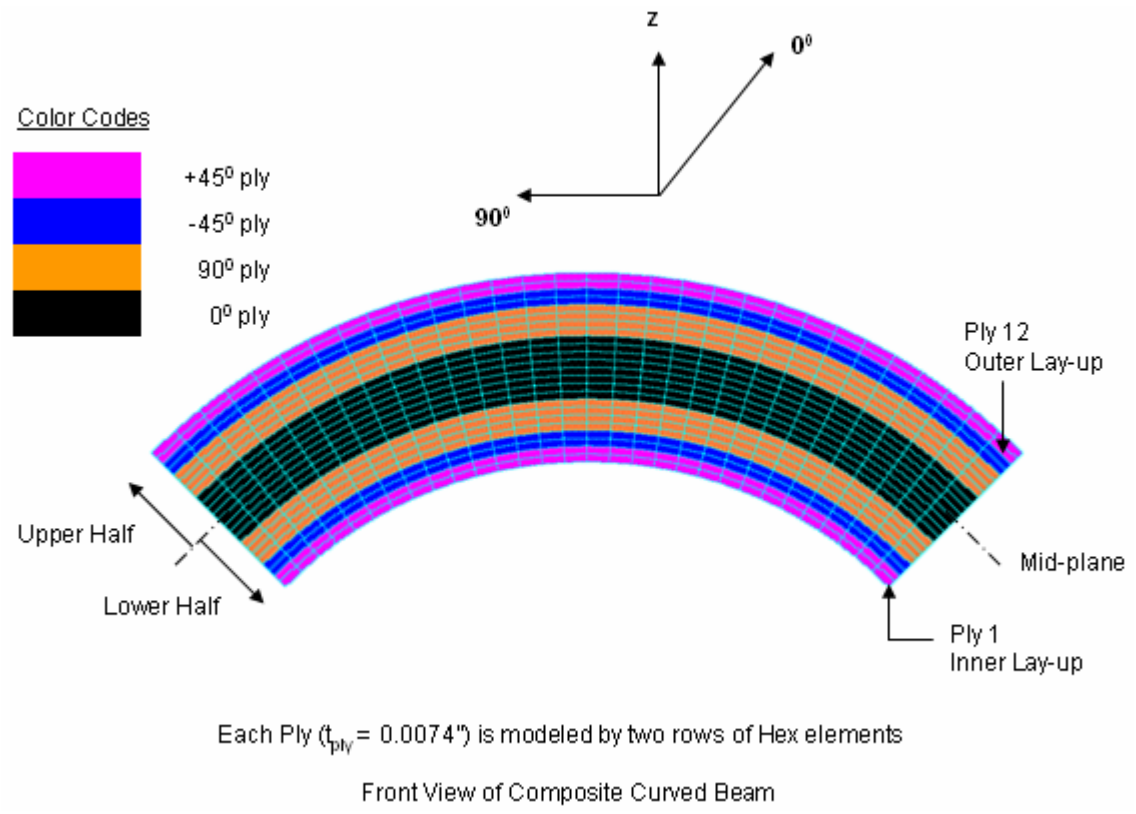

Figure 4.1. The lay-up sequence of composite curved beam.

The stress distributions of eight selected plies are shown in the figures over the next pages.

4.1.1.1 Stress Distribution for 0^0 ply

Figures 4.2 and 4.3 show the tangential and radial stress contours of ply #6 and #7. As shown, the higher stress is located at the vicinity of both free edges of the curved and straight sides. Both tangential and radial stresses are somewhat uniform at the place away from the free edges.

Tangential stress σ_θ of ply #6 Tangential stress σ_θ of ply #7

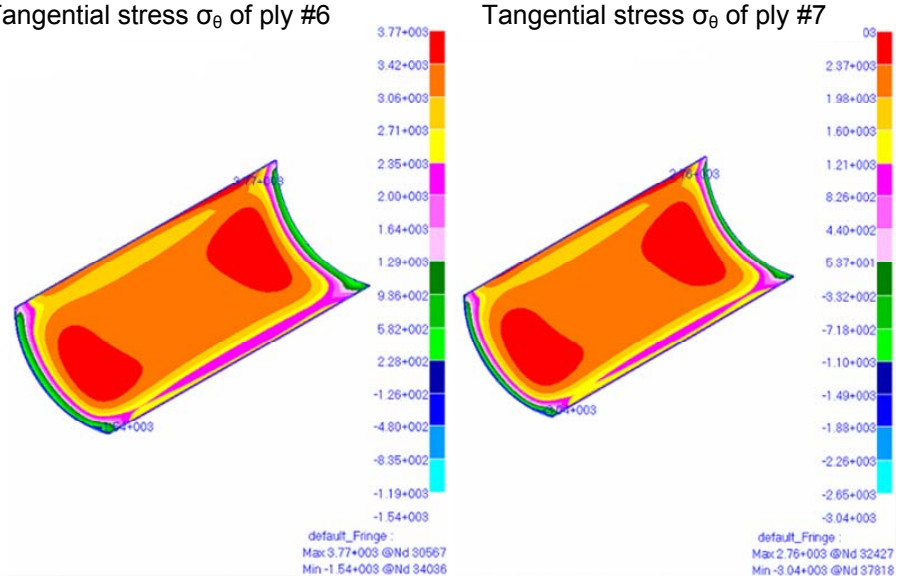

Figure 4.2. The distribution of tangential stress σ_θ in 0^0 ply.

Radial stress σ_r of ply #6 Radial stress σ_r of ply #7

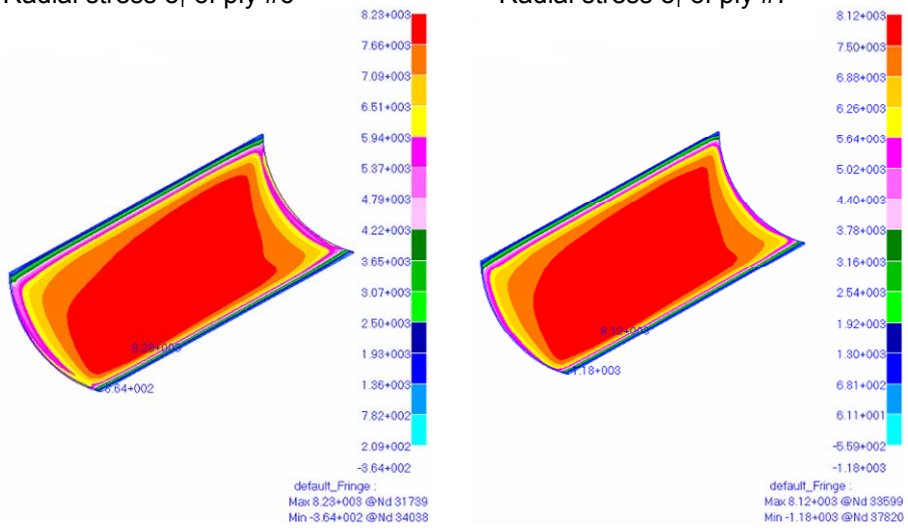

Figure 4.3. The distribution of radial stress σ_r in 0^0 ply.

4.1.1.2 Stress Distribution for -45^0 ply and +45^0 ply

The σ_θ and σ_r stress contours are plotted in Figures 4.4 and 4.5 for -45^0 ply and Figures 4.6 and 4.7 for +45^0 ply. Comparing σ_θ of plies #1 and #2, the maximum magnitude occurs along its fiber direction. The radial stress seems to be not significantly affected by the positive or negative fiber direction.

Tangential stress σ_θ of ply #2 Tangential stress σ_θ of ply #11

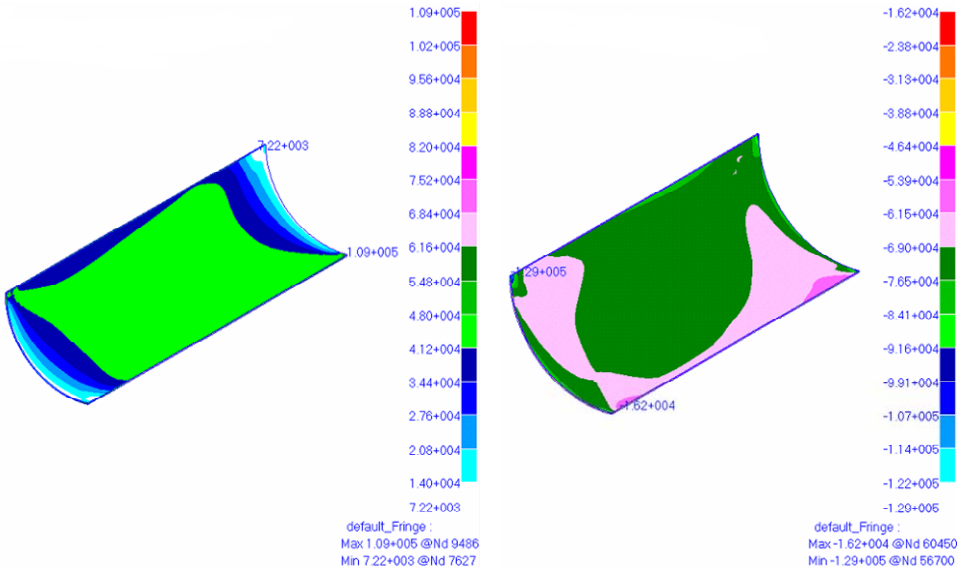

Figure 4.4. The distribution of tangential stress σ_θ in -45^0 ply.

Radial stress σ_r of ply #2 Radial stress σ_r of ply #11

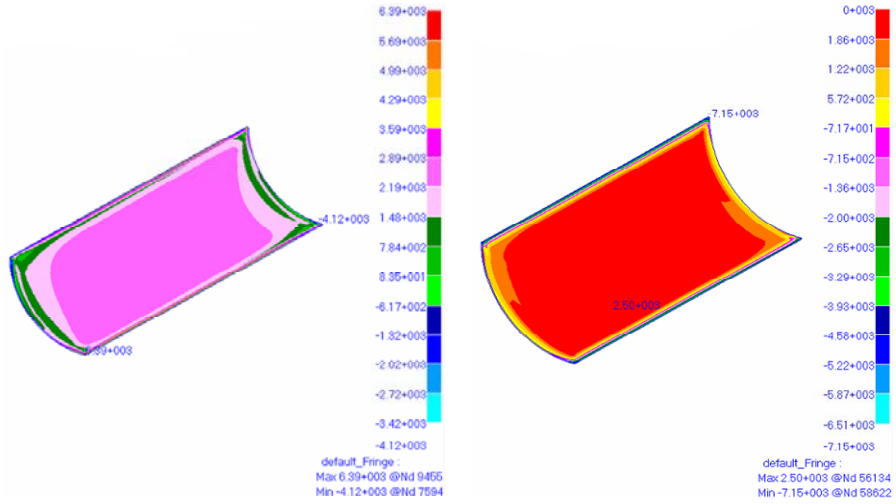

Figure 4.5. The distribution of radial stress σ_r in -45^0 ply.

Tangential stress σ_θ of ply #1

Tangential stress σ_θ of ply #12

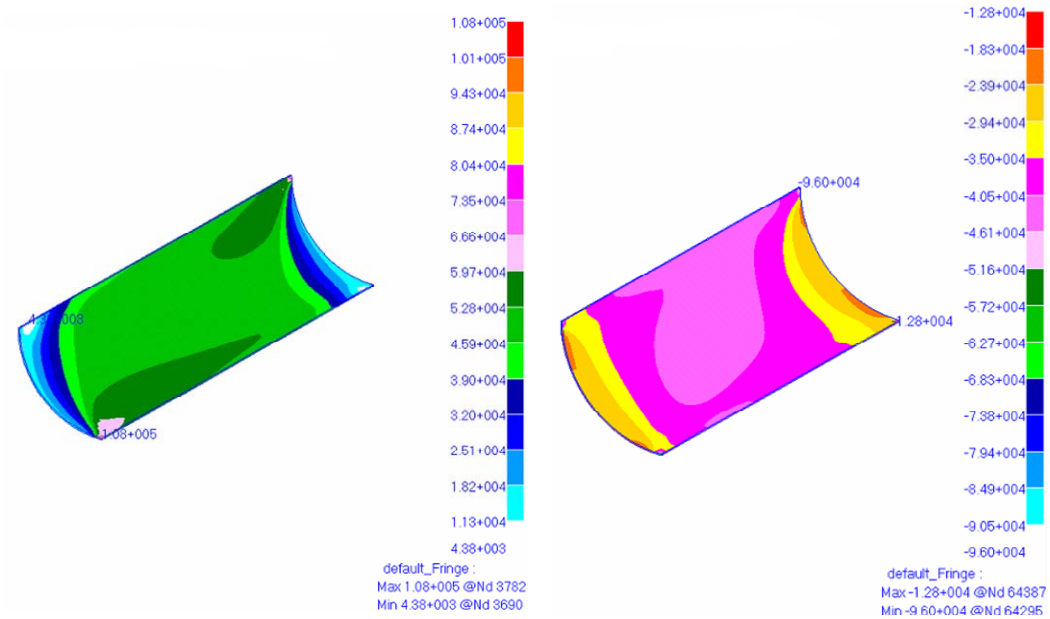

Figure 4.6. The distribution of tangential stress σ_θ in $+45^0$ ply.

Radial stress σ_r of ply #1

Radial stress σ_r of ply #12

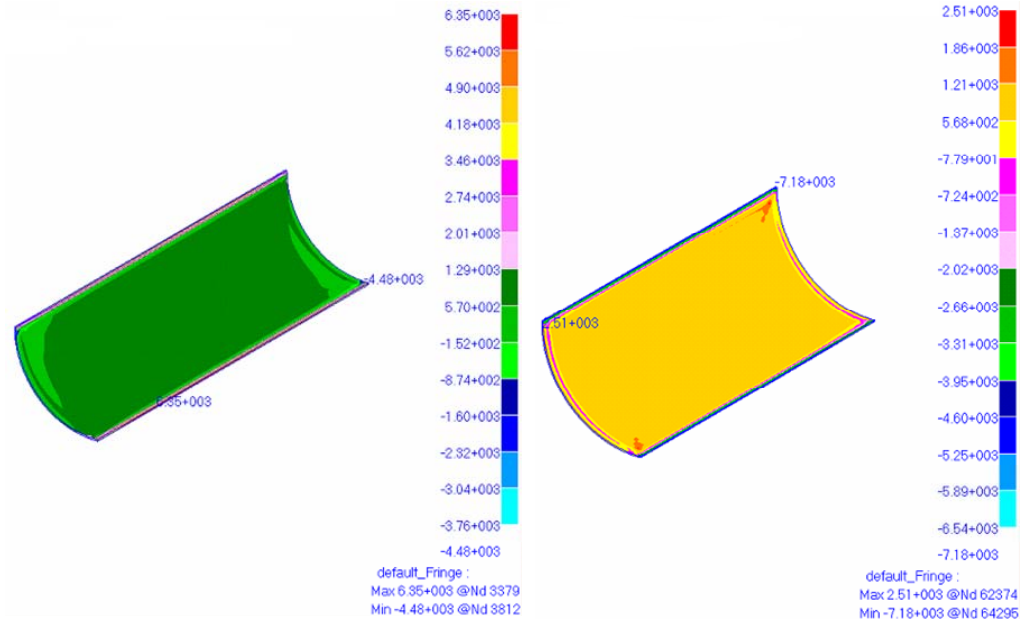

Figure 4.7. The distribution of radial stress σ_r in $+45^0$ ply.

4.1.1.3 Stress Distribution for 90^0 ply

Since the moment is applied in the θ direction, 90^0 ply is the major load carrying ply of the laminate in this case. Figures 4.8 and 4.9 show the tangential and the radial stress contours of ply # 4 and ply #9, respectively. σ_θ is the highest stress component among all the plies in the laminate. If there is no curvature in the laminate, σ_θ in ply #4 and #9 should be equal in magnitude but opposite sign because of symmetrical laminate. However, this is not the case for the curved laminate. As shown, σ_θ in ply #4 is larger than σ_θ in ply #9.

Tangential stress σ_θ of ply #4 Tangential stress σ_θ of ply #9

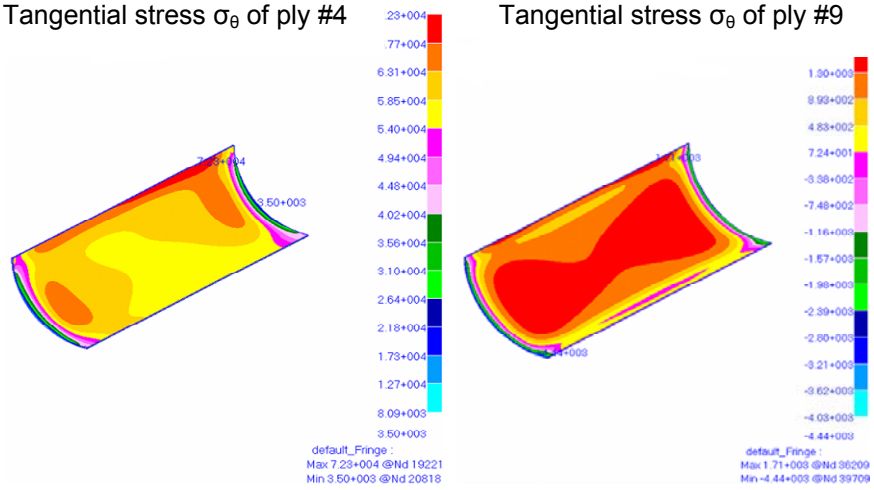

Figure 4.8. The distribution of tangential stress σ_θ in 90^0 ply.

Radial stress σ_r of ply #4 Radial stress σ_r of ply #9

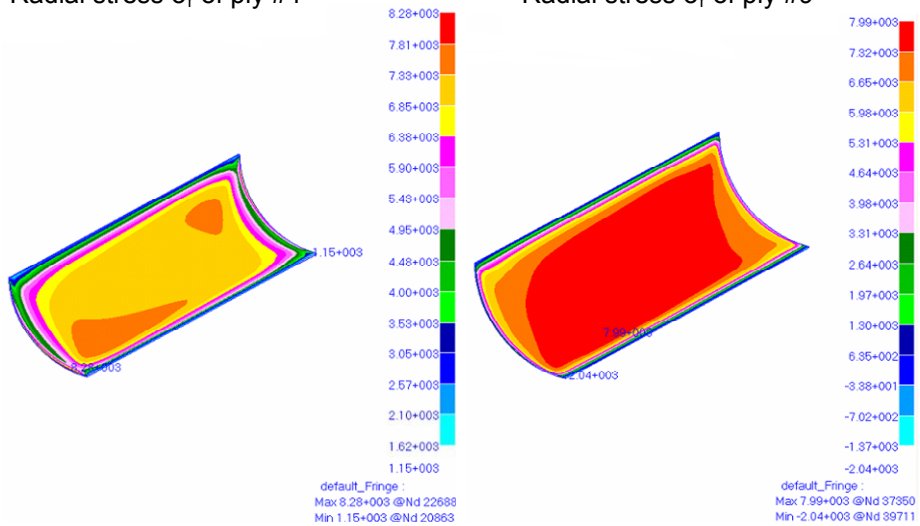

Figure 4.9. The distribution of radial stress σ_r in 90^0 ply.

4.1.2 Stress Comparison

Curved beam Model I, Model II and Model III with three different mid-plane curvatures were examined and analyzed using PATRAN/NASTRAN. The geometrical dimensions of these three models are shown in Table 2.1. Four different plies (0^0 ply#6, -45^0 ply#2, $+45^0$ ply#1 & and 90^0 ply#4) from the lower half of these models were selected for stress comparison. Twenty different elements which associated with twenty different angle positions from each ply, as shown in Figure 4.10, were selected to eliminate the "edge effective".

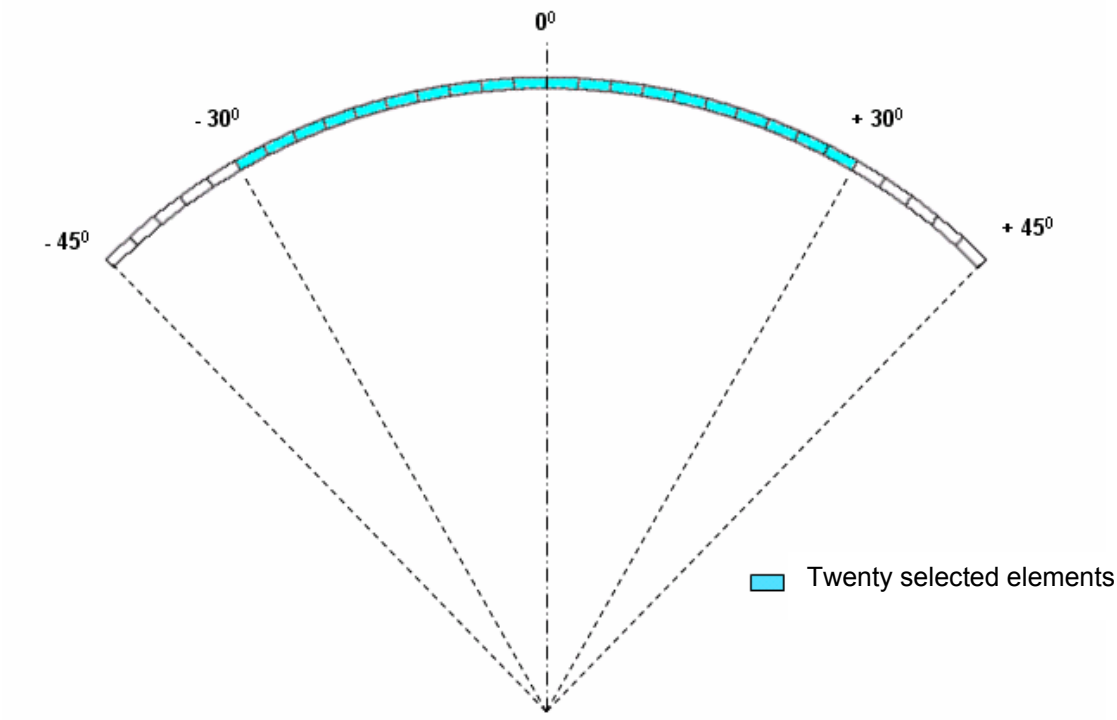

Figure 4.10. Elements on each ply at different angle position.

The values of radial stress σ_r and tangential stress σ_θ for these twenty elements were recorded from the PATRAN/NASTRAN output. These stress values were then plotted into different graphs. Each of these graphs shows the stress variation of each individual ply at a different angle of fiber orientation from three different analyzed curved beam models. The behavior and the variation of interlaminar stresses from each different layer due to the changing in curvature of each model highlighted clearly from these graphs.

4.1.2.1 The Stress Variation for +45^0 ply#1

Table 4.2. The stress values for +45^0 ply#1.

(deg)	Model I (R_1 = 0.2444)		Model II (R_2 = 0.6444)		Model III (R_3 = 1.8444)	
Angle Position	σ_r (psi)	σ_θ (psi)	σ_r (psi)	σ_θ (psi)	σ_r (psi)	σ_θ (psi)
30	5.11E+02	5.48E+04	4.70E+02	4.74E+04	1.43E+02	4.50E+04
27	5.13E+02	5.49E+04	4.61E+02	4.72E+04	1.44E+02	4.50E+04
24	5.14E+02	5.50E+04	4.64E+02	4.70E+04	1.46E+02	4.51E+04
21	5.15E+02	5.50E+04	4.60E+02	4.69E+04	1.41E+02	4.52E+04
18	5.16E+02	5.51E+04	4.60E+02	4.67E+04	1.49E+02	4.54E+04
15	5.16E+02	5.51E+04	4.59E+02	4.66E+04	1.46E+02	4.55E+04
12	5.16E+02	5.51E+04	4.59E+02	4.66E+04	1.37E+02	4.55E+04
9	5.16E+02	5.52E+04	4.58E+02	4.65E+04	1.50E+02	4.56E+04
6	5.17E+02	5.52E+04	4.59E+02	4.65E+04	1.40E+02	4.56E+04
3	5.17E+02	5.52E+04	4.58E+02	4.65E+04	1.54E+02	4.57E+04
-3	5.17E+02	5.52E+04	4.58E+02	4.65E+04	1.32E+02	4.57E+04
-6	5.18E+02	5.53E+04	4.59E+02	4.65E+04	1.51E+02	4.57E+04
-9	5.18E+02	5.53E+04	4.58E+02	4.66E+04	1.46E+02	4.57E+04
-12	5.19E+02	5.54E+04	4.60E+02	4.66E+04	1.41E+02	4.57E+04
-15	5.20E+02	5.54E+04	4.59E+02	4.67E+04	1.45E+02	4.56E+04
-18	5.21E+02	5.55E+04	4.62E+02	4.68E+04	1.52E+02	4.56E+04
-21	5.22E+02	5.57E+04	4.60E+02	4.70E+04	1.34E+02	4.55E+04
-24	5.25E+02	5.59E+04	4.66E+02	4.71E+04	1.57E+02	4.56E+04
-27	5.28E+02	5.62E+04	4.61E+02	4.73E+04	1.34E+02	4.55E+04
-30	5.31E+02	5.65E+04	4.75E+02	4.76E+04	1.59E+02	4.57E+04

The tangential stress σ_θ and radial stress σ_r are found to be positive for +45^0 lay-up #1, as shown in Figure 4.11 and Figure 4.12 on the next page. As expected, the stresses σ_θ and σ_r along the curve angle position are fairly constant. However, these stresses decrease with the increasing of curvatures. Figure 4.12 clearly highlights the effect of curvature on radial stress σ_r. Model I (R_1 = 0.2444) with the lowest in radius of curvature produces the highest in interlaminar stresses. On the other hand, Model III (R_3 = 1.8444) with the highest in radius of curvature produces the lowest in interlaminar stresses.

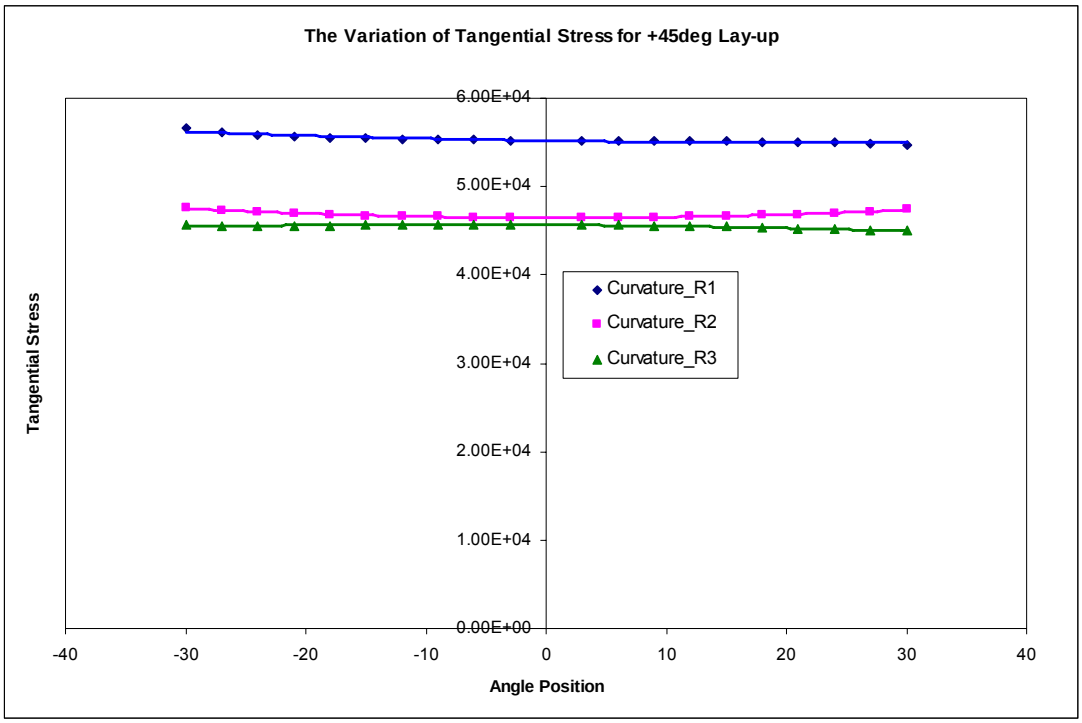

Figure 4.11. Tangential stress for $+45^0$ lay-up.

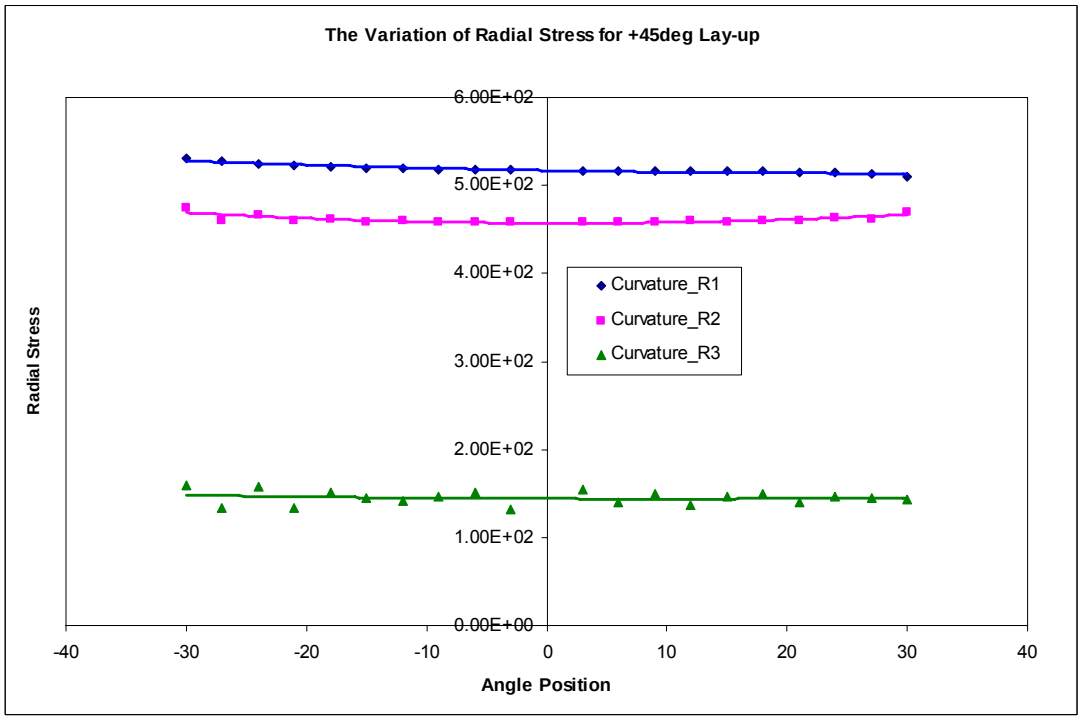

Figure 4.12. Radial stress for $+45^0$ lay-up.

4.1.2.2 The Stress Variation for -45^0 ply#2

Table 4.3. The stress values for -45^0 ply#2.

(deg)	Model I (R_1 = 0.2444)		Model II (R_2 = 0.6444)		Model III (R_3 = 1.8444)	
Angle Position	σ_r (psi)	σ_θ (psi)	σ_r (psi)	σ_θ (psi)	σ_r (psi)	σ_θ (psi)
30	2.89E+03	4.02E+04	1.01E+03	4.24E+04	3.17E+02	4.34E+04
27	2.93E+03	4.04E+04	1.01E+03	4.27E+04	3.21E+02	4.36E+04
24	2.96E+03	4.06E+04	1.01E+03	4.29E+04	3.14E+02	4.38E+04
21	2.97E+03	4.06E+04	1.01E+03	4.31E+04	3.17E+02	4.40E+04
18	2.98E+03	4.07E+04	1.01E+03	4.33E+04	3.15E+02	4.41E+04
15	2.98E+03	4.08E+04	1.01E+03	4.34E+04	3.18E+02	4.42E+04
12	2.98E+03	4.08E+04	1.01E+03	4.35E+04	3.05E+02	4.44E+04
9	2.99E+03	4.08E+04	1.02E+03	4.36E+04	3.23E+02	4.44E+04
6	2.99E+03	4.09E+04	1.02E+03	4.37E+04	3.07E+02	4.45E+04
3	2.99E+03	4.09E+04	1.02E+03	4.37E+04	3.16E+02	4.45E+04
-3	3.00E+03	4.09E+04	1.02E+03	4.37E+04	3.08E+02	4.45E+04
-6	3.00E+03	4.09E+04	1.02E+03	4.37E+04	3.16E+02	4.45E+04
-9	3.01E+03	4.09E+04	1.02E+03	4.36E+04	3.18E+02	4.44E+04
-12	3.01E+03	4.09E+04	1.02E+03	4.35E+04	3.07E+02	4.43E+04
-15	3.02E+03	4.10E+04	1.01E+03	4.34E+04	3.14E+02	4.42E+04
-18	3.03E+03	4.10E+04	1.02E+03	4.33E+04	3.23E+02	4.41E+04
-21	3.05E+03	4.10E+04	1.01E+03	4.31E+04	3.08E+02	4.39E+04
-24	3.07E+03	4.11E+04	1.02E+03	4.30E+04	3.25E+02	4.36E+04
-27	3.09E+03	4.12E+04	1.01E+03	4.28E+04	3.10E+02	4.34E+04
-30	3.11E+03	4.14E+04	1.02E+03	4.25E+04	3.32E+02	4.32E+04

The tangential stress σ_θ and radial stress σ_r are found to be positive for -45^0 lay-up #2, as shown in Figure 4.13 and Figure 4.14 on the next page. For this -45^0 lay-up, the tangential stress σ_θ increases with the increasing of curvature. The radial stress σ_r decreases with the increasing of curvature. Model I (R_1 = 0.2444) with the lowest in radius of curvature produces the highest in radial stress and lowest in tangential stress. On the other hand, Model III (R_3 =1.8444) with the highest in curvature produces the lowest in radial stress and highest tangential stress.

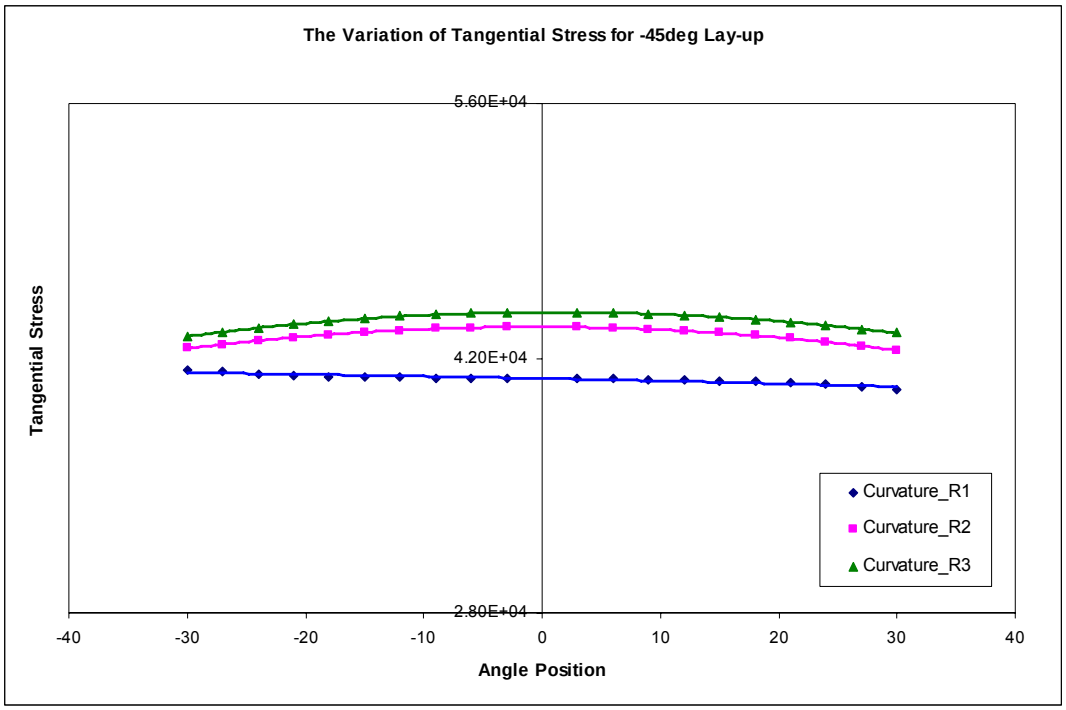

Figure 4.13. Tangential stress for -45^0 lay-up.

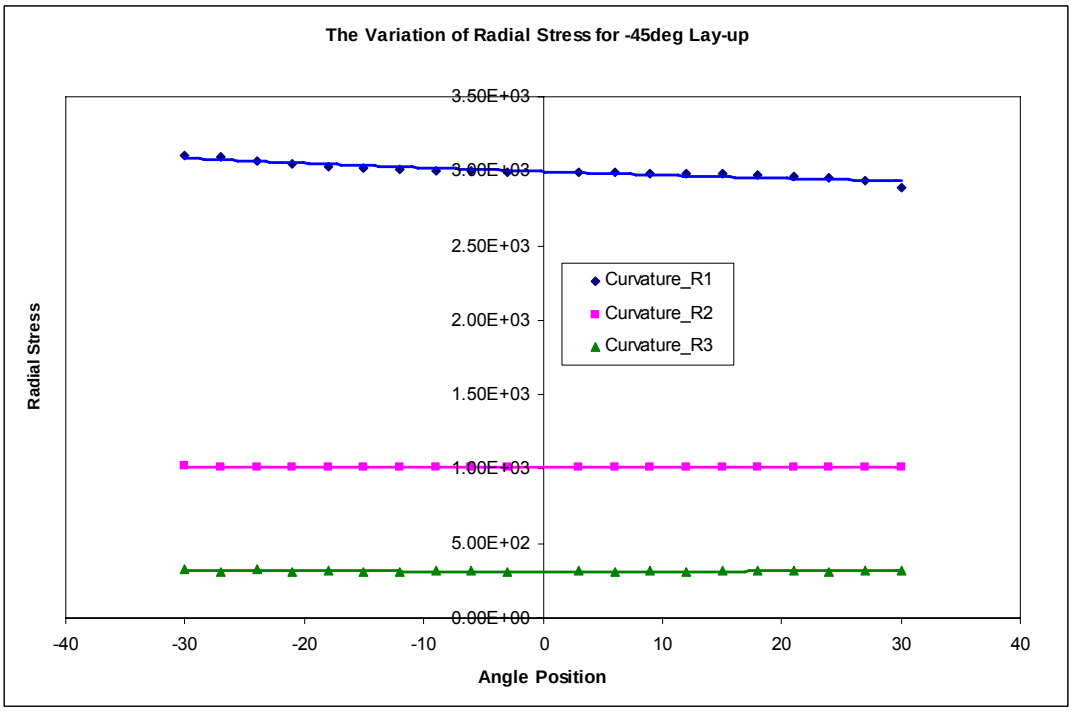

Figure 4.14. Radial stress for -45^0 lay-up.

4.1.2.3 The Stress Variation for 90^0 ply#4

Table 4.4. The stress values for 90^0 ply#4.

(deg)	Model I (R_1 = 0.2444)		Model II (R_2 = 0.6444)		Model III (R_3 = 1.8444)	
Angle Position	σ_r (psi)	σ_θ (psi)	σ_r (psi)	σ_θ (psi)	σ_r (psi)	σ_θ (psi)
30	7.38E+03	5.11E+04	2.91E+03	6.29E+04	1.05E+03	7.81E+04
27	7.49E+03	5.09E+04	2.91E+03	6.29E+04	1.05E+03	7.98E+04
24	7.54E+03	5.08E+04	2.91E+03	6.29E+04	1.07E+03	8.11E+04
21	7.56E+03	5.08E+04	2.92E+03	6.28E+04	1.06E+03	8.24E+04
18	7.57E+03	5.08E+04	2.92E+03	6.28E+04	1.08E+03	8.34E+04
15	7.58E+03	5.08E+04	2.92E+03	6.28E+04	1.07E+03	8.43E+04
12	7.58E+03	5.07E+04	2.92E+03	6.28E+04	1.06E+03	8.48E+04
9	7.58E+03	5.07E+04	2.92E+03	6.28E+04	1.09E+03	8.53E+04
6	7.59E+03	5.07E+04	2.93E+03	6.28E+04	1.07E+03	8.55E+04
3	7.59E+03	5.07E+04	2.93E+03	6.28E+04	1.09E+03	8.58E+04
-3	7.60E+03	5.07E+04	2.93E+03	6.28E+04	1.06E+03	8.57E+04
-6	7.60E+03	5.06E+04	2.93E+03	6.28E+04	1.09E+03	8.56E+04
-9	7.61E+03	5.05E+04	2.93E+03	6.28E+04	1.06E+03	8.53E+04
-12	7.62E+03	5.04E+04	2.93E+03	6.28E+04	1.08E+03	8.49E+04
-15	7.64E+03	5.03E+04	2.92E+03	6.28E+04	1.07E+03	8.43E+04
-18	7.67E+03	5.01E+04	2.92E+03	6.29E+04	1.07E+03	8.35E+04
-21	7.70E+03	4.97E+04	2.92E+03	6.29E+04	1.07E+03	8.25E+04
-24	7.74E+03	4.93E+04	2.92E+03	6.29E+04	1.06E+03	8.13E+04
-27	7.78E+03	4.87E+04	2.92E+03	6.29E+04	1.06E+03	7.99E+04
-30	7.79E+03	4.81E+04	2.93E+03	6.29E+04	1.05E+03	7.84E+04

The tangential stress σ_θ and radial stress σ_r are found to be positive for 90^0 lay-up #4, as shown in Figure 4.15 and Figure 4.16 on the next page. For this 90^0 lay-up, the tangential stress σ_θ increases with the increasing of curvature. The radial stress σ_r decreases with the increasing of curvature. Model I (R_1 = 0.2444) with the lowest in radius of curvature produces the highest in radial stress and lowest in tangential stress. On the other hand, Model III (R_3 = 1.8444) with the highest in radius of curvature produces the lowest in radial stress and highest tangential stress.

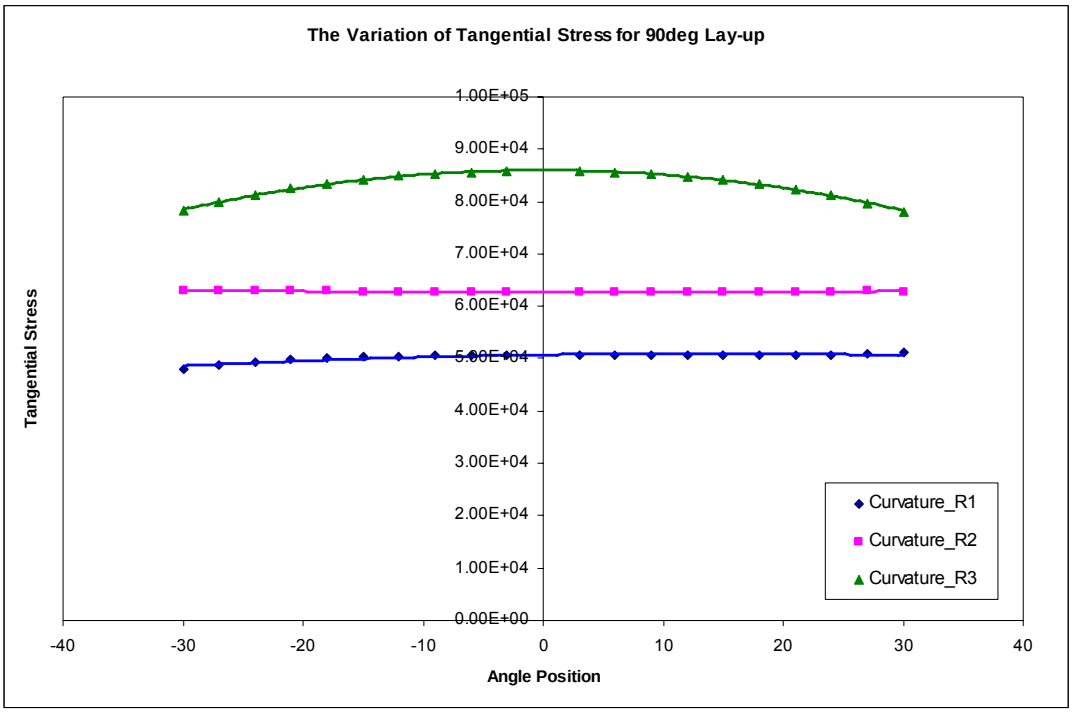

Figure 4.15. Tangential stress for 90^0 lay-up.

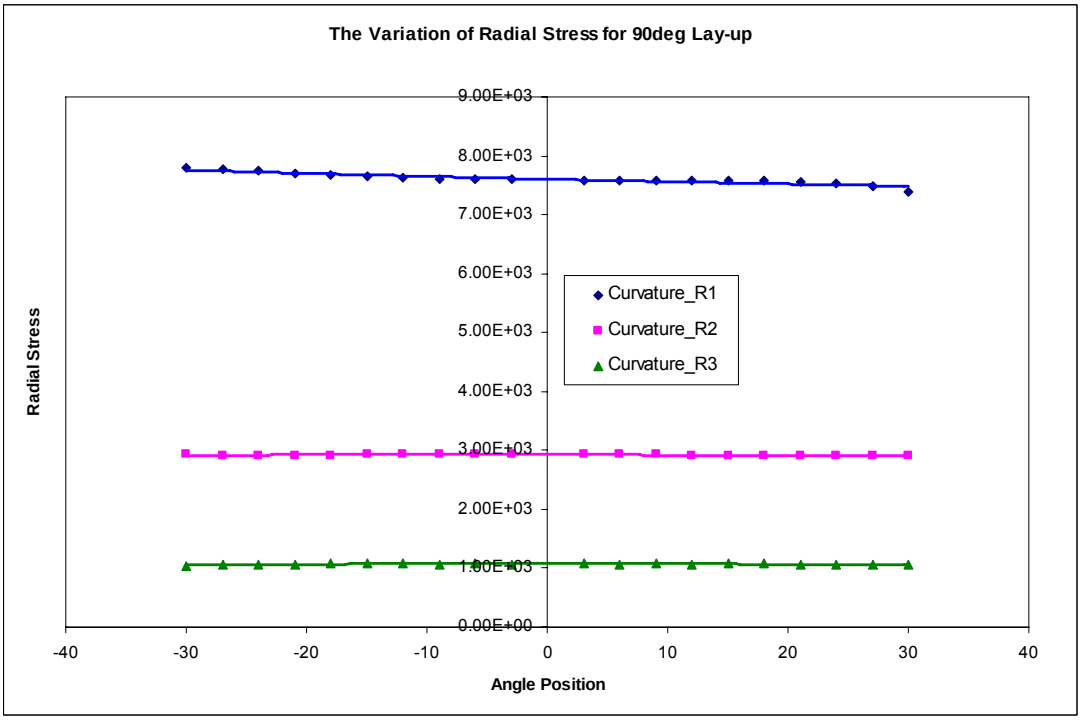

Figure 4.16. Radial stress for 90^0 lay-up.

4.1.2.4 The Stress Variation for 0^0 ply#6

Table 4.5. The stress values for 0^0 ply#6.

(deg)	Model I (R_1 = 0.2444)		Model II (R_2 = 0.6444)		Model III (R_3 = 1.8444)	
Angle Position	σ_r (psi)	σ_θ (psi)	σ_r (psi)	σ_θ (psi)	σ_r (psi)	σ_θ (psi)
30	7.59E+03	2.63E+03	3.04E+03	1.67E+03	1.07E+03	1.82E+03
27	7.67E+03	2.71E+03	3.04E+03	1.67E+03	1.07E+03	1.88E+03
24	7.70E+03	2.76E+03	3.04E+03	1.67E+03	1.07E+03	1.96E+03
21	7.72E+03	2.79E+03	3.05E+03	1.67E+03	1.08E+03	2.02E+03
18	7.72E+03	2.80E+03	3.05E+03	1.67E+03	1.07E+03	2.07E+03
15	7.72E+03	2.81E+03	3.05E+03	1.67E+03	1.08E+03	2.12E+03
12	7.72E+03	2.82E+03	3.05E+03	1.67E+03	1.08E+03	2.15E+03
9	7.72E+03	2.82E+03	3.06E+03	1.66E+03	1.08E+03	2.18E+03
6	7.73E+03	2.82E+03	3.06E+03	1.66E+03	1.08E+03	2.19E+03
3	7.73E+03	2.82E+03	3.06E+03	1.66E+03	1.07E+03	2.20E+03
-3	7.73E+03	2.82E+03	3.06E+03	1.66E+03	1.08E+03	2.20E+03
-6	7.74E+03	2.82E+03	3.06E+03	1.66E+03	1.07E+03	2.19E+03
-9	7.74E+03	2.82E+03	3.06E+03	1.66E+03	1.08E+03	2.18E+03
-12	7.76E+03	2.82E+03	3.06E+03	1.66E+03	1.08E+03	2.15E+03
-15	7.77E+03	2.81E+03	3.06E+03	1.66E+03	1.08E+03	2.12E+03
-18	7.80E+03	2.81E+03	3.05E+03	1.66E+03	1.07E+03	2.08E+03
-21	7.83E+03	2.78E+03	3.05E+03	1.66E+03	1.08E+03	2.03E+03
-24	7.88E+03	2.74E+03	3.05E+03	1.67E+03	1.07E+03	1.96E+03
-27	7.93E+03	2.66E+03	3.05E+03	1.67E+03	1.07E+03	1.88E+03
-30	7.96E+03	2.52E+03	3.06E+03	1.67E+03	1.06E+03	1.79E+03

The tangential stress σ_θ and radial stress σ_r are found to be positive for 0^0 lay-up #6, as shown in Figure 4.17 and Figure 4.18 on the next page. For this 0^0 lay-up, the tangential stress σ_θ are found highest for Model I (R_1 = 0.2444), and lowest for Model II (R_2 = 0.6444). The radial stress σ_r decreases with the increasing of curvature. Model I (R_1 = 0.2444) with the lowest in radius of curvature produces the highest in radial stress. Model III (R_3 = 1.8444) with the highest in radius of curvature produces the lowest in radial stress.

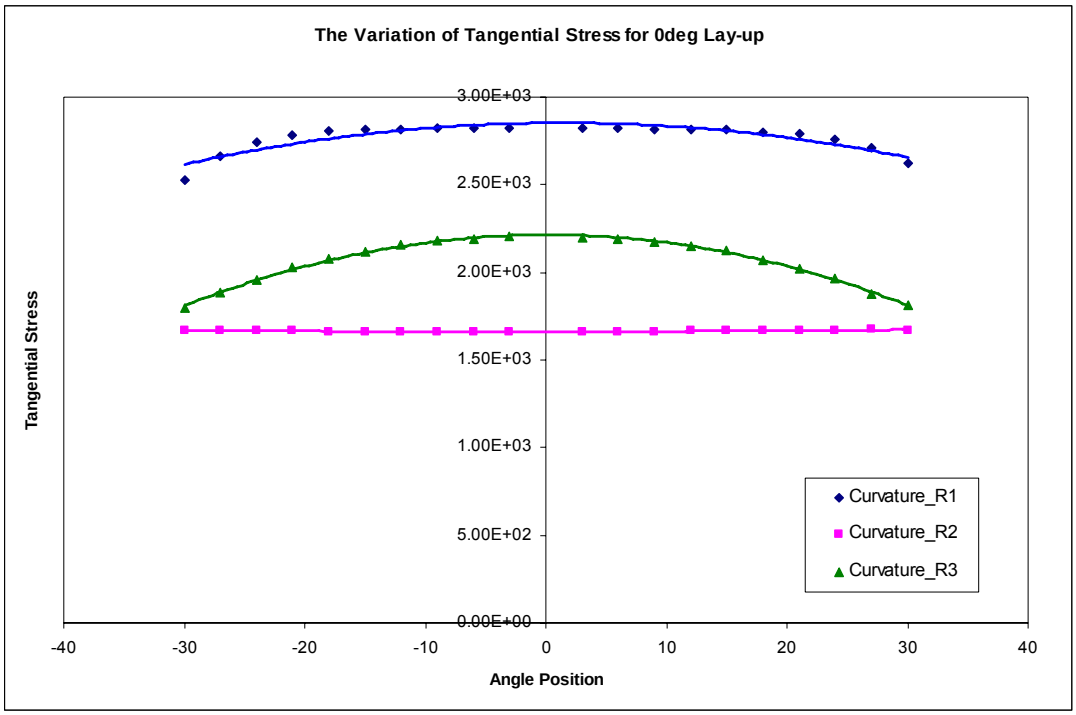

Figure 4.17. Tangential stress for 0^0 lay-up.

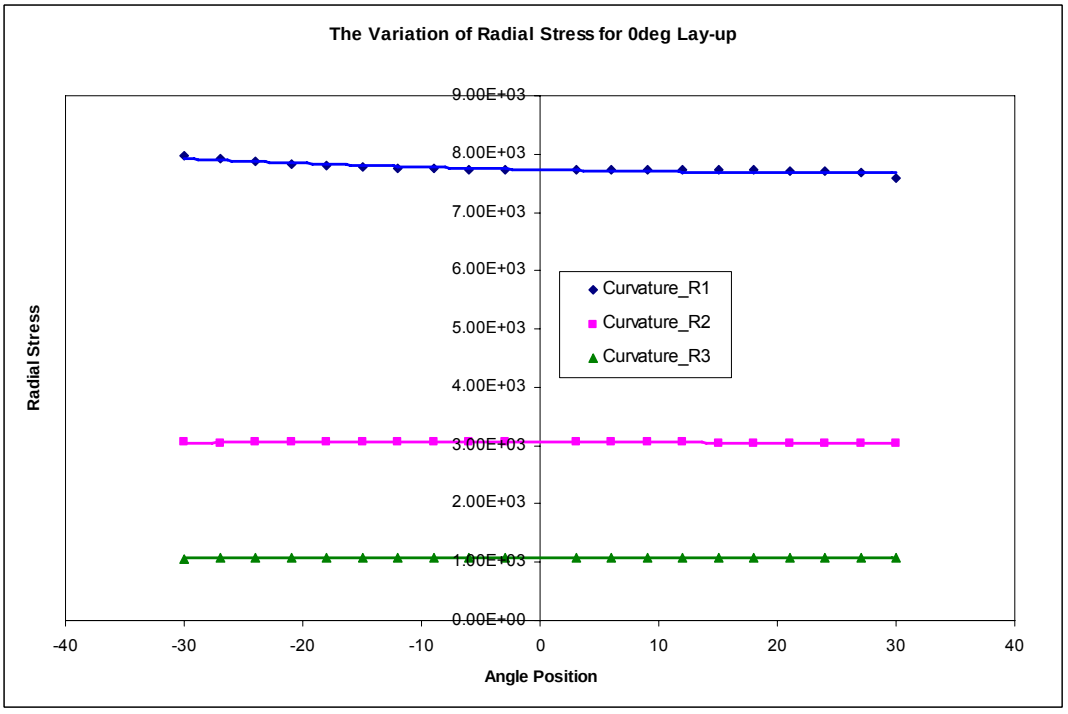

Figure 4.18. Radial stress for 0^0 lay-up.

4.1.3 Stacking Sequence $[+45^0/-45^0/90^0_2/0^0_2]_S$

The tangential stresses along the θ direction of -45^0 (ply#2), $+45^0$ (ply #1) and 90^0 (ply #4) are calculated using the closed-form solution in Chapter 3. These calculated stress values are used to validate the obtained tangential stress values in Section 4.1.2. The comparison between FEM and the closed-form solution is shown in Table 4.6.

Table 4.6. The comparison for tangential stress.

	Applied bending moment $M_{\theta\theta}$ = 100 lbs-in					
	Tangential stress, $\sigma_{\theta\theta}$ (psi)					
	R_1 = 0.2444 inches		R_2 = 0.6444 inches		R_3 = 1.8444 inches	
	FEM	Present	FEM	Present	FEM	Present
-45^0 Ply	4.09E+04	4.20E+04	4.37E+04	4.03E+04	4.45E+04	3.97E+04
$+45^0$ Ply	5.52E+04	5.36E+04	4.65E+04	4.97E+04	4.57E+04	4.83E+04
90^0 Ply	5.07E+04	5.21E+04	6.28E+04	5.64E+04	8.58E+04	7.13E+04
	% Different		% Different		% Different	
-45^0 Ply	2.62		8.44		12.09	
$+45^0$ Ply	2.99		6.44		5.38	
90^0 Ply	2.69		11.35		20.34	

The difference in tangential stress between the FEM result and the closed-form solution is predictable. This difference takes place due to the fact that the FEM includes 3D material properties while the closed-form solution includes only 1D material property.

4.2 The Fiber Orientation Effect on Laminate Stresses

The effect of fiber orientation is also investigated. Model I (R_1 = 0.2444) was examined. The meshing, the number of elements, boundary conditions and material coordinate systems for this model were remained the same as defined in Sections 2.1 and 2.2.

4.2.1 Symmetric and Balanced Laminates

A T300/977-2 graphite/epoxy laminate with stacking sequence of $[\pm\theta/\pm\theta/90^0_2]_S$ was used for the selected models, where $\theta = 15^0$, 30^0, 45^0, 60^0, and 75^0. A different local coordinate was created for each different angle of fiber orientation: 0^0, $+15^0$, -15^0, $+30^0$, -30^0, $+45^0$, -45^0, $+60^0$, -60^0, $+75^0$, and -75^0. There are five different stacking sequences were applied for this model. They are: $[\pm15^0/\pm15^0/90^0_2]_S$, $[\pm30^0/\pm30^0/90^0_2]_S$, $[\pm45^0/\pm45^0/90^0_2]_S$, $[\pm60^0/\pm60^0/90^0_2]_S$, and $[\pm75^0/\pm75^0/90^0_2]_S$.

S.S #1	S.S #2	S.S #3	S.S #4	S.S #5
$+15^0$	$+30^0$	$+45^0$	$+60^0$	$+75^0$
-15^0	-30^0	-45^0	-60^0	-75^0
$+15^0$	$+30^0$	$+45^0$	$+60^0$	$+75^0$
-15^0	-30^0	-45^0	-60^0	-75^0
90^0	90^0	90^0	90^0	90^0
90^0	90^0	90^0	90^0	90^0
90^0	90^0	90^0	90^0	90^0
90^0	90^0	90^0	90^0	90^0
-15^0	-30^0	-45^0	-60^0	-75^0
$+15^0$	$+30^0$	$+45^0$	$+60^0$	$+75^0$
-15^0	-30^0	-45^0	-60^0	-75^0
$+15^0$	$+30^0$	$+45^0$	$+60^0$	$+75^0$

Figure 4.19. Description of laminate coding for five different stacking sequences.

The interlaminar stresses for the elements in 90^0 layer are expected to be different for each stacking sequence. To study the effect of changing in stacking sequence, three different elements in the 90^0 layer #6 from the lower half of the curved beam model were examined.

These three elements were selected from three different angle positions (27^0, 33^0 and 39^0), as shown in Figure 4.20. The element at 45^0 angle position was not selected for this case study since the result at this position may be strongly affected by the end condition enforced by FEM.

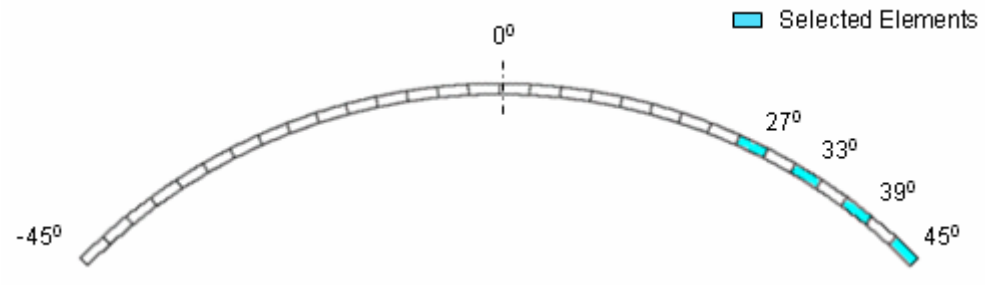

Figure 4.20. The selected elements in 90^0 layer #6 at different angle positions.

The variation of σ_θ and σ_r stresses for the selected elements in 90^0 layer #6 at various angle positions (27^0, 33^0, and 39^0) are shown below for five different stacking sequences.

Color Codes

S.S #1: Stacking Sequence 1
S.S #2: Stacking Sequence 2
S.S #3: Stacking Sequence 3
S.S #4: Stacking Sequence 4
S.S #5: Stacking Sequence 5

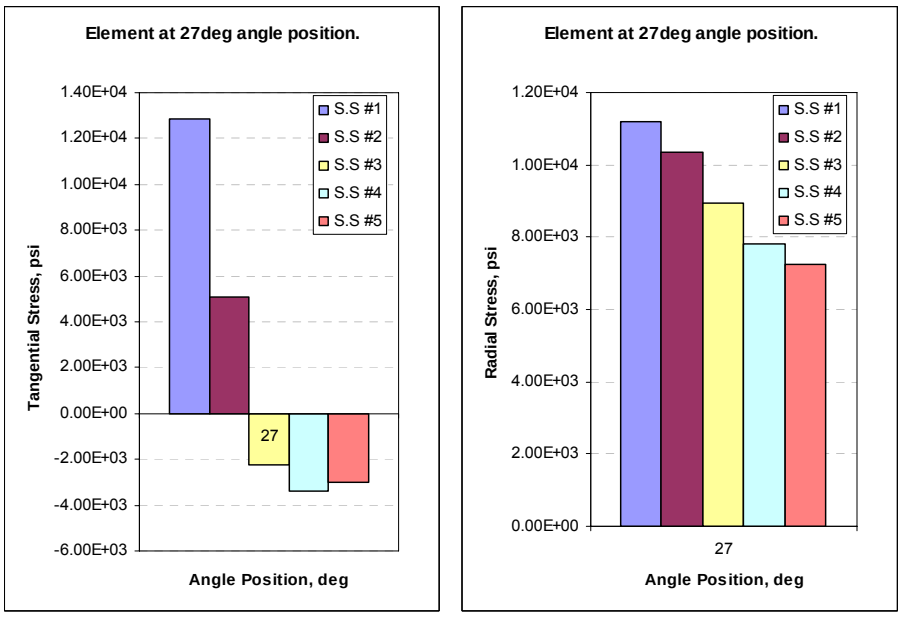

Figure 4.21. Stress for element at 27^0 angle position.

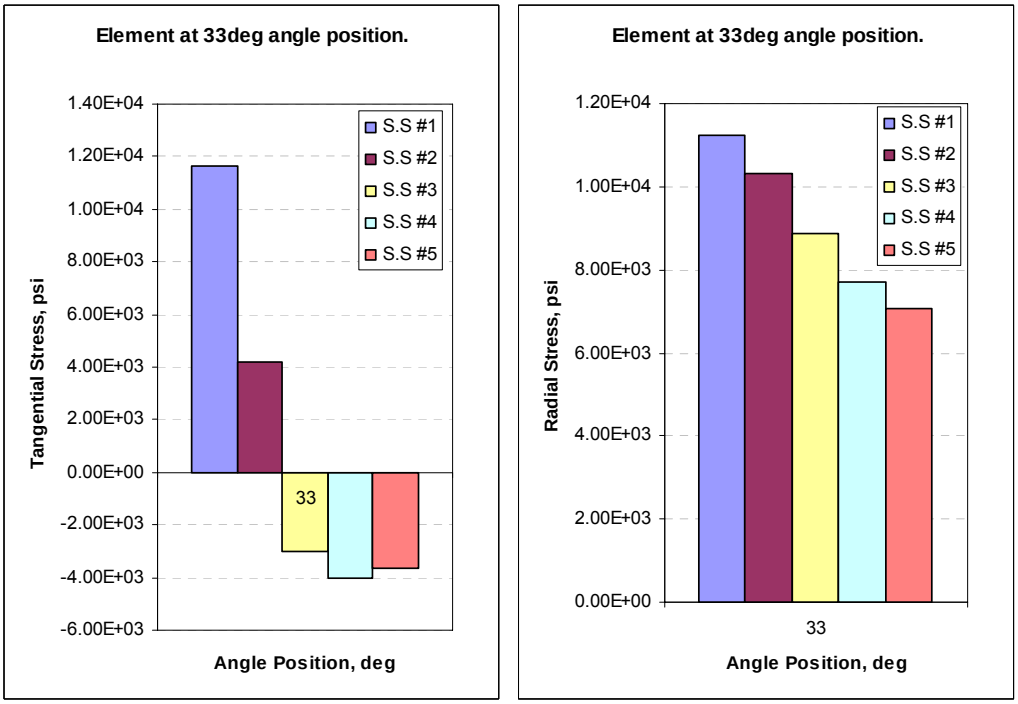

Figure 4.22. Stress for element at 33^0 angle position.

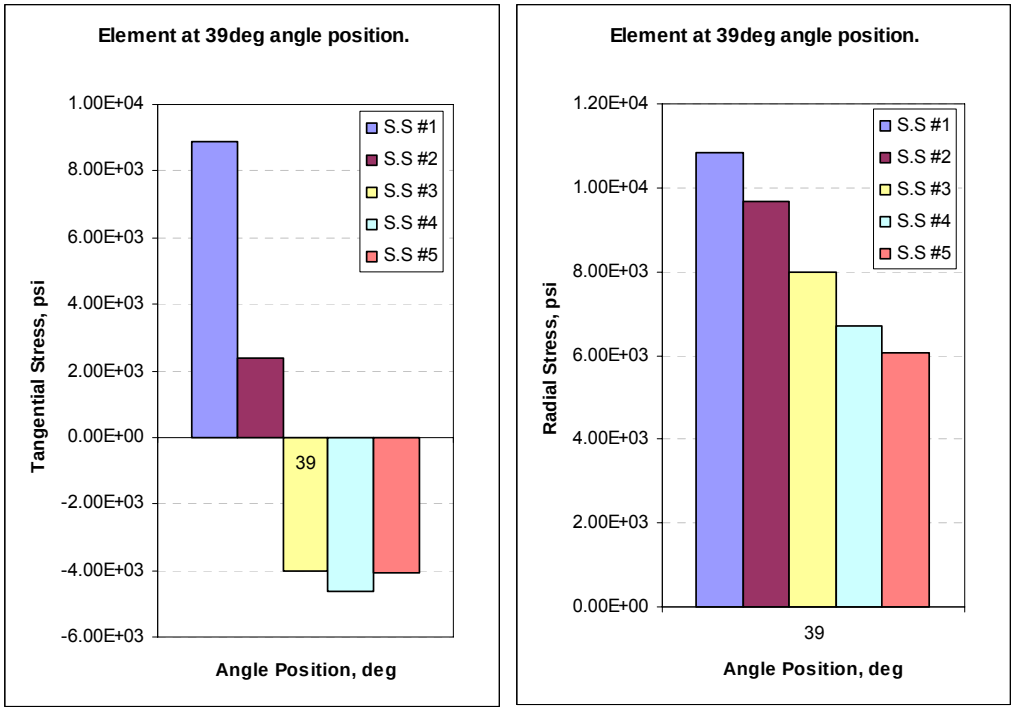

Figure 4.23. Stress for element at 39^0 angle position.

Figures 4.21, 4.22 and 4.23 highlight clearly the effect of fiber orientations on the interlaminar stresses (σ_θ and σ_r). The radial stress σ_r is found positive for all stacking sequences at all selected angle positions. The stacking sequences #1 & #2 produced positive tangential stress σ_θ and the stacking sequences #3, #4, & #5 produced negative tangential stress σ_θ at all selected angle positions. This is because of the shift of the neutral axis of the curved laminate as the fiber orientation changes. The stacking sequence #1, $[\pm 15^0/\pm 15^0/ 90^0{}_2]_S$, produced the highest interlaminar stresses (σ_θ and σ_r) for elements in 90^0 layer #6.

4.2.2 Symmetric / Unsymmetrical and Balanced / Unbalanced Laminates

The effects of three other stacking sequences on the tangential stress were also investigated. The symmetric and balanced laminate $\left[\pm 45^0{}_2/90^0{}_4/\mp 45^0{}_2\right]_T$, unsymmetrical and balanced laminate $\left[\pm 45^0{}_2/\pm 45^0{}_2/90^0{}_4\right]_T$, and unsymmetrical and unbalanced laminate $\left[+45^0{}_8/90^0{}_4\right]_T$ were applied in the same Model I (R_1 = 0.2444). The layer #1 of $+45^0$ fiber orientation was selected to show the different in tangential stress. The stacking sequences are shown below.

S.S #1	S.S #2	S.S #3
$+45^0$	$+45^0$	$+45^0$
-45^0	-45^0	$+45^0$
$+45^0$	$+45^0$	$+45^0$
-45^0	-45^0	$+45^0$
90^0	$+45^0$	$+45^0$
90^0	-45^0	$+45^0$
90^0	$+45^0$	$+45^0$
90^0	-45^0	$+45^0$
-45^0	90^0	90^0
$+45^0$	90^0	90^0
-45^0	90^0	90^0
$+45^0$	90^0	90^0

Figure 4.24. Description of laminate coding for three different stacking sequences.

Twenty different elements which associated with twenty different angle positions, as shown in Figure 4.10, were selected for this study. The tangential stresses from three different stacking sequences were plotted in the same graph for comparison purposes.

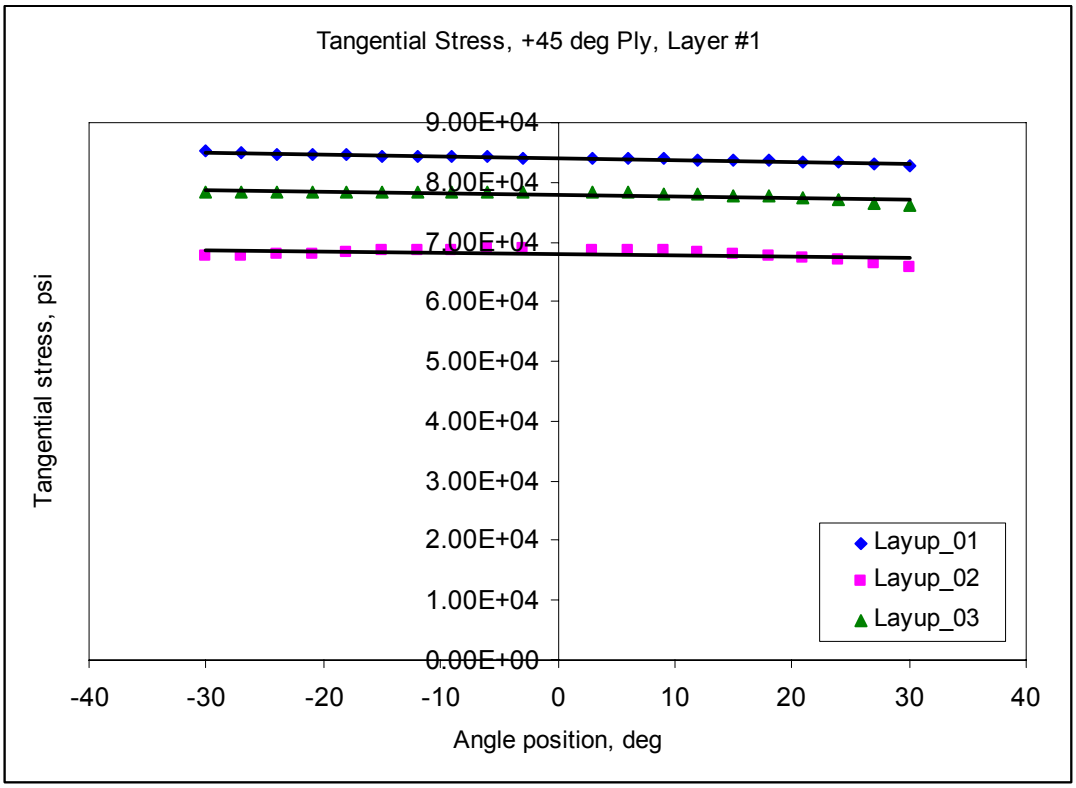

Figure 4.25. The variation of tangential stress.

The tangential stress σ_θ was found positive for all stacking sequences. The symmetric and balanced laminate $\left[\pm 45^0{}_2 / 90^0{}_4 / \mp 45^0{}_2\right]_T$ produced the highest tangential stress for $+45^0$ layer #1. The unsymmetrical and balanced laminate $\left[\pm 45^0{}_2 / \pm 45^0{}_2 / 90^0{}_4\right]_T$ produced the lowest tangential stress for $+45^0$ layer #1.

4.3 The Effect of Stacking Sequence

Five different laminates were examined to show the effect of the lay-up stacking sequences on the extensional stiffness matrix [A], extensional-bending coupling stiffness matrix [B], and bending stiffness matrix [D]. These five laminates and their lay-up stacking sequences are shown in Table 4.7 below.

Table 4.7. Laminate stacking sequences.

LAMINATE 1	$[0^0/0^0/+45^0/-45^0/90^0/90^0]_S$	Symmetric and Balanced
LAMINATE 2	$[+45^0/0^0/0^0/-45^0/90^0/90^0]_S$	Symmetric and Balanced
LAMINATE 3	$[+45^0/-45^0/0^0/0^0/90^0/90^0]_S$	Symmetric and Balanced
LAMINATE 4	$[+45^0/-45^0/90^0/90^0/0^0/0^0]_S$	Symmetric and Balanced
LAMINATE 5	$[+45^0{}_2/-45^0{}_2/0^0{}_4/90^0{}_4]_T$	Unsymmetrical and Balanced

The calculated values of matrices $A_{\theta\theta}$, $B_{\theta\theta}$, and $D_{\theta\theta}$ using Equations 3-16, 3-17, and 3-18 with different laminate stacking sequences and/or different mid-plane radius R are shown in the following table.

Table 4.8. Matrices comparison for laminate 3.

	R_1 = 0.2444	R_2 = 0.6444	R_3 = 1.8444	R → ∞
$A_{\theta\theta}$ (10^5 lb/in)	9.055	9.002	8.995	8.994
$B_{\theta\theta}$ (10^2 lb)	-14.88	-5.54	-1.93	0.00
$D_{\theta\theta}$ (10^2 lb-in)	3.64	3.57	3.56	3.56

As indicated in Table 4.8, $A_{\theta\theta}$ and $D_{\theta\theta}$ fairly remain constant as R increases. However, the magnitude of $B_{\theta\theta}$ strongly decreases as R increases. The values of matrices $A_{\theta\theta}$, $B_{\theta\theta}$ and $D_{\theta\theta}$ are then re-evaluated with four different laminates (1, 2, 3, and 4) and one mid-plane radius, R = 0.2444 inches. These values are shown in Table 4.9. Unlike the plate laminate, the changing of stacking sequence in the curved laminate does affect the axial stiffness, $A_{\theta\theta}$.

It should be also noted that $B_{\theta\theta} \neq 0$ for curved laminates as listed in Table 4.9. This Table 4.9 also indicates that increasing R gives significant reduction of $B_{\theta\theta}$.

Table 4.9. Matrices comparison for mid-plane radius R_1 = 0.2444 inches.

	LAMINATE 1	LAMINATE 2	LAMINATE 3	LAMINATE 4
$A_{\theta\theta}$ (10^5 lb/in)	9.031	9.044	9.055	9.099
$B_{\theta\theta}$ (10^2 lb)	-9.03	-12.34	-14.88	-25.74
$D_{\theta\theta}$ (10^2 lb-in)	2.21	3.02	3.64	6.29

The effect of symmetric and balanced laminate and unsymmetrical and balanced laminate was also investigated. Laminate 3 and laminate 5 were examined with four mid-plane radius R_1 = 0.2444 inches, R_2 = 0.6444 inches, R_3 = 1.8444 inches, and R → ∞. The values of matrices $A_{\theta\theta}$, $B_{\theta\theta}$ and $D_{\theta\theta}$ are shown below.

Table 4.10. Matrices comparison for laminate 3 & 5.

	R_1 = 0.2444		R_2 = 0.6444	
	LAMINATE	LAMINATE 5	LAMINATE 3	LAMINATE 5
$A_{\theta\theta}$ (10^5 lb/in)	9.055	8.588	9.002	8.810
$B_{\theta\theta}$ (10^2 lb)	-14.88	99.22	-5.54	118.40
$D_{\theta\theta}$ (10^2 lb-in)	3.64	7.69	3.57	7.92
	R_3 = 1.8444		R → ∞	
	LAMINATE	LAMINATE 5	LAMINATE 3	LAMINATE 5
$A_{\theta\theta}$ (10^5 lb/in)	8.995	8.925	8.994	8.994
$B_{\theta\theta}$ (10^2 lb)	-1.93	126.33	0.00	130.69
$D_{\theta\theta}$ (10^2 lb-in)	3.56	8.05	3.56	8.12

As the radius of curvature R goes to infinity, a curved laminate becomes a plate laminate. In this case, extensional-bending coupling stiffness matrix [B] is only affected by the stacking sequence in laminate. This indication is shown in Table 4.10. For laminate 3 (symmetric and balanced), $B_{\theta\theta}$ is equal to zero when the radius of curvature R goes to infinity. For laminate 5 (unsymmetrical and balanced), $B_{\theta\theta}$ is not equal to zero when the radius of curvature R goes to infinity.

CHAPTER 5

CONCLUSIONS AND FUTURE WORK

The research has studied the variation of both tangential and radial stresses respect to the changing in curvatures, stacking sequences and fiber orientations in a curved laminated beam subjected to a bending moment. Three 3-D finite element models of the curved laminated beam have been developed in PATRAN / NASTRAN. These models have been validated for isotropic material, Al-2014-T6, and orthotropic material, T300/977-2 graphite/epoxy, with all 0^0 plies lay-up. The finite element models of the curved laminated beam provide solutions showing an excellent agreement with the exact solutions for both tangential and radial stresses.

An analytical method to calculate the tangential stress was also developed for a curved laminated beam subjected to a bending moment. The tangential stress results from this method were compared well with the results from finite element method. The analytical closed-form expressions of axial, coupling and bending stiffness, as well as their characteristics were also investigated.

From this research, the following conclusions can be made.

For the same stacking sequence, $[+45^0/-45^0/90^0_2/0^0_2]_S$ with three different given radius of curvatures:

- In $+45^0$ (layer #1, the bottom layer) and -45^0 (layer #2, the 2^{nd} to the bottom), the tangential and radial stresses increase with the decreasing in radius of curvatures.
- In 90^0 (layer #4, from the bottom layer), the tangential stress decreases with the decreasing in radius of curvature. The radial stress increases with the decreasing in curvature.

- In 0^0 (layer #6, from the bottom), the tangential stress is highest for radius of curvature R_1 and lowest for radius of curvature R_2. The radial stress increases with the decreasing in curvature.

For a given radius of curvature with five different symmetric and balanced stacking sequences, the stress for elements on 90^0 layer #6 from the bottom layer:

- The radial stress is positive for all stacking sequences.
- The tangential stresses from stacking sequence #1, $[\pm 15^0/\pm 15^0/90^0{}_2]_S$, and stacking sequence #2, $[\pm 30^0/\pm 30^0/90^0{}_2]_S$, are positive.
- The tangential stresses from stacking sequence #3, $[\pm 45^0/\pm 45^0/90^0{}_2]_S$, stacking sequence #4, $[\pm 60^0/\pm 60^0/90^0{}_2]_S$, and stacking sequence #5, $[\pm 75^0/\pm 75^0/90^0{}_2]_S$, are negative.
- The tangential and radial stresses from stacking sequence #1, $[\pm 15^0/\pm 15^0/90^0{}_2]_S$, are highest.

For a given radius of curvature with three different stacking sequences: $\left[\pm 45^0{}_2/90^0{}_4/\mp 45^0{}_2\right]_T$, $\left[\pm 45^0{}_2/\pm 45^0{}_2/90^0{}_4\right]_T$, and $\left[+45^0{}_8/90^0{}_4\right]_T$, the stress for elements on $+45^0$ layer #1, bottom layer:

- The tangential stresses σ_θ are positive for all stacking sequences.
- The symmetric and balanced laminate, $\left[\pm 45^0{}_2/90^0{}_4/\mp 45^0{}_2\right]_T$, produced the highest tangential stress.
- The unsymmetrical and balanced laminate, $\left[\pm 45^0{}_2/\pm 45^0{}_2/90^0{}_4\right]_T$, produced the lowest tangential stress.

For a symmetric and balanced laminate:

- $A_{\theta\theta}$ and $D_{\theta\theta}$ fairly remain constant as R increases.
- The magnitude of $A_{\theta\theta}$ is affected by the changing of stacking sequence in the curved laminate.
- $B_{\theta\theta}$ is not equal to zero for curved laminated beam but its magnitude strongly decreases as R increases.
- The increasing of radius curvature gives significant reduction of $B_{\theta\theta}$.

In future studies, the developed analytical method could be extended to laminated cylindrical shell. The hygrothermal effects on the tangential and radial stresses can be included. Effect of stress components due to the boundary conditions and loading of the curved beam can be investigated.

APPENDIX A

GENERAL PROCEDURE TO CREATE A 3D FEM FOR AN ISOTROPIC AND A CURVED LAMINATED BEAM IN PATRAN

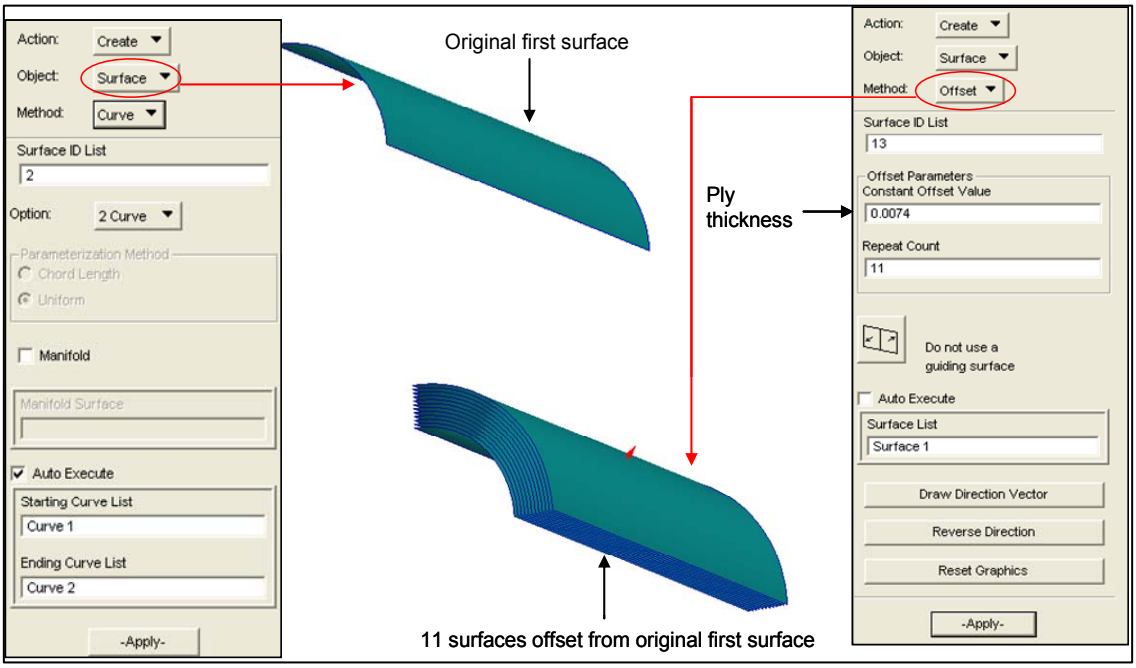

Figure A1. The creation of 12 surfaces.

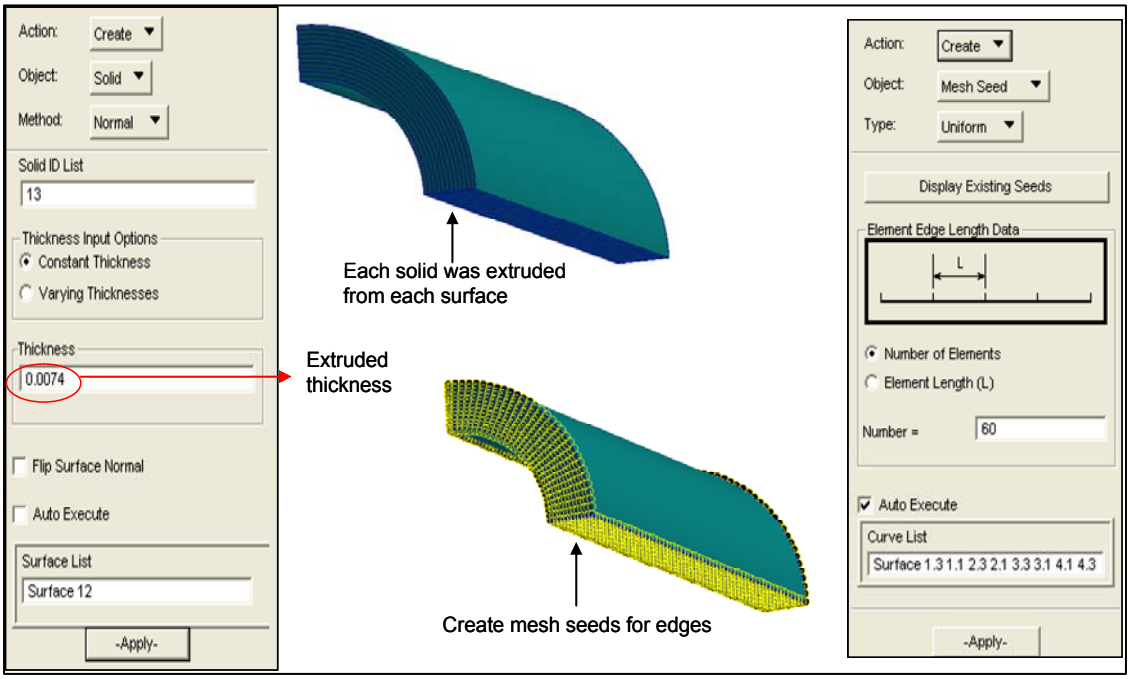

Figure A2. The creation of 12 solids and mesh seeds.

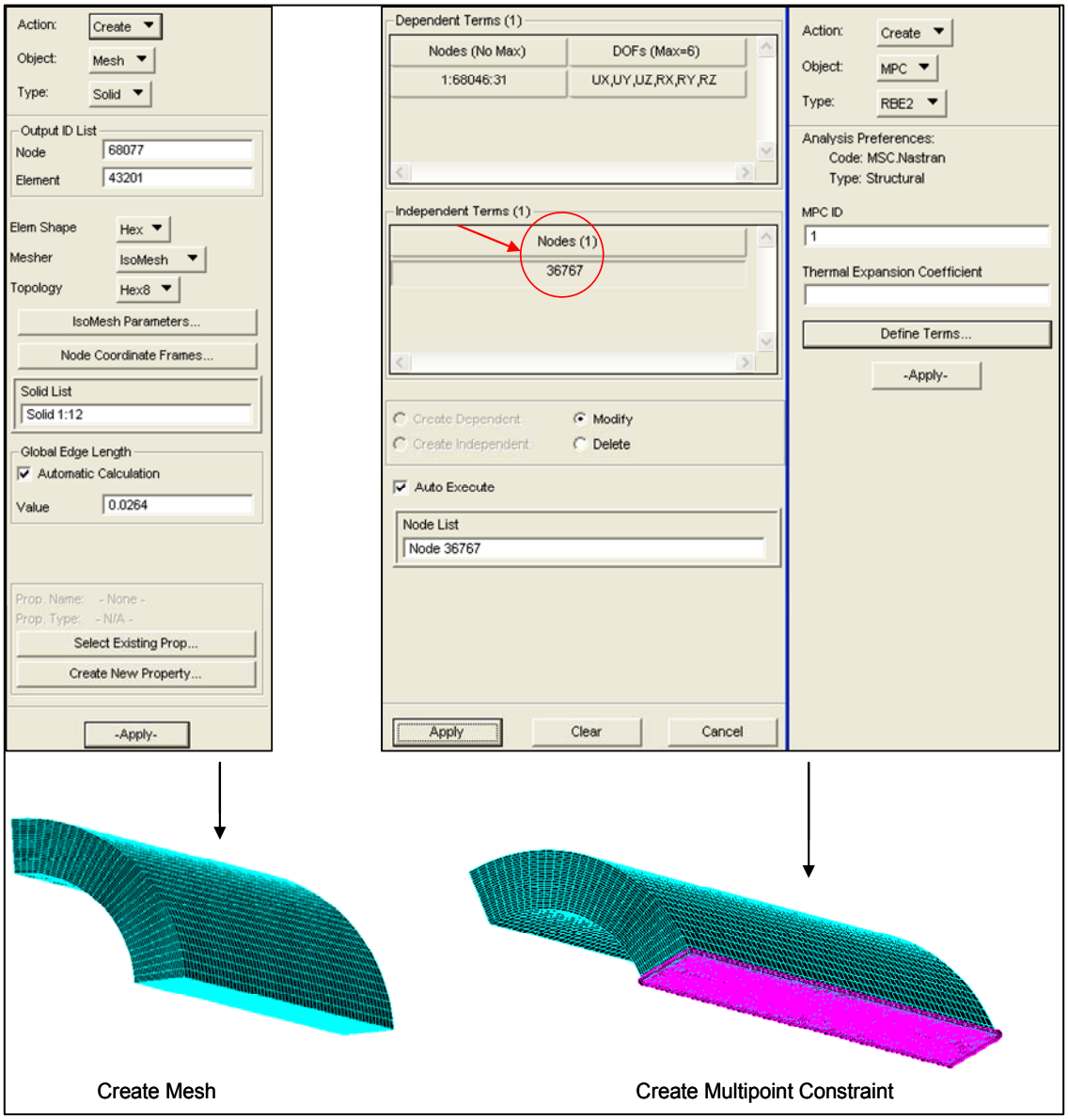

Figure A3. The creation for the mesh and MPC.

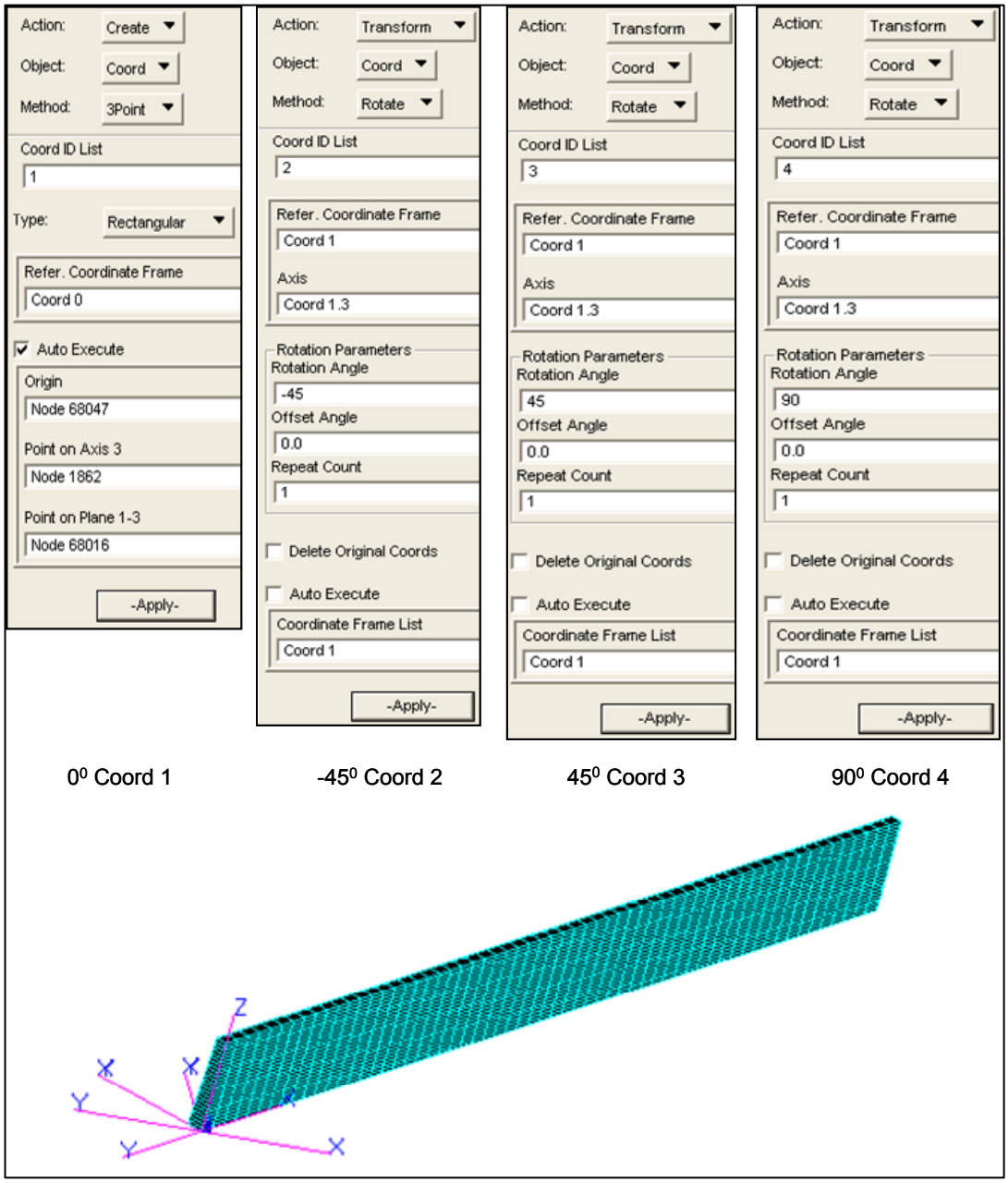

Figure A4. The creation of local coordinates for each element group in laminate.

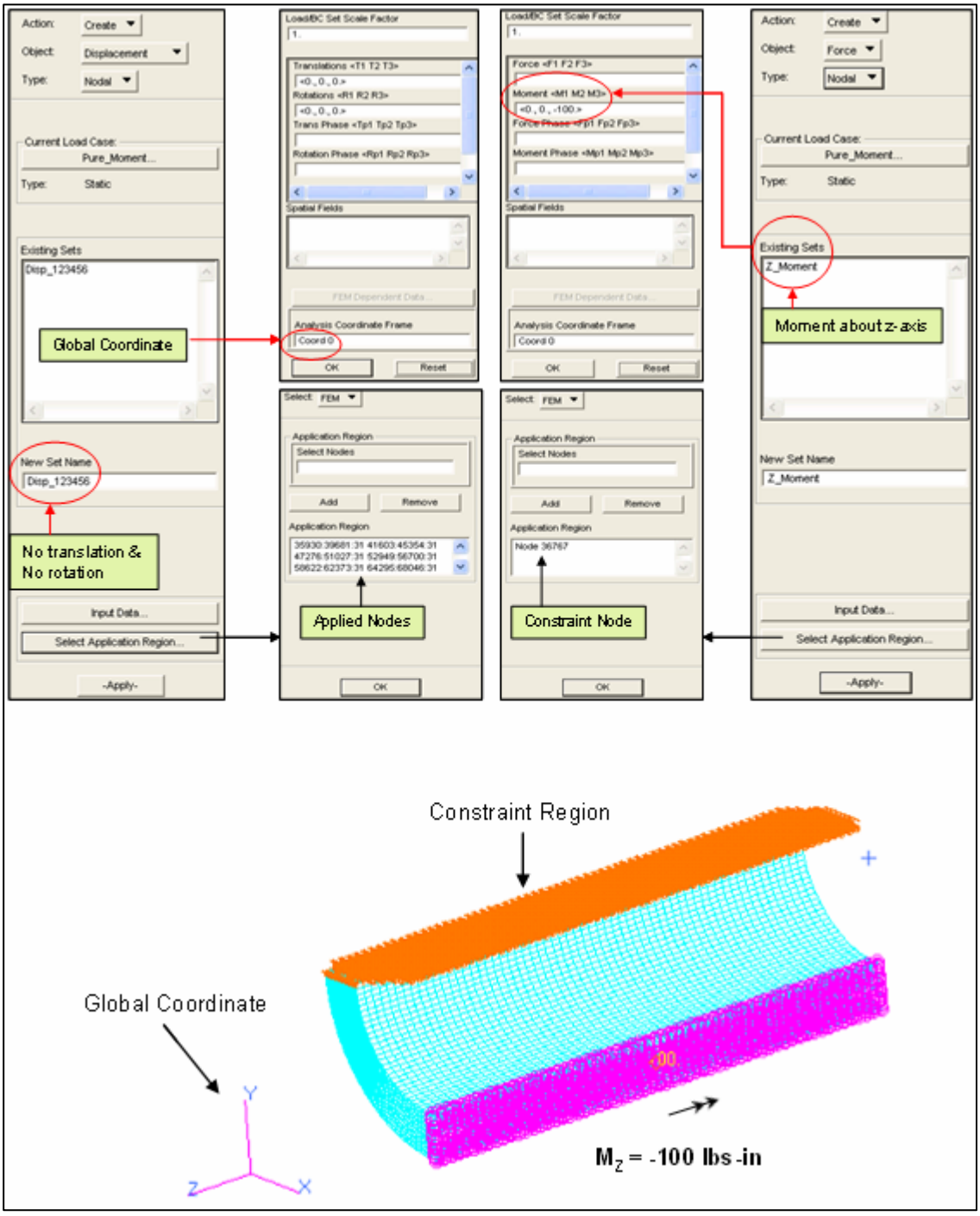

Figure A5. The creation of displacement and applied moment.

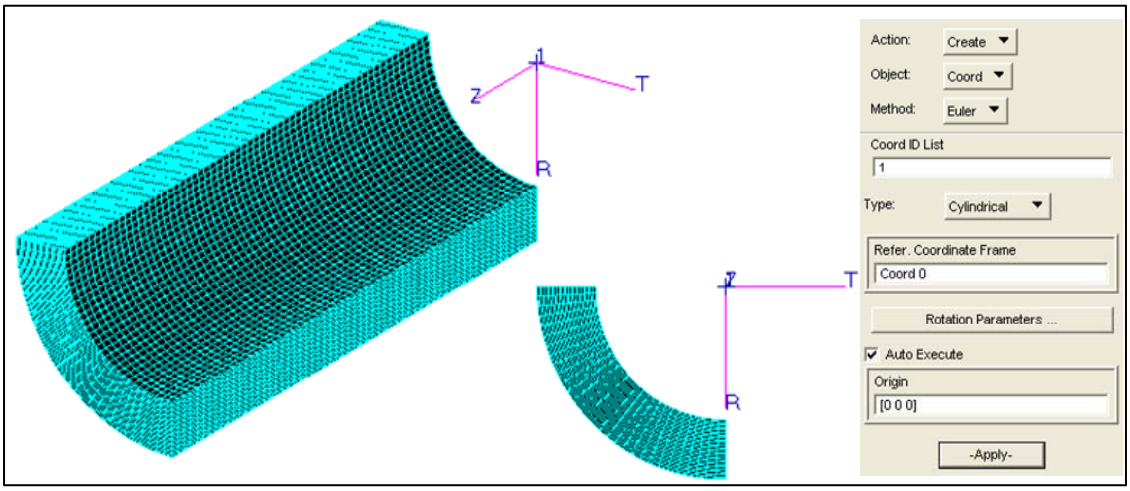

Figure A6. The creation of cylindrical coordinate system for isotropic.

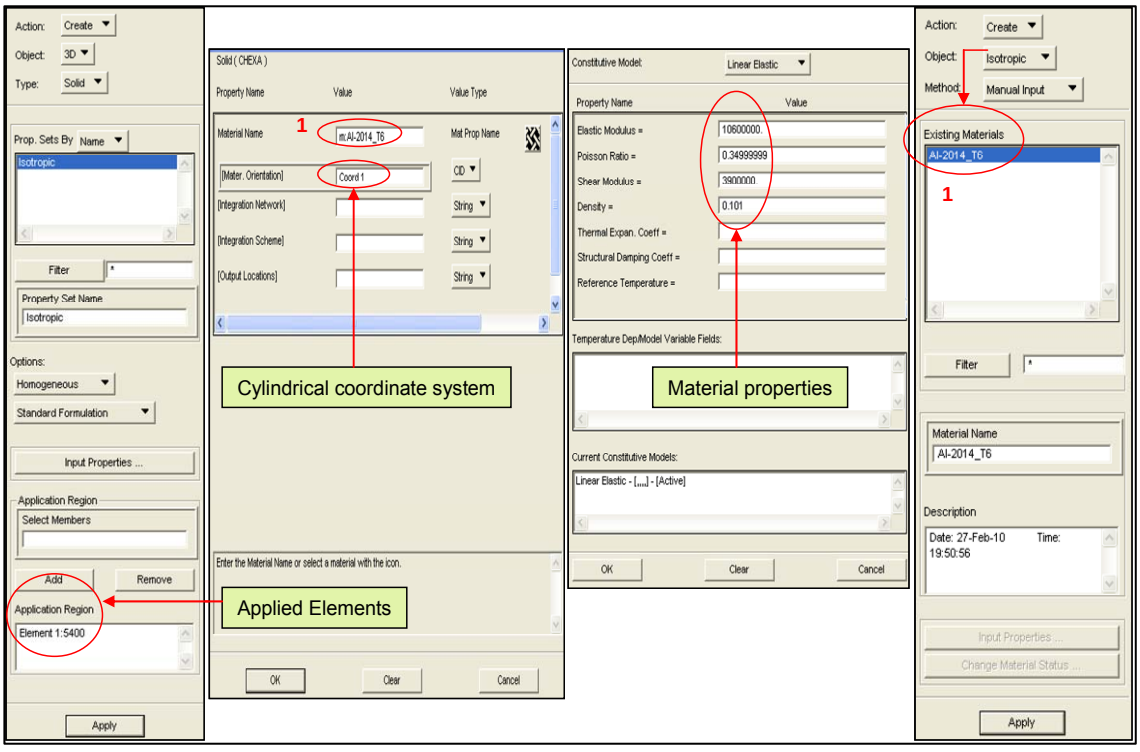

Figure A7. The creation of Isotropic material and 3D solid elements.

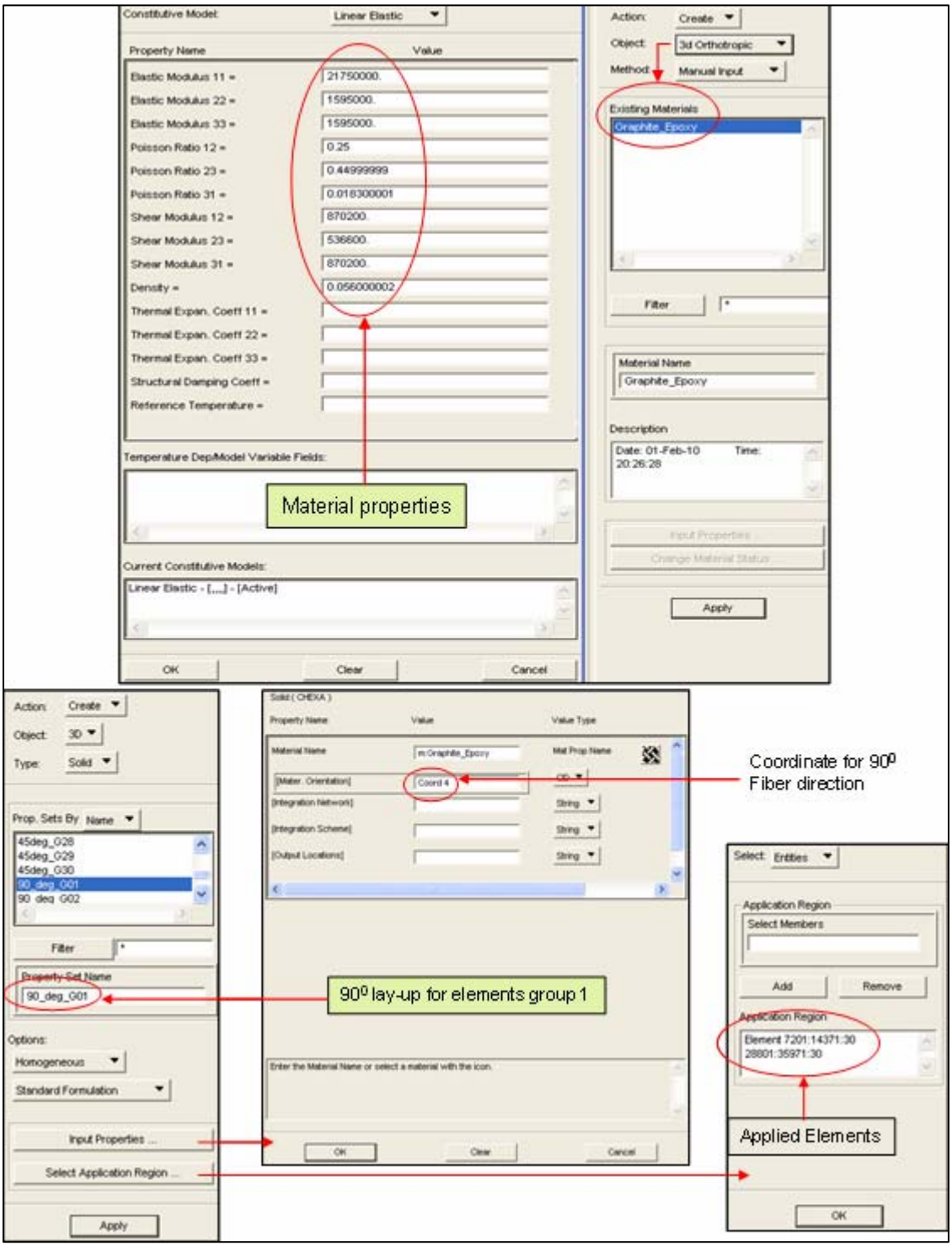

Figure A8. The creation of 3D orthotropic material and 3D solid group elements.

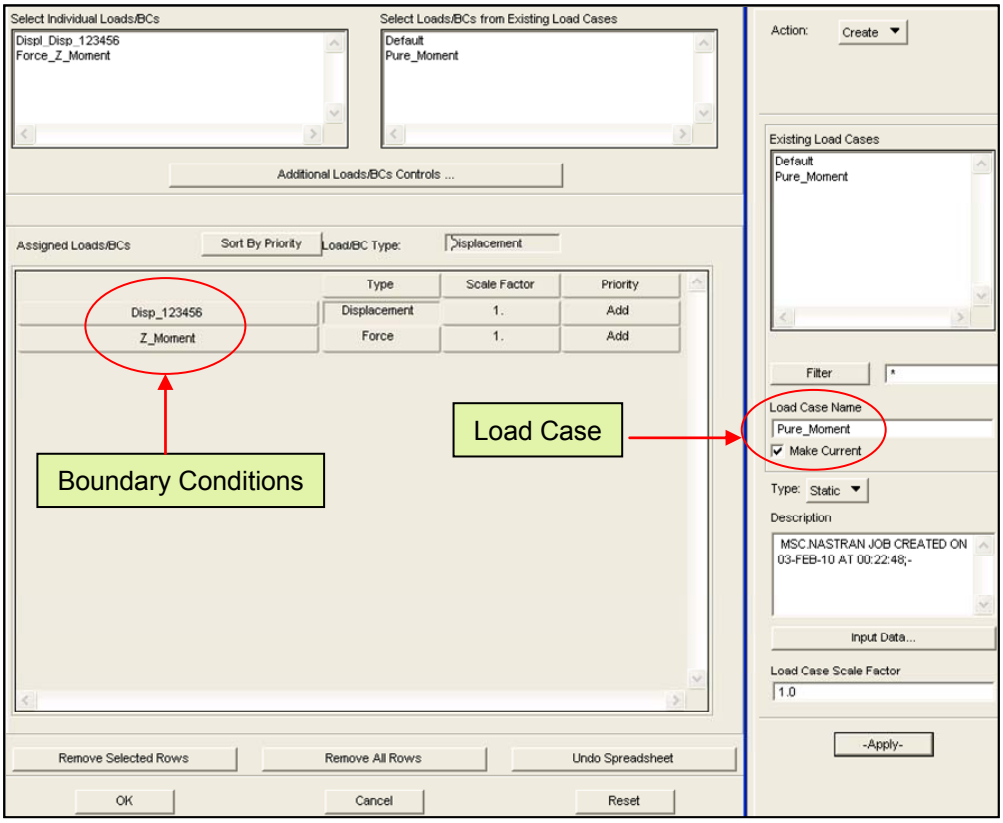

Figure A9. The creation of analysis Load case.

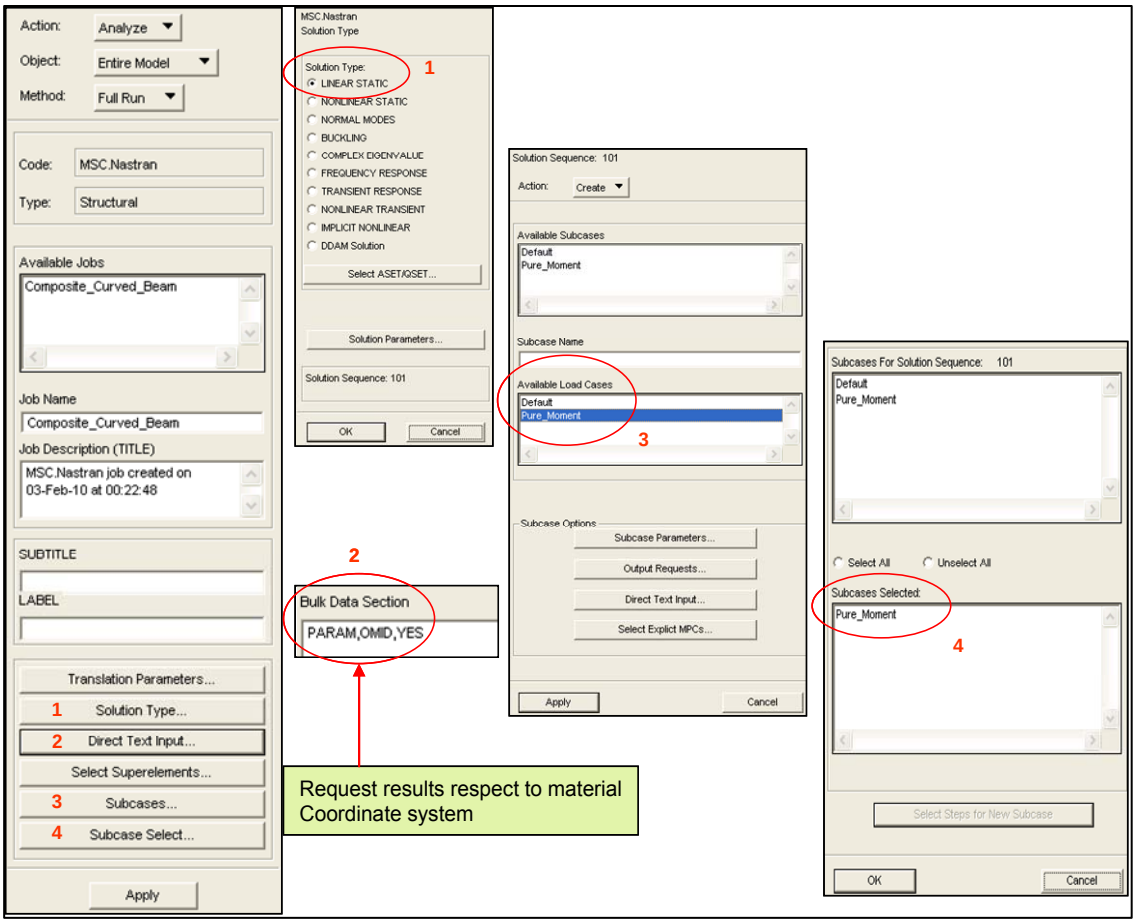

Figure A10. The procedure to set up the analysis.

APPENDIX B

MATHEMATICAL PROCEDURE TO VERIFY THE ACCURACY OF MATRIX [A], [B], AND [D] WHEN THE CURVATURE GOES TO INFINITY

THE EXTENSIONAL STIFFNESS MATRIX [A]:

From Equation 3-16, $A_{\theta\theta} = R\sum_{k=1}^{n} \overline{Q}_{\theta\theta,k} \ln \frac{R+z_k}{R+z_{k-1}}$

$$\lim_{R\to\infty} A_{\theta\theta} = \lim_{R\to\infty} R\sum_{k=1}^{n} \overline{Q}_{\theta\theta,k} \ln \frac{R+z_k}{R+z_{k-1}} = \sum_{k=1}^{n} \overline{Q}_{\theta\theta,k} \lim_{R\to\infty} R\ln \frac{R+z_k}{R+z_{k-1}} \tag{B1}$$

where $\overline{Q}_{\theta\theta,k}$ is material constant.

$$\lim_{R\to\infty} R\cdot \ln \frac{R+z_k}{R+z_{k-1}} = \lim_{R\to\infty} R\cdot \ln\left(1+\frac{z_k - z_{k-1}}{R+z_{k-1}}\right) = \lim_{R\to\infty} R\cdot \ln(1+x) \tag{B-2}$$

where $x = \frac{z_k - z_{k-1}}{R+z_{k-1}}$ and $|x| < 1.$

Taylor series: $\ln(1+x) = x - \frac{1}{2}x^2 + \frac{1}{3}x^3 - \frac{1}{4}x^4 + \ldots$

$$R\cdot \ln(1+x) = R\cdot\left(x - \frac{1}{2}x^2 + \frac{1}{3}x^3 - \frac{1}{4}x^4 + \ldots\right) \approx R\cdot x$$

$$R\cdot \ln(1+x) \approx R\cdot \frac{z_k - z_{k-1}}{R+z_{k-1}} = \frac{z_k - z_{k-1}}{1+\frac{z_{k-1}}{R}} \tag{B-3}$$

Substitute (B-3) into (B-2) yields:

$$\lim_{R\to\infty} R\cdot \ln \frac{R+z_k}{R+z_{k-1}} = \lim_{R\to\infty} \frac{z_k - z_{k-1}}{1+\frac{z_{k-1}}{R}} = z_k - z_{k-1} \tag{B-4}$$

Hence, we have:

$$\lim_{R\to\infty} A_{\theta\theta} = \sum_{k=1}^{n} \overline{Q}_{\theta\theta,k}\left(z_k - z_{k-1}\right)$$ (Plate Lamination Theory).

THE EXTENSIONAL-BENDING COUPLING STIFFNESS MATRIX [B]:

From Equation 3-17, $B_{\theta\theta} = R\sum_{k=1}^{n}\overline{Q}_{\theta\theta,k}\left[\left(z_k - z_{k-1}\right) - R\cdot\ln\frac{R+z_k}{R+z_{k-1}}\right]$

$$\lim_{R\to\infty} B_{\theta\theta} = \lim_{R\to\infty}\sum_{k=1}^{n}\overline{Q}_{\theta\theta,k}\left[R\cdot\left(z_k - z_{k-1}\right) - R^2\cdot\ln\frac{R+z_k}{R+z_{k-1}}\right]$$

$$\lim_{R\to\infty} B_{\theta\theta} = \sum_{k=1}^{n}\overline{Q}_{\theta\theta,k}\left(\lim_{R\to\infty} R\cdot\left(z_k - z_{k-1}\right) - \lim_{R\to\infty} R^2\cdot\ln\frac{R+z_k}{R+z_{k-1}}\right) \tag{B-5}$$

$$\lim_{R\to\infty} R^2\cdot\ln\frac{R+z_k}{R+z_{k-1}} = \lim_{R\to\infty} R^2\cdot\ln(1+x), \qquad \text{where } x = \frac{z_k - z_{k-1}}{R+z_{k-1}} \text{ and } |x| < 1.$$

$$\lim_{R\to\infty} R^2\cdot\ln(1+x) = \lim_{R\to\infty} R^2\cdot\left(x - \frac{1}{2}x^2 + \frac{1}{3}x^3 - \frac{1}{4}x^4 + \ldots\right) \approx \lim_{R\to\infty}\left(R^2\cdot x - \frac{1}{2}(R\cdot x)^2\right) \tag{B-6}$$

$$\lim_{R\to\infty} R^2\cdot x = \lim_{R\to\infty} R^2\cdot\frac{z_k - z_{k-1}}{R+z_{k-1}} = \lim_{R\to\infty} R\cdot\left(\frac{z_k - z_{k-1}}{1+\frac{z_{k-1}}{R}}\right) = \lim_{R\to\infty} R(z_k - z_{k-1})\frac{1}{(1+y)} \tag{B-7}$$

where $y = \frac{z_{k-1}}{R}$ and $|y| < 1$

Taylor series: $\frac{1}{1+y} = 1 - y + y^2 - y^3 + \ldots$ for $|y| < 1$ (B-8)

Substitute (B8) into (B7) yields:

$$\lim_{R\to\infty} R^2\cdot x = \lim_{R\to\infty} R\cdot\left(z_k - z_{k-1}\right)\cdot\left(1 - \frac{z_{k-1}}{R} + \left(\frac{z_{k-1}}{R}\right)^2 - \left(\frac{z_{k-1}}{R}\right)^3 + \ldots\right)$$

$$\lim_{R\to\infty} R^2\cdot x \approx \lim_{R\to\infty} R\cdot\left(z_k - z_{k-1}\right) - \lim_{R\to\infty} z_{k-1}\cdot\left(z_k - z_{k-1}\right)$$

$$= \lim_{R\to\infty} R\cdot\left(z_k - z_{k-1}\right) - z_{k-1}\cdot\left(z_k - z_{k-1}\right) \tag{B-9}$$

$$\lim_{R\to\infty}\frac{(R\cdot x)^2}{2}=\frac{1}{2}\lim_{R\to\infty}\left(R\cdot\frac{z_k-z_{k-1}}{R+z_{k-1}}\right)^2=\frac{1}{2}\lim_{R\to\infty}\left((z_k-z_{k-1})^2\cdot\left(\frac{1}{1+\frac{z_{k-1}}{R}}\right)^2\right)$$

Taylor series: $\frac{1}{1+\frac{z_{k-1}}{R}}=\left(1-\frac{z_{k-1}}{R}+\left(\frac{z_{k-1}}{R}\right)^2-\left(\frac{z_{k-1}}{R}\right)^3+\ldots\right)$

Then, $\lim_{R\to\infty}\frac{(R\cdot x)^2}{2}=\frac{1}{2}\lim_{R\to\infty}(z_k-z_{k-1})^2=\frac{1}{2}(z_k-z_{k-1})^2$ (B-10)

Equation B-6 becomes:

$$\lim_{R\to\infty}R^2\cdot\ln\frac{R+z_k}{R+z_{k-1}}=\lim_{R\to\infty}R\cdot(z_k-z_{k-1})-\lim_{R\to\infty}z_{k-1}\cdot(z_k-z_{k-1})-\frac{1}{2}\lim_{R\to\infty}(z_k-z_{k-1})^2$$

$$\lim_{R\to\infty}R^2\cdot\ln\frac{R+z_k}{R+z_{k-1}}=-z_{k-1}\cdot(z_k-z_{k-1})-\frac{1}{2}(z_k-z_{k-1})^2+\lim_{R\to\infty}R\cdot(z_k-z_{k-1})$$

$$\lim_{R\to\infty}R^2\cdot\ln\frac{R+z_k}{R+z_{k-1}}=\frac{1}{2}(z_{k-1}^2-z_k^2)+\lim_{R\to\infty}R\cdot(z_k-z_{k-1})$$ (B-11)

Substitute B-11 into B-5 yields:

$$\lim_{R\to\infty}B_{\theta\theta}=\sum_{k=1}^{n}\overline{Q}_{\theta\theta,k}\left(\lim_{R\to\infty}R\cdot(z_k-z_{k-1})-\frac{1}{2}(z_{k-1}^2-z_k^2)-\lim_{R\to\infty}R\cdot(z_k-z_{k-1})\right)$$

$$\lim_{R\to\infty}B_{\theta\theta}=\frac{1}{2}\sum_{k=1}^{n}\overline{Q}_{\theta\theta,k}(z_k^2-z_{k-1}^2)$$ (Plate Lamination Theory).

THE BENDING STIFFNESS MATRIX [D]:

From Equation 3-18:

$$D_{\theta\theta} = R\sum_{k=1}^{n}\overline{Q}_{\theta\theta,k}\left[\frac{1}{2}\left(z_k^2 - z_{k-1}^2\right) - R\left(z_k - z_{k-1}\right) + R^2\ln\left(\frac{R+z_k}{R+z_{k-1}}\right)\right]$$

$$\lim_{R\to\infty} D_{\theta\theta} = \sum_{k=1}^{n}\overline{Q}_{\theta\theta,k}\lim_{R\to\infty}\left[\frac{R}{2}\left(z_k^2 - z_{k-1}^2\right) - R^2\left(z_k - z_{k-1}\right) + R^3\ln\left(\frac{R+z_k}{R+z_{k-1}}\right)\right] \qquad \text{(B-12)}$$

$$R^3\ln\left(\frac{R+z_k}{R+z_{k-1}}\right) = R^3\ln(1+x) = R^3\left(x - \frac{1}{2}x^2 + \frac{1}{3}x^3 - \ldots\right) \approx R^3\cdot x - \frac{R^3}{2}x^2 + \frac{R^3}{3}x^3$$

$$R^3\ln\left(\frac{R+z_k}{R+z_{k-1}}\right) \approx R^3\cdot x - \frac{R^3}{2}x^2 + \frac{R^3}{3}x^3 \qquad \text{(B-13)}$$

where $x = \dfrac{z_k - z_{k-1}}{R + z_{k-1}}$; (See Equation B-6)

$$R^3\cdot x = R^3\cdot\frac{z_k - z_{k-1}}{R+z_{k-1}} = R^2\left(\frac{z_k - z_{k-1}}{1+\dfrac{z_{k-1}}{R}}\right) \approx R^2\left(z_k - z_{k-1}\right)\cdot\left[1 - \frac{z_{k-1}}{R} + \left(\frac{z_{k-1}}{R}\right)^2\right]$$

$$R^3\cdot x \approx R^2\left(z_k - z_{k-1}\right)\cdot\left[1 - \frac{z_{k-1}}{R} + \left(\frac{z_{k-1}}{R}\right)^2\right]; \qquad \text{(See equation B-8)}$$

$$R^3\cdot x = R^2\cdot\left(z_k - z_{k-1}\right) - R\cdot\left(z_k - z_{k-1}\right)\cdot z_{k-1} + \left(z_k - z_{k-1}\right)\cdot z_{k-1}^2 \qquad \text{(B-14)}$$

$$\frac{R^3}{2}x^2 = \frac{R}{2}\cdot\left(R\cdot x\right)^2 = \frac{R}{2}\cdot\left(R\cdot\frac{z_k - z_{k-1}}{R+z_{k-1}}\right)^2 = \frac{R}{2}\cdot\left(\frac{z_k - z_{k-1}}{1+\dfrac{z_{k-1}}{R}}\right)^2$$

$$= \frac{R}{2}\cdot\left(z_k - z_{k-1}\right)^2\cdot\left[1 - 2\cdot\frac{z_{k-1}}{R} + 3\left(\frac{z_{k-1}}{R}\right)^2 - \ldots\right] \text{ for } \left|\frac{z_{k-1}}{R}\right| < 1 \quad \text{(Taylor series)}$$

$$\frac{R^3}{2}x^2 \approx \frac{R}{2}\cdot\left(z_k - z_{k-1}\right)^2 - z_{k-1}\cdot\left(z_k - z_{k-1}\right)^2 \qquad \text{(B-15)}$$

$$\frac{R^3}{3}x^3 = \frac{1}{3}\cdot(R\cdot x)^3 = \frac{1}{3}\cdot\left(R\cdot\frac{z_k - z_{k-1}}{R + z_{k-1}}\right)^3 \approx \frac{1}{3}\cdot(z_k - z_{k-1})^3 \qquad \text{(B-16)}$$

(Using the same approach in Equation B-15)

Substitute B-14, B-15, and B-16 into B-12 yields:

$$\lim_{R\to\infty} D_{\theta\theta} = \sum_{k=1}^{n} \overline{Q}_{\theta\theta,k}\left[\begin{array}{l} \lim_{R\to\infty}\frac{R}{2}\left(z_k^2 - z_{k-1}^2\right) - \lim_{R\to\infty} R^2\left(z_k - z_{k-1}\right) + \lim_{R\to\infty} R^2\cdot\left(z_k - z_{k-1}\right) \\ -\lim_{R\to\infty} R\cdot\left(z_k - z_{k-1}\right)\cdot z_{k-1} + \lim_{R\to\infty}\left(z_k - z_{k-1}\right)\cdot z_{k-1}^2 - \lim_{R\to\infty}\frac{R}{2}\cdot\left(z_k - z_{k-1}\right)^2 \\ +\lim_{R\to\infty} z_{k-1}\cdot\left(z_k - z_{k-1}\right)^2 + \lim_{R\to\infty}\frac{1}{3}\cdot\left(z_k - z_{k-1}\right)^3 \end{array}\right]$$

$$\lim_{R\to\infty} D_{\theta\theta} = \sum_{k=1}^{n} \overline{Q}_{\theta\theta,k}\left[\begin{array}{l} \left(z_k - z_{k-1}\right)\cdot z_{k-1}^2 + z_{k-1}\cdot\left(z_k - z_{k-1}\right)^2 + \frac{1}{3}\cdot\left(z_k - z_{k-1}\right)^3 \\ +\lim_{R\to\infty}\frac{R}{2}\left(z_k^2 - z_{k-1}^2 - 2z_k\cdot z_{k-1} + 2\cdot z_{k-1}^2 - z_k^2 + 2z_k\cdot z_{k-1} - z_{k-1}^2\right) \end{array}\right]$$

$$\lim_{R\to\infty} D_{\theta\theta} = \sum_{k=1}^{n} \overline{Q}_{\theta\theta,k}\left[\left(z_k - z_{k-1}\right)\cdot z_{k-1}^2 + z_{k-1}\cdot\left(z_k - z_{k-1}\right)^2 + \frac{1}{3}\cdot\left(z_k - z_{k-1}\right)^3\right]$$

$$\lim_{R\to\infty} D_{\theta\theta} = \frac{1}{3}\sum_{k=1}^{n} \overline{Q}_{\theta\theta,k}\left(z_k^3 - z_{k-1}^3\right) \qquad \text{(Plate Lamination Theory).}$$

REFERENCES

1) Sayegh A. F. and Dong S. B., M.ASCE, “Analysis of Laminated Curved Beams”, Journal of the Engineering Mechanics Division, August 1970.
2) Cheung C. K. and Sorensen H. C., “Effect of axial loads on radial stress in curved beams”, Wood and Fiber Science Journal, Volume 15, Number 3 / July 1983.
3) Graff E. and Springer G. S., “Stress analysis of thick, curved composite laminates”, Computers & Structures journal, Volume 38, Issue 1, 1991, Pages 41-55.
4) Barbero, E. J., Fu, S. H., and Raftoyiannis, I., “Ultimate bending strength of composite beams “, ASCE J. Mater, Civil Engng 3, 1991, pp. 293-306.
5) Madabhusi-Raman, P. and Davalos J. F., Static shear correction factor for laminated rectangular beams. Composites Part B: Engineering, 1996. 27(3-4): p. 285-293.
6) Kasal B. and Heiduschle A., “Radial reinforcement of curved glue laminated wood beams with composite materials”, Forest Products Journal, Jan 2004.
7) Wang W. and Shenoi R. A., “Analytical Solutions to Predict Flexural Behavior of Curved Sandwich Beams”, Journal of Sandwich Structures and Materials, Vol. 6, No. 3, 199-216 (2004).
8) Qatu M. S., Vibration of Laminated Shells and Plates, Elsevier Academic Press, 2004.
9) Ugural A. C. and Fenster S. K., Advanced Strength and Applied Elasticity 4th ed., Pearson Education, Inc., 2003.
10) Daniel, I.M. and Ishai, O., Engineering Mechanics of Composite Materials, 2nd edition, Oxford University Press, 2006.
11) Chan W. S., Composite Lecture Notes, University of Texas at Arlington, Spring 2008.

BIOGRAPHICAL INFORMATION

Thien Nguyen received his Bachelor Degree in Mechanical Engineering from the University of Texas at Arlington in 2007. He graduated with Summa Cum Laude Honor and received numerous recognitions during his years as a undergraduate student. Thien was a member of both Pi Tau Sigma and Alpha Chi Honor Society.

He started his Master's degree in Mechanical Engineering at the University of Texas at Arlington immediately after he received his Bachelor's Degree. While pursuing his Master's Degree, Thien works for Vought Aircraft Industry as a Structural Engineer.

His research interests include composite structure analysis, finite element analysis, and behavior of composite materials. Thien Nguyen received Master of Science Degree in Mechanical Engineering from the University of Texas at Arlington in May 2010.